

Signals of Supersymmetry and Higgs at the Large Hadron Collider

Nishita Desai
Harish-Chandra Research Institute

A thesis submitted to the
Board of Studies in Physical Sciences
Homi Bhabha National Institute

In partial fulfillment of requirements for the degree of
Doctor of Philosophy



April 2012

Chhatnag Road, Jhansi, Allahabad 211019

CERTIFICATE

This is to certify that this Ph. D. thesis titled ‘Signals of Supersymmetry and Higgs at the Large Hadron Collider,’ submitted by Nishita Desai is a record of bona fide research work done under my supervision. It is further certified that this thesis represents independent work by the candidate and collaboration was necessitated by the nature and scope of the problems dealt with.

Date:

Prof. Biswarup Mukhopadhyaya
Thesis Advisor

DECLARATION

This thesis is a presentation of my original research work. Whenever contributions of others are involved, every effort is made to indicate this clearly, with due reference to the literature and acknowledgement of collaborative research and discussions. The work is original and has not been submitted earlier as a whole or in part for a degree or diploma at this or any other Institution or University. This work was done under supervision of Prof. Biswarup Mukhopadhyaya, at Harish-Chandra Research Institute, Allahabad.

Date:

Nishita Desai
Ph. D. Candidate

Acknowledgements

I am indebted to many people for their support during the work on this thesis. First, to my thesis advisor, Biswarup Mukhopadhyaya for his unwavering goodwill, support and guidance. I particularly appreciate the timely advice in matters both physics and non-physics given by Dileep Jatkar, Dilip Kumar Ghosh, Aresh Datta and the faculty at Harish-Chandra Research Institute.

My thanks also go to the particle physics community in India, I have learned much from the regular schools, conferences, meetings and ready informal discussion. I would also particularly like to thank Bruce Mellado for helping me understand the working of particle detectors and statistics.

My sincerest thanks to Peter Skands for the opportunity to work on PYTHIA 8 at CERN. Those four months opened up a new world to me.

I have benefited from discussion and advice from many colleagues, in particular, Priyotosh Bandyopadhyay, Subhaditya Bhattacharya, Sanjoy Biswas, Shailesh Lal and Satyanarayan Mukhopadhyay.

Finally, I would like to thank my family — my parents, for their encouragement and support and for putting up with my long absences, and my husband for being with me as always, across distances and timezones.

CONTENTS

| | |
|-----------------------------|-------------|
| Acknowledgements | vii |
| Synopsis | xvii |
| List of Publications | xxi |

INTRODUCTION

| | |
|---|----------|
| 1 The Standard Model and Beyond | 3 |
| 1.1 The Standard Model Lagrangian | 4 |
| 1.2 Experimental confirmations | 8 |
| 1.2.1 QCD as an SU(3) theory | 8 |
| 1.2.2 Proof of SU(2) × U(1) structure | 11 |
| 1.2.3 Evidence for Higgs | 13 |
| 1.3 Shortcomings of the SM | 14 |
| 1.3.1 Anomalous magnetic moment of the muon $(g - 2)_\mu$ | 15 |
| 1.3.2 Neutrino masses and mixing | 15 |
| 1.3.3 Dark Matter, Dark energy and Baryon asymmetry in the Universe | 16 |
| 1.3.4 Higgs mass stabilisation | 16 |
| 1.3.5 The flavour problem | 17 |
| 1.4 The Large Hadron Collider | 17 |
| 1.4.1 Detection of particles | 18 |

| | | |
|---|---|-----------|
| 1.4.2 | Physics goals of the LHC | 19 |
| 2 | Supersymmetry | 23 |
| 2.1 | The Minimal Supersymmetric Standard Model | 24 |
| 2.1.1 | The SUSY algebra and superfields | 24 |
| 2.1.2 | Constructing the Lagrangian | 26 |
| 2.2 | SUSY breaking and the sparticle spectrum | 28 |
| 2.2.1 | MSSM particle spectrum | 29 |
| 2.2.2 | Neutralinos and Charginos | 29 |
| 2.2.3 | Squarks and sleptons | 30 |
| 2.3 | Phenomenological Modelling of the MSSM | 31 |
| 2.3.1 | The constrained MSSM | 31 |
| 2.3.2 | The phenomenological MSSM | 33 |
| 2.4 | Summary | 34 |
| SIGNATURES OF SUPERSYMMETRY | | |
| 3 | Signals for squarks of the third generation | 37 |
| 3.1 | Choice of parameters and benchmarks | 39 |
| 3.2 | Signals and Backgrounds | 40 |
| 3.2.1 | Identification of physics objects: | 43 |
| 3.2.2 | Dilepton Channels: $1b + 2l$, $1b + 2l_{(SSD)}$ and $2l_{(SSD)}$ | 46 |
| 3.2.3 | Multi-b Channels: $2b + l$ and $3b$ | 47 |
| 3.2.4 | Channels with reconstructed Higgs | 48 |
| 3.3 | Distinction from cMSSM scenarios | 50 |
| 3.4 | Summary | 53 |
| 4 | Constraints on third generation squarks from LHC data | 55 |
| 4.1 | Simulation of the signal and ATLAS exclusion curves in cMSSM | 57 |
| 4.2 | Parameterisation of the third generation sector | 60 |
| 4.3 | Results | 62 |
| 4.3.1 | Case A | 63 |
| 4.3.2 | Case B | 65 |
| 4.3.3 | Case C | 65 |
| 4.3.4 | Case D | 67 |
| 4.4 | High-scale non-universal scalar scenarios | 68 |
| 4.5 | Caveat: Non-universality in the gaugino sector | 70 |
| 4.6 | Summary | 70 |

| | | |
|----------|--|-----------|
| 5 | R-parity violating resonant top squark production | 71 |
| 5.1 | Resonant stop production and decays | 74 |
| 5.1.1 | Stop production | 74 |
| 5.1.2 | Stop decays and choice of benchmark points | 76 |
| 5.2 | Event generation and selection | 79 |
| 5.2.1 | Event generation | 79 |
| 5.2.2 | Event selection | 79 |
| 5.3 | Results | 81 |
| 5.3.1 | Limits at $\sqrt{s} = 14, 10$ TeV | 81 |
| 5.3.2 | Observability at the early run of 7 TeV | 83 |
| 5.3.3 | Differentiating from R-conserving signals | 85 |
| 5.4 | Non- $\tilde{\chi}_1^0$ LSPs | 87 |
| 5.5 | Summary | 88 |

SIGNATURES OF HIGGS

| | | |
|----------|---|------------|
| 6 | Probing the CP-violating nature of HWW couplings | 91 |
| 6.1 | The anomalous coupling and its simulation | 93 |
| 6.1.1 | Simulation | 93 |
| 6.1.2 | Backgrounds and Cuts | 94 |
| 6.2 | Numerical Results | 95 |
| 6.3 | Effect of showering and hadronisation | 104 |
| 6.4 | Conclusions | 106 |
| 7 | Conclusions | 109 |

APPENDIX

| | | |
|----------|--|------------|
| A | MSSM in Pythia 8 | 113 |
| A.1 | Couplings | 114 |
| A.2 | R-parity violation | 115 |
| A.3 | Cross Sections | 116 |
| A.4 | Sparticle Decays | 117 |
| A.5 | Showers in R-parity violating case | 118 |
| A.6 | Validation | 121 |

| | | |
|--|---------------------|------------|
| | Bibliography | 140 |
|--|---------------------|------------|

LIST OF FIGURES

| | | |
|-----|---|----|
| 1.1 | Results from the JADE Collaboration | 9 |
| 1.2 | Summary of measurements of R | 10 |
| 1.3 | Best fit values for triple gauge boson vertices | 12 |
| 1.4 | Electroweak constraints on Higgs mass | 14 |
| 1.5 | A schematic slice of the CMS detector. (Image by CMS Collaboration). | 18 |
| 1.6 | Summary of Tevatron's $t\bar{t}$ asymmetry | 20 |
| | | |
| 2.1 | Spectrum for point SPS1a | 33 |
| | | |
| 3.1 | Energy distribution of tops for 1A | 41 |
| 3.2 | Energy distribution of tops for 1C | 42 |
| 3.3 | p_T distribution of b-quarks | 42 |
| 3.4 | Missing transverse energy (E_T^{miss}) and effective mass M_{eff} distributions | 45 |
| 3.5 | p_T for the two hardest leptons | 46 |
| 3.6 | Chargino branching fractions into Higgs | 48 |
| 3.7 | p_T and θ of jets from Higgs decay | 49 |
| 3.8 | Comparison of M_{eff} distributions for points 1C, S1 and S2. | 52 |
| | | |
| 4.1 | Comparison of our exclusion curves with the ATLAS | 59 |
| 4.2 | The dependence of the exclusion curves on different values of μ | 63 |
| 4.3 | Comparison of LO and NLO exclusion curves | 64 |
| 4.4 | Exclusion curves for Case-A | 65 |
| 4.5 | Exclusion curves for Case-B | 66 |

| | | |
|------|--|-----|
| 4.6 | Exclusion curves for Case-C | 66 |
| 4.7 | Exclusion curves for Case-D | 67 |
| 4.8 | Comparison of exclusion curves from three high-scale non-universal scenarios | 69 |
| 5.1 | Stop production cross section at the LHC $\lambda''_{eff} = 0.2$ | 75 |
| 5.2 | Lighter stop decay branching fractions | 76 |
| 5.3 | M_{eff} distributions at $\sqrt{s} = 14$ TeV | 84 |
| 5.4 | Normalised effective mass (M_{eff}) and missing energy (\cancel{E}_T) distributions | 87 |
| 6.1 | The behaviour of the cross section in the SSD channel | 95 |
| 6.2 | Δp_T distribution | 97 |
| 6.3 | Distribution of cosine of the angle between two same-sign leptons | 97 |
| 6.4 | Effect of $\text{Re}(\tilde{b})$ on the $\Delta\phi$ distributions | 98 |
| 6.5 | The asymmetry A_{SSD1} | 99 |
| 6.6 | The asymmetry A_{SSD2} | 100 |
| 6.7 | Effect of $\text{Im}(\tilde{b})$ on the $\Delta\eta$ distributions | 100 |
| 6.8 | Effect of $\text{Im}(\tilde{b})$ on the $\Delta \eta $ | 101 |
| 6.9 | The asymmetry A_{SSD3} | 102 |
| 6.10 | The asymmetry A_{SSD4} | 102 |
| 6.11 | Normalised Δp_T distribution | 104 |
| 6.12 | $\Delta\phi$ distribution after including ISR and FSR | 105 |
| 6.13 | $\Delta\eta$ distribution after including ISR and FSR | 105 |
| 6.14 | $\Delta \eta $ distribution after including ISR and FSR | 106 |
| A.1 | Gluon emission from RPV vertices with ϵ -tensor. | 119 |

LIST OF TABLES

| | | |
|-----|---|----|
| 1.1 | Summary of central values for neutrino masses and mixing parameters. | 15 |
| 3.1 | Third generation squark and gluino masses in GeV for the benchmark points considered. | 40 |
| 3.2 | Chargino and Neutralino masses in GeV for all the benchmark points. | 40 |
| 3.3 | Cross section after basic cuts | 46 |
| 3.4 | Signal and background events | 47 |
| 3.5 | Signal and background events for different channels with Higgs identification | 50 |
| 3.6 | Third generation squark and gluino masses in GeV | 51 |
| 3.7 | Number of events at 300 fb^{-1} for the cMSSM points | 51 |
| 4.1 | The values of cross section times acceptance from ATLAS analysis | 60 |
| 4.2 | The parameters of the scan in $M_{\tilde{t}_1}$ - M_2 space. | 62 |
| 5.1 | Benchmark points and the dominant decay modes of the lighter stop. | 78 |
| 5.2 | Effect of cuts on signal and SM background cross sections (in fb) | 82 |
| 5.3 | Same as Table 5.2, but for the SSD + b channel. | 83 |
| 5.4 | Effect of cuts on signal and SM background cross sections | 85 |
| 5.5 | Values of minimum λ''_{eff} that can be ruled out at 95% CL with 10 fb^{-1} of data | 85 |
| 5.6 | Benchmark points for studying RPV stop production at $\sqrt{s} = 7 \text{ TeV}$ | 86 |
| 6.1 | The effect of cuts on the SSD cross section | 96 |

| | | |
|-----|---|-----|
| 6.2 | Asymmetries after ISR and FSR | 106 |
| A.1 | List of SUSY production processes. In all cases, charge conjugate processes are turned on by default. | 116 |
| A.2 | Cross sections for various SUSY processes using PYTHIA 8 | 122 |
| A.3 | Masses and mixing matrices corresponding to SPS1a calculated using SoftSusy 2.0.5 | 123 |

SYNOPSIS

This PhD thesis focusses on phenomenological studies and addresses two questions. First, that of looking for Supersymmetry (SUSY) by detecting squarks of the third generation (in theories both with and without R-parity). The problem of Higgs mass stabilisation is solved in theories with SUSY by the cancellation of the corrections to the Higgs mass from the top and stop (top- squark) loops. To avoid fine-tuning, we would require stop mass to be within a TeV, and hence, we expect stops to be produced at the LHC. Search for top-squarks is therefore a robust way to searching for Supersymmetry.

Secondly, I address the question of determining Higgs couplings to gauge bosons. Assuming that a Higgs-like resonance is observed at the LHC, the next step will be to confirm whether it indeed corresponds to the Standard Model (SM) Higgs. For this, one needs to measure its couplings to gauge bosons since it is here that the structure of the underlying theory will be reflected. I propose a solution to the question of measuring any anomalous contributions to the HWW vertex and to pinpoint its CP property.

Signatures of squarks of the third family

The primary SUSY searches hinge on signatures with jets and missing energy which are tailored to look for squarks of the first two generations and the gluino (which decays into light-quark jets if these squarks are not very heavy). The limits from these searches are then translated to limits on stop mass using a high-scale model like the cMSSM. We address the question of how to detect the stop in the framework where the first two generations are very heavy (and therefore inaccessible) by using a non-universal scalar sector. In light of recent data from LHC experiments, we reinterpret the 1.04 fb^{-1} data in jets+MET channel and 0.83 fb^{-1} data in b-jets+MET channel from ATLAS to determine the limits on masses of third family squarks . Besides this, we have worked

on determining the best signatures for discovery if the stop and gluino masses are near the limit of LHC reach. We perform a detailed background simulation using ALPGEN and find that channels with b-tagged jets and channels with like-sign dileptons have the best reach for discovering such scenarios.

R-parity violating resonant stop production

Even though R-parity is commonly assumed in models of SUSY, it is not a consistency requirement. Therefore, putting limits on R-parity violating couplings by explicitly searching for signatures is a valid mode of determining the nature of BSM physics. Many of these couplings are strongly constrained by observation of meson decays, EDMs etc. However, the baryon number violating UDD-type couplings, λ''_{312} is almost entirely unconstrained. Such a coupling would result in resonant production of a stop which could dominate over the pair-production cross section. We study this particular case for various possible stop decays using Herwig 6.5 for simulating the signal and ALPGEN for the background. Due to the Majorana nature of the neutralino, the like-sign top final state occurs 50% of the time and hence, like-sign dilepton signature is a powerful discriminator. We find that we can better the current limit on λ''_{312} by up to two orders of magnitude for stop masses less than a TeV.

Anomalous HWW couplings at the LHC

The problem of determining Higgs couplings has been well studied in the case of the HZZ coupling because the Z boson can be cleanly reconstructed in its leptonic decay mode. However, it is a difficult problem in the case of the HWW coupling since (a) the event is not fully reconstructible due to the presence of two neutrinos in the final state, and because (b) the opposite-sign dilepton channel has a large SM background. We show that the best production channel to observe this vertex is not $gg \rightarrow h$ but $qq \rightarrow Wh$ followed by $h \rightarrow WW$. We develop certain asymmetry variables that are capable of determining the CP violating nature of the anomalous couplings and also explicitly show that they are largely unaffected by initial state radiation effects. This project involved the use of form to calculate exact matrix elements for both production and decay, writing our own parton-level event generator and interfacing it to Pythia 8 using the Les Houches Event File (LHEF) format for showering and hadronisation.

Implementation of SUSY in Pythia 8

Part of my PhD was spent in working on the generator PYTHIA 8 as an ‘Early Stage Researcher’ working with the Marie Curie Network ‘MCnet’. PYTHIA 8 is a general

purpose Monte-Carlo Generator written in C++ and is capable of simulating various SM and BSM processes. My work on Pythia 8 consists of implementing the production and decay of SUSY particles. I started by generalising the coupling structure so that any BSM couplings can be implemented as an add on to the Standard Model couplings. Following this, all the production cross sections — gluino-pair, squark-pair, squark-gluino, gaugino-pair, squark-gaugino and R-parity violating resonant squark production — were encoded. I also implemented the two body decays of all SUSY particles, the R-parity violating decays of squarks and the R-parity violating three- body decay of the neutralinos (via UDD coupling). The implementation is available for use in the current public release (version 8.160) of PYTHIA 8. My contribution will be detailed in an Appendix.

LIST OF PUBLICATIONS

Publications included in Thesis

1. **Signals of supersymmetry with inaccessible first two families at the Large Hadron Collider.**
Nishita Desai, Biswarup Mukhopadhyaya
Phys. Rev. D 80, 055019 (2009) [arXiv:0901.4883]
2. **R-parity violating resonant stop production at the Large Hadron Collider**
Nishita Desai, Biswarup Mukhopadhyaya
JHEP 1010 (2010) 060. [arXiv:0102.2339]
3. **CP-violating HWW couplings at the Large Hadron Collider**
Nishita Desai, Dilip Kumar Ghosh, Biswarup Mukhopadhyaya
Phys. Rev. D 83, 113004 (2011) [arXiv:1104.3327]
4. **Constraints on supersymmetry with light third family from LHC data**
Nishita Desai, Biswarup Mukhopadhyaya
Preprint [arXiv:1111.2830] *Submitted to JHEP*

Other Publications

1. **Supersymmetry and Generic BSM Models in PYTHIA 8**
Nishita Desai and Peter Skands
Preprint [arXiv:1109.5852]

INTRODUCTION

CHAPTER

1

THE STANDARD MODEL AND BEYOND

“There are many hypotheses in science that are wrong. That’s perfectly alright; it’s the aperture to finding out what’s right. Science is a self-correcting process. To be accepted, new ideas must survive the most rigorous standards of evidence and scrutiny.”

– Carl Sagan, Cosmos

The full theoretical framework describing the fundamental constituents of the universe and their interactions is called the “Standard Model”. In the description of the micro-world, it refers to a gauge-theoretic description of the strong, weak and electromagnetic interactions of elementary particles. Complementarily, the Standard Model of Cosmology encapsulates the current knowledge of gravitational interactions (at a classical level) described by the General Theory of Relativity with the addition of a cosmological constant term. These two together represent the experimentally established pillars of current fundamental science. This thesis deals with the Standard Model of particle physics (hereafter referred to as the SM), its shortcomings, and some proposals of probing new physics beyond the SM.

Although the field of modern particle physics can be said to start with the discovery of the electron in 1897, the confirmation of the gauge-theoretical description came only

in 1983, with the discovery of the W and Z bosons at CERN ¹. The gauge sector of the SM consists of two massless bosons — the gluon (g) and the photon (γ), and two massive bosons — the W and Z . Besides the gauge sector of the SM, there is also a rich fermionic sector containing six leptons ($e, \mu, \tau, \nu_e, \nu_\mu, \nu_\tau$) and six quarks (d, u, s, c, b, t). All fermions are now known to be massive, with neutrino masses of the order of eV and the heaviest being the top quark with a mass of about 172 GeV. This completes the known particle spectrum of the SM. The massive gauge bosons W and Z are believed to get their mass due to the Higgs mechanism which would also imply the existence of a massive, neutral scalar boson, commonly called the Higgs boson (h) which is currently the focus of the Large Hadron Collider (LHC) experiment at CERN.

1.1 The Standard Model Lagrangian

Given the particle content of the SM, the various components of the Lagrangian can be written as

$$\mathcal{L} = \mathcal{L}_{\text{matter}} + \mathcal{L}_{\text{QCD}} + \mathcal{L}_{\text{gauge}} + \mathcal{L}_{\text{electro-weak}} + \mathcal{L}_{\text{Higgs}} + \mathcal{L}_{\text{Yukawa}} \quad (1.1)$$

where each term corresponds to a separate origin of the terms in the Lagrangian and will be explained below. The first term $\mathcal{L}_{\text{matter}}$ corresponds to the Dirac Lagrangian for all fermions. The neutrinos are a special case and we should note that the SM particle spectrum only contains massless, left-handed neutrinos.

$$\mathcal{L}_{\text{matter}} = \sum_{i=\text{fermions}} \bar{f}_i (i\gamma^\mu \partial_\mu - m_i) f_i \quad (1.2)$$

The first gauge group we consider is $SU(3)_c$. All the quarks are charged under colour and both left- and right-handed quarks have the same interaction strength. In the following expression, g_s is the coupling strength, G_μ^a are the gluons, t^a are the generators of $SU(3)_c$ and $G_{\mu\nu}^a$ is the field strength tensor.

$$\mathcal{L}_{\text{QCD}} = -\frac{1}{4} G_{\mu\nu}^a G^{a,\mu\nu} - g_s \sum_{i=d,u,s,c,b,t} \bar{q}_i \gamma^\mu t^a q_i G_\mu^a \quad (1.3)$$

The most complicated part of the SM is the weak sector. The gauge group is $SU(2)_L \times U(1)_Y$ which is broken spontaneously to the electromagnetic gauge group $U(1)_{\text{EM}}$. The particular complexity of the SM arises from this sector. Firstly, after the symmetry is broken spontaneously, the corresponding gauge bosons are massive.

¹The history of experimental confirmations of the SM can be found e.g. in [1].

The Higgs mechanism believed to be responsible for this phenomenon is outlined below. (Moreover, the same Higgs field that gives masses to the gauge bosons also gives masses to the chiral fermions.) Secondly, the subscript ‘L’ denotes the fact the only the left-handed fermions are charged under this SU(2) group. This leads to explicit parity violation in the standard model. The pure gauge-theoretic part of the SU(2)_L × U(1)_Y sector is given by:

$$\mathcal{L}_{\text{gauge}} = -\frac{1}{4}W_{\mu\nu}W^{\mu\nu} - \frac{1}{4}B_{\mu\nu}B^{\mu\nu} \quad (1.4)$$

We now give a brief outline of the Higgs mechanism which gives mass to the gauge bosons. We start with a complex SU(2) doublet scalar field with the gauge-invariant lagrangian given by

$$\mathcal{L}_{\text{Higgs}} = \frac{1}{2}D_{\mu}\phi^{\dagger}D^{\mu}\phi + \mu^2\phi^{\dagger}\phi - \lambda(\phi^{\dagger}\phi)^2 \quad (1.5)$$

Where the covariant derivative, $D_{\mu} = \partial_{\mu} - igW_{\mu}^i\tau^i - ig'B_{\mu}$.

The general field ϕ can be re-written as follows

$$\phi = \begin{pmatrix} \phi_1 + i\phi_2 \\ \phi_3 + i\phi_4 \end{pmatrix} = U(x)\frac{1}{\sqrt{2}}\begin{pmatrix} 0 \\ v + h(x) \end{pmatrix} \quad (1.6)$$

where $U(x)$ is a general SU(2) gauge transformation and v is the vacuum expectation value of the field ϕ obtained by minimising the potential. SU(2) being a 3-parameter group, the three degrees of freedom removed from the scalar doublet can be contained in $U(x)$. Thus, it is possible to work in a gauge, called the ‘unitary gauge’, where the only non-zero component of the higgs doublet corresponds to a neutral scalar field. Working in the unitary gauge and substituting the form of ϕ into $\mathcal{L}_{\text{Higgs}}$ gives us the mass eigenstates of the gauge bosons:

$$A_{\mu} = \frac{(g'W_{\mu}^3 + gB_{\mu})}{\sqrt{g^2 + g'^2}} \quad ; \quad Z_{\mu} = \frac{(gW_{\mu}^3 - g'B_{\mu})}{\sqrt{g^2 + g'^2}} \quad (1.7)$$

$$W_{\mu}^{\pm} = \frac{W^1 \pm iW^2}{\sqrt{2}} \quad (1.8)$$

The masses of W^{\pm} and Z are given by

$$m_W = g\frac{v}{2} \quad ; \quad m_Z = (\sqrt{g^2 + g'^2})\frac{v}{2} \quad (1.9)$$

whereas the photon is massless. The ratio $\sin \theta_W = \frac{g'}{\sqrt{g^2+g'^2}}$ defines the Weinberg mixing angle θ_W . In the unitary gauge, the full Higgs sector Lagrangian then becomes:

$$\begin{aligned} \mathcal{L}_{\text{Higgs}} = & \frac{1}{2} \partial_\mu h \partial^\mu h - \mu^2 h^2 - \lambda v h^3 - \frac{1}{4} \lambda h^4 \\ & + m_W^2 W_\mu^+ W^{-\mu} + m_Z^2 Z_\mu Z^\mu + m_W h W_\mu^+ W^{-\mu} + m_Z h Z_\mu Z^\mu \end{aligned} \quad (1.10)$$

The mass of the remaining degree of freedom of the scalar field (called the Higgs boson) is given by $m_h = \sqrt{2}\mu = \sqrt{2\lambda}v$.

As mentioned above, the masses of chiral fermions are also generated when the Higgs field gets a vacuum expectation value. The Higgs field is charged under $U(1)_Y$ with the charge $Y = \frac{1}{2}$ and therefore the $SU(2)_L \times U(1)_Y$ invariant couplings to fermions are

$$-\mathcal{L}_{\text{fermion-higgs}} = \sum_{i,j=\text{generations}} \lambda_{dij} \bar{Q}_{Li} \phi d_{Rj} + \lambda_{uij} \bar{Q}_{Li} (i\sigma_2 \phi^\dagger) u_{Rj} + \text{h.c.} \quad (1.11)$$

The second term (which eventually corresponds to a mass term for an up-type quark) contains the charge conjugate of the the higgs field. The basis in which the Higgs couplings are diagonal is called the mass basis of the fermions. The corresponding transformations are

$$u'_{Li} = (V_u)_{ij} \bar{u}_{Li}; \quad d'_{Li} = (V_d)_{ij} d_{Li} \quad (1.12)$$

The mass terms are generated when the higgs field acquires a vev with the mass of the fermion f given by $m_{fi} = \lambda_{fi}v$, where λ_{fi} is the eigenvalue corresponding to the fermion f . We must note that in the SM, the fermion sector differs from the quark sector in that there are no right handed neutrinos. Therefore, only the down-type term exists in the lepton sector of the SM.

The mass terms thus generated have been already written in $\mathcal{L}_{\text{matter}}$ as a part of the Dirac lagrangian. The couplings of the higgs boson to the fermions are given by:

$$\mathcal{L}_{\text{Yukawa}} = - \sum_{\text{fermions}} m_i \frac{h}{v} \bar{f}_i f_i + \text{h.c.} \quad (1.13)$$

It is possible to simultaneously diagonalise the Higgs couplings to the fermions and the strong gauge couplings to the fermions. However, the W boson couplings mix both up and down-type fermions which need not be simultaneously diagonalisable. The fact that they are not simultaneously diagonalisable leads to a mixing matrix in the quark sector, called the Cabbibo-Kobayashi-Masakawa (CKM) mixing matrix.

$$(V)_{ij} = (V_u^\dagger)_{ik} (V_d)_{kj} \quad (1.14)$$

The coupling of the fermions to the gauge bosons is then given by

$$\begin{aligned}
-\mathcal{L}_{\text{electro-weak}} &= \frac{g}{\sqrt{2}} \sum_{jk} \bar{Q}_j V_{jk} \gamma^\mu P_L (T^+ W_\mu^+ + T^- W_\mu^-) Q_k \\
&+ \frac{g}{\sqrt{2}} \sum_j \bar{L}_j \gamma^\mu P_L (T^+ W_\mu^+ + T^- W_\mu^-) L_j \\
&+ \frac{g}{2 \cos \theta_W} \sum_{i=\text{fermions}} \bar{f}_i \gamma^\mu (g_V^i - g_A^i \gamma_5) f_i Z_\mu \\
&+ e \sum_{i=\text{charged fermions}} q^i \bar{f}_i \gamma^\mu f_i A_\mu
\end{aligned} \tag{1.15}$$

The W^\pm bosons, which are components only of the $SU(2)_L$, interact only with left-handed fermions. This is assured by the projection operator P_L . T^\pm are the $SU(2)_L$ generators. The symbol Q refers to the quark doublet $(u_i \ d_i)^T$ whereas L is the lepton doublet $(\nu_i \ e_i)^T$ (all in the mass basis) and V is the CKM matrix defined above.

The Z boson contains both W^3 and B and therefore has couplings to both left- and right-handed fermions. The couplings are described in terms of the $SU(2)_L$ charge T^3 and the electric charge q as $g_V^i = (T_L^3)^i - 2q^i \sin^2 \theta_W$ and $g_A^i = (T_L^3)^i$. The couplings of the photon are left-right symmetric, as expected, and the coupling is the electric charge of the fermion. Since the transformation matrices for going from flavour to mass eigenstates cancel in Z -fermion-fermion couplings, there are no flavour changing neutral currents (FCNC) at tree-level in the SM. This fact has been verified experimentally to a high accuracy and can be used to restrict any models of new physics.

It should again be noted that right-handed neutrinos are not included in the SM spectrum and, even if present, would not interact with any SM fields since they would not carry any charge under SM gauge groups.

The higgs mechanism has another important consequence in improving the consistency of the SM. The scattering amplitudes for massive gauge bosons of the form $f\bar{f} \rightarrow W^+W^-$ are expected to diverge with the center-of mass-energy due to the presence of the longitudinal component, thus posing a problem of unitarity of the SM. However, since in the case of the Higgs mechanism, the longitudinal component comes from the absorption of the Goldstone boson degree of freedom, unitarity is restored. The renormalisability of spontaneously broken theories was also proved by 'tHooft and Veltman [2]. The SM with a light higgs boson is therefore a renormalisable, unitary gauge theory.

The theoretical basis of quantum field theory and the SM have been addressed in many books and review articles (see e.g. [3, 4]). The testing of the gauge structure of the SM was performed to a high accuracy at Large Electron Positron (LEP) collider. A partial summary of the experimental verification of the SM is presented in the next section.

1.2 Experimental confirmations

Although the experimental confirmation of the SM has by no means been a linear journey, we shall summarise the first proofs of the $SU(3)_C \times SU(2)_L \times U(1)_Y$ structure of the standard model. The experimental results discussed below are supplemented by measurements of masses of the particles, their decays and branching ratios, the mixing angles in the CKM matrix and the CP-violating phase. There have also been explicit measurements confirming the renormalisation-group running and accuracy of higher-order perturbative calculations which validate the quantum field theoretic description of the SM and are intimately connected with verification of the SM. However, we focus here on a few main results.

First, for the confirmation of QCD, we shall discuss (a) the observation of 3-jet events e^+e^- collisions events which proved the existence of the gluon and, (b) the measurement of the ratio of cross section for $e^+e^- \rightarrow \text{hadrons}$ to $e^+e^- \rightarrow \mu^+\mu^-$. Second, for the evidence of $SU(2)_L \times U(1)_Y$ structure, we describe (a) the measurement of triple gauge vertex at LEP and, (b) the forward-backward asymmetry due to Z bosons. Finally, we talk briefly about the indirect evidence for Higgs bosons and current status of the Higgs bosons searches.

1.2.1 QCD as an $SU(3)$ theory

The JADE Collaboration working on the PETRA e^+e^- collider published a paper [5] in 1980 with the following conclusion:

[T]opological distributions of hadrons show significant deviation from two-jet structure at high energies of $\sqrt{s} \simeq 30$ GeV. The deviation appears in the form of jet broadening and an excess of planar events. A model-independent analysis shows that planar events actually possess three-jet structure. Both the qualitative nature of these planar, three-jet events and the rate at which they occur are in good agreement with what is expected from the process $e^+e^- \rightarrow q\bar{q}g$.

The above paper refers to a study of events of the type $e^+e^- \rightarrow \text{multi-hadrons}$ to decipher the jet structure of the events. They tested the compatibility of the data with two different hypothesis. First, that the final states contained only $q\bar{q}$ events with the spread of jets given by phenomenological model of fragmentation. And, second, the QCD-based hypothesis that there would be certain events where the “fatter” jet can be thought of as comprised of two jets — one due to the quark and one due to a hard gluon radiated off the quark, i.e. $e^+e^- \rightarrow q\bar{q}g$ events. Since the total momentum of the three jets has to sum to zero by momentum conservation, the three jets must be coplanar. The analysis therefore consisted of selecting highly planar events and studying their distributions.

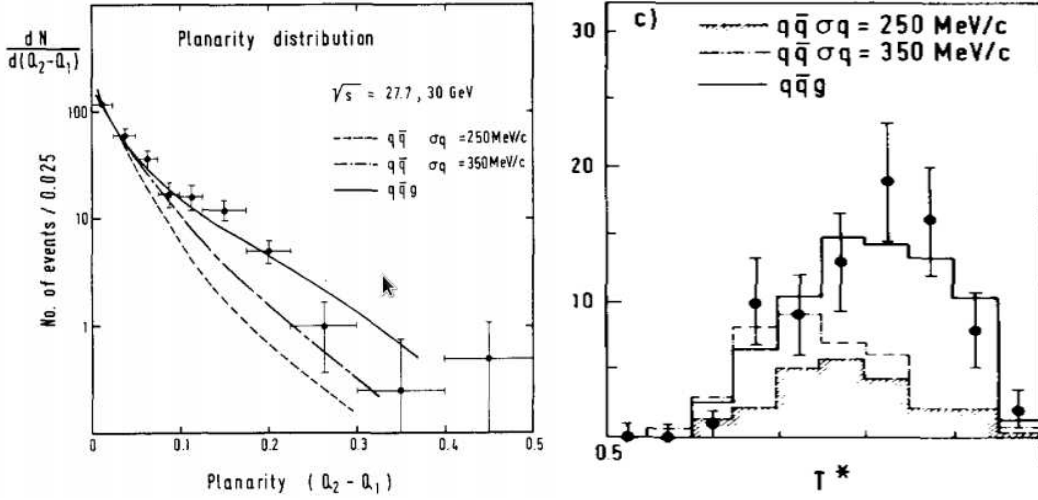


Figure 1.1: Results from the JADE Collaboration[5] comparing the distributions of (a) Planarity and (b) Thrust for events observed at $\sqrt{s} \simeq 27, 30$ GeV.

We first define the event shape variables used for the study. The normalised sphericity tensor is defined as

$$T_{\alpha\beta} = \frac{\sum_i P_{i\alpha} P_{i\beta}}{\sum_i P_i^2} \quad (1.16)$$

where P_i is the momentum of the i^{th} particle and the sum is over all particles in the event. This tensor is diagonalised and the three eigenvalues are denoted by Q_i where $Q_1 < Q_2 < Q_3$. Planarity is defined as $Q_2 - Q_1$ and coplanar events correspond to $Q_1 \ll Q_2$. The JADE analysis selects events with $Q_2 - Q_1 > 0.07$ (which corresponds to highly coplanar events) for which they observe 78 events as opposed to the 24 expected if only $q\bar{q}$ processes (no QCD hypothesis) were present.

A similar variable is the thrust T , defined by² the same study as

$$T = \max \left\{ \frac{\sum_i P_i \cdot \hat{n}}{\sum_i |P_i|} \right\} \quad (1.17)$$

where the direction \hat{n} is chosen to maximize T . The JADE study calculates the rest-frame thrust (denoted by T^*) for particles falling in the “fat” jet. The rest frame in question is calculated from the sum of the four momenta of all particles in the “fat” jet. Figure 1.1 shows the distribution of both, planarity and T^* . Both are found to agree with the $q\bar{q}g$ hypothesis.

Now that the existence of gluons was conclusively proven, it remained still to count the number of quarks, their flavours and colours. The number of colours in particular,

²This definition has since been generalised to multiple jet axes. See e.g. chapter 9 of [4].

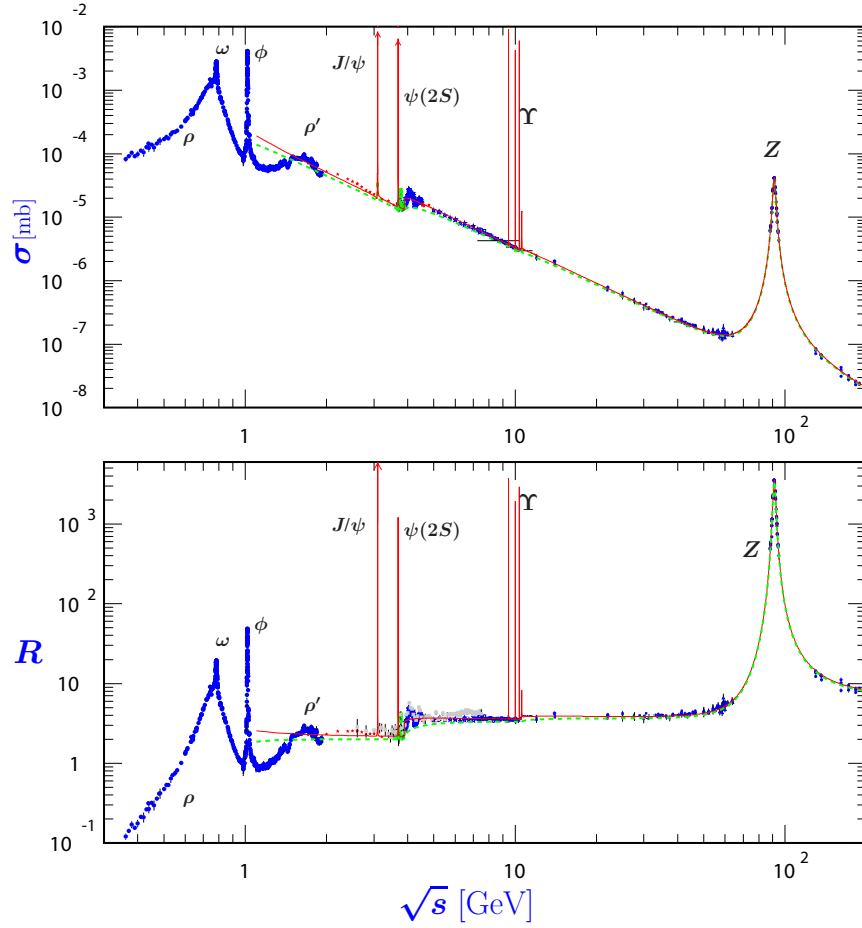


Figure 1.2: The lower panel gives a summary of measurements of R from various e^+e^- collider experiments with different center-of-mass energies. The dotted green line gives the naive estimate discussed in the text whereas the solid red line gives the prediction from 3-loop QCD calculations. Figure has been taken from the 2011 update of Review of Particle Physics[6].

would confirm the 3 in SU(3). This was done by measuring the ratio

$$R = \frac{\sigma(e^+e^- \rightarrow \text{hadrons})}{\sigma(e^+e^- \rightarrow \mu^+\mu^-)} \quad (1.18)$$

$$= N_c \sum_q e_q^2 \quad (1.19)$$

Since the diagrams leading to both $e^+e^- \rightarrow q\bar{q}$ and $e^+e^- \rightarrow \mu^+\mu^-$ are the same, we expect the functional form of the numerator and denominator to be identical. Therefore, it is only the charges of the quarks (e_q) and the number of colours they come in (N_c) that are different and the measurement of this ratio would be measuring both these quantities.

It must be noted that there can be extra contributions to both the numerator and denominator by $e^+e^- \rightarrow \tau^+\tau^-$ events. In the numerator, one would expect a contribution of the form $\sigma(e^+e^- \rightarrow \tau^+\tau^-) \times \text{BR}(\tau \rightarrow \nu_\tau \text{hadrons})^2$ whereas in the denominator we would have $\sigma(e^+e^- \rightarrow \tau^+\tau^-) \times \text{BR}(\tau \rightarrow \mu\bar{\nu}_\mu\nu_\tau)^2$. However, due to the square of the branching fractions involved, these contributions are much smaller than the dominant contributions. Moreover, due to the presence of a ν_τ in the final state, it may be possible to eliminate them further by demanding that no missing momentum be observed in the events.

The naive expectation for three flavours u , d and s and three colours (with quark charges assumed to be as suggested from hadron spectroscopy) is $R = 2$. This increases to $R = \frac{10}{3}$ when the center-of-mass of the collider exceeds twice the mass of the c quark and to $R = \frac{11}{3}$ when it exceeds twice the mass of the b quark. The actual measurements of R along with these simple predictions and predictions from 3-loop QCD calculations can be seen in Figure 1.2. Also seen in the bottom-right of the figure, is the resonant Z -pole. The Z boson comes from the electroweak sector of the SM, which we discuss in the next sub-section.

1.2.2 Proof of SU(2) \times U(1) structure

We now come to the verification of the electroweak gauge structure of the SM Lagrangian. First, we discuss the non-abelian nature of the SU(2) \times U(1) theory, which leads to triple gauge-boson vertices. In the SM, there are no triple neutral boson ($\gamma\gamma\gamma$, ZZZ , $\gamma\gamma Z$ and γZZ) vertices. The remaining couplings are of the form W^+W^-V (where $V = Z, \gamma$) and, along with possible anomalous couplings, can be parametrised by a generalised Lagrangian given as:

$$\begin{aligned} \mathcal{L} = & ig_{WWV} \left\{ g_{1V}(W_{\mu\nu}^+ W^{-\nu} - W_{\mu\nu}^- W^{+\nu})V + \kappa_V W_\mu^+ W_\nu^- V^{\mu\nu} \right. \\ & \left. + \frac{\lambda_V}{M_W^2} W_\mu^{+\nu} W_\nu^{-\rho} V_\rho^\mu \right\} \end{aligned} \quad (1.20)$$

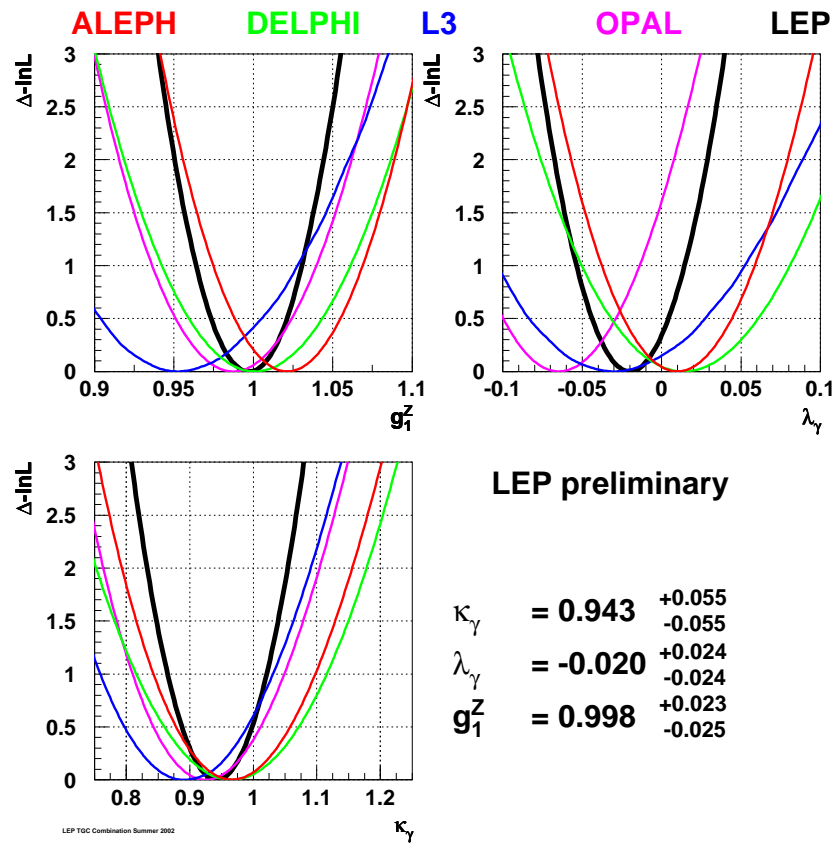


Figure 1.3: Best fit values for the triple gauge vertex parameters as measured by the four experiments of the LEP experiment. Figure taken from the analysis by the LEP Electroweak Working Group [7].

The coupling g_{WWV} corresponds to the tree-level SM coupling. The W^+W^-Z coupling is of particular importance here both because it confirms the non-abelian nature of the gauge theory and because it is responsible for regularisation of the divergence in $e^+e^- \rightarrow W^+W^-$ cross section (when the masses of the gauge bosons are assumed to be derived from the Higgs mechanism).

The measurement of the couplings g_{1V} , κ_V and λ_V was first done at LEP [7] and then updated at the Tevatron. For a recent review of the status of the EW precision constraints, see e.g. [8]. The SM tree level values correspond to $g_1^Z = \kappa_Z = \kappa_\gamma = 1$ and $\lambda_Z = \lambda_\gamma = 0$. The status of the measurement from LEP can be seen from Figure 1.3. As can be seen from this, all measured values are consistent with the SM within the errors.

Another consequence of the EW sector is the presence of a ‘‘forward-backward asymmetry’’ in $f\bar{f} \rightarrow f'f'$ events. As can be seen from the electroweak lagrangian describing the coupling of the Z boson to the fermions (equation 1.15), the couplings are not symmetric for left- and right-handed particles. The consequence of this is that a forward-backward asymmetry (A_{FB}) can be observed in events of the type $f\bar{f} \rightarrow f'f'$ due to the addition of Z -mediated diagrams and their interference with γ -mediated diagrams. If θ is the angle made by the final state fermion with the z -axis, the asymmetry A_{FB} is generally defined as

$$A_{FB} = \frac{\sigma(\cos\theta > 0) - \sigma(\cos\theta < 0)}{\sigma(\cos\theta > 0) + \sigma(\cos\theta < 0)} \quad (1.21)$$

The expressions $\sigma(\cos\theta > 0)$ and $\sigma(\cos\theta < 0)$ refer to the cross sections integrated over the corresponding values of θ . The measurement of the forward-backward asymmetry requires an unambiguous z -axis and therefore can be done reliably either at e^+e^- or $p\bar{p}$ colliders, where one of the beam directions can be designated as the z -axis³. Similar measurements are harder at a symmetric collider like the LHC because of the absence of an unambiguous z -axis. The values of A_{FB} measured at the Z -pole for all the fermions can be found in the Review of Particle Physics [6].

1.2.3 Evidence for Higgs

The ratio of the masses of the W and Z bosons serve as a crucial pointer to the true mechanism for the spontaneous breaking of the $SU(2) \times U(1)$. The value of the ρ -parameter, defined as

$$\rho = \frac{M_W^2}{M_Z^2 \cos^2 \theta_W} = 1 \text{ (for SM)} \quad (1.22)$$

³As we shall see in the next section, the Tevatron $t\bar{t}$ forward-backward asymmetry is one of the indications of new physics we currently have

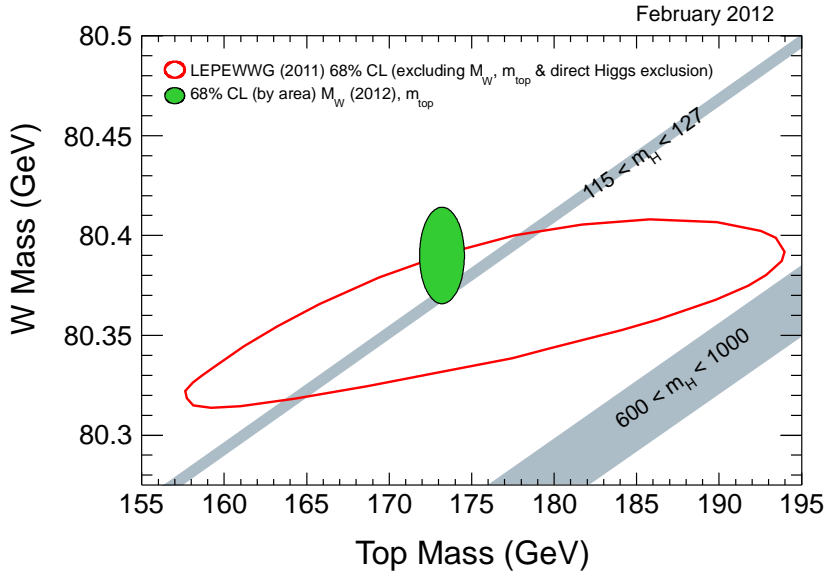


Figure 1.4: Current bound on Higgs mass from the LEP EW working group with updated W mass measurement from CDF [9, 10].

is a consequence of the doublet nature of the Higgs in the SM. The independent measurements of W and Z masses at LEP and the weak mixing angle $\sin\theta_W$ at NuTeV results in a value of ρ compatible with the SM and is a strong indirect evidence in favour of the doublet Higgs.

The coupling of the Higgs to a SM particle is proportional to its masses. Moreover, it is possible to calculate the Higgs contributions to radiative corrections to the mass of each particle in the SM. Therefore, we can check the consistency of a given Higgs mass hypothesis with observed masses for heavy particles. The consistency of the Higgs mass in the range $115 < M_H < 127$ GeV with the latest measurement of the masses of the W boson[9] and the mass of the top quark [6] can be seen from Figure 1.4. The band $115 < M_H < 127$ GeV corresponds to allowed mass region for a SM Higgs as of writing this thesis [11, 12]. The direct search for the Higgs has progressed considerably at the two experiments at the LHC, viz. ATLAS and CMS. (The details of LHC and its experiments will be discussed in section 1.4.) Both experiments see an excess in the $h \rightarrow \gamma\gamma$ decay channel at $M_H \simeq 125$ GeV [13, 12] with a local significance of about 3σ .

1.3 Shortcomings of the SM

As discussed above, the SM has been incredibly successful in predicting measured quantities and the search for the Higgs boson is ongoing with promising signals. However,

there are some observational discrepancies and theoretical dissatisfactions that hint at some new physics beyond the SM. We summarise the some of these below.

1.3.1 Anomalous magnetic moment of the muon $(g - 2)_\mu$

The measurement of anomalous magnetic moment of the muon is one of the strongest indicators of disagreement of data with the SM. If the electromagnetic vertex is given by

$$(-ie)\bar{u}(p') \left[\gamma^\alpha F_1(q^2) + i \frac{\sigma^{\alpha\beta} q_\beta}{2m_\mu} F_2(q^2) \right] u(p) \quad (1.23)$$

then, the anomalous magnetic moment $a_\mu = F_2(0)$. The current values from theory and experiment are[14, 15]:

$$a_\mu^{\text{Exp.}} = 1.16592080(63) \times 10^{-3}; \quad a_\mu^{\text{Theory}} = 1.16591790(65) \times 10^{-3} \quad (1.24)$$

The resultant discrepancy is $\delta a_\mu = (290 \pm 90) \times 10^{-11}$ which corresponds to 3.2σ deviation.

1.3.2 Neutrino masses and mixing

The SM particle spectrum contains three left-handed, massless neutrinos. The neutrino was first postulated to explain the apparent missing momentum in measurements of beta-decay. However, the direct detection of neutrinos is extremely difficult due to their very feeble interaction with matter through weak boson exchange. The first evidence of a neutrino anomaly was measured from the solar neutrino rate in 1968 with a possible explanation in terms of oscillation of electron neutrinos to other flavours. Since then, there has been enormous progress both in theory and experiment for explaining the origin of neutrino masses as well as oscillations. For a review, see e.g.[16]. More recently, there have been measurements of a non-zero value of the neutrino mixing angle θ_{13} [17, 18]. The recent results are summarised in Table 1.1. Since the explanation of neutrino mass needs either the addition of more fundamental fields or lepton-number violating interactions, these measurements are a clear indication of physics beyond the SM.

| | |
|----------------------------|---|
| Solar mass splitting | $\Delta m_{12}^2 = (7.58 \pm 0.21)10^{-5}\text{eV}^2$ |
| Atmospheric mass splitting | $ \Delta m_{23} ^2 = (2.40 \pm 0.15)10^{-3}\text{eV}^2$ |
| Solar Mixing angle | $\tan^2 \theta_{12} = 0.484 \pm 0.048$ |
| Atmospheric mixing angle | $\sin^2 2\theta_{23} = 1.02 \pm 0.04$ |
| θ_{13} mixing angle | $\sin^2 2\theta_{13} = 0.092 \pm 0.017$ |

Table 1.1: Summary of central values for neutrino masses and mixing parameters.

1.3.3 Dark Matter, Dark energy and Baryon asymmetry in the Universe

The first evidence for Dark Matter (DM) came from the measurement of the rotation curves of galaxies in the 1930's. The rotation curves were found to be inconsistent with the amount of matter visible in the galaxy [19]. The curves were found to fit better with the hypothesis that the visible part of the galaxy was immersed in a halo of invisible matter. The presence of large amounts of such dark matter in the universe has now also been confirmed by photographs taken by high power telescopes that show gravitational lensing disproportionate to the amount of visible matter [20]. The observations from Cosmic Microwave Background radiation currently set the value of the DM abundance to $h^2\Omega_{DM} = 0.1123 \pm 0.0035$ [21]. For a recent review of the status of indirect DM determination experiments, see e.g. [22].

There is no SM particle that can be considered a candidate for DM. It cannot be strongly charged — both because such a candidate could not satisfy the relic density conditions and because a strongly charged particle would be required to form colour singlet bound states which would be observable by their transition spectra. A similar argument applies if it is electrically charged, it would again likely form bound states like atoms which would again be observable by its spectral lines. It therefore has to be both electrically and colour neutral and the only possible interactions such a particle might have is via the weak force. Going to the other extreme, one may postulate candidates that are uncharged even under the weak force. However, such a component could not thermalise and therefore does not agree with current observations.

The largest component of the universe is the so called “Dark Energy” [21] which can be modelled as a cosmological constant term in the Einstein equation. However, we do not at the present have any explanation for the origin of such a term.

Finally, Baryon asymmetry of the universe refers to the observation that almost the entire baryonic component of the Universe is matter and not anti-matter. For this to be explained, there would need to be a large CP violating interaction. Currently, the only source of CP violation in the SM is the phase in the CKM mixing matrix and has been found insufficient to explain the observed baryon asymmetry.

1.3.4 Higgs mass stabilisation

As is well known, a tree-level calculation is only the simplest approximation of the full matrix element. Consistent inclusion of higher order terms leads to radiative corrections that modify the couplings and masses via the renormalisation procedure. Any quadratic corrections to the mass cancel for the gauge bosons due to the gauge symmetry and for fermions due to chiral symmetry, leaving only a weak, logarithmic dependence. However, the Higgs, being a scalar, does not have any such safeguards and its mass would naturally be driven to the scale of new physics (or the cutoff where the SM no longer

remains the fundamental theory). Requiring the Higgs mass to be small is equivalent to demanding a very fine cancellation between the loop contributions and this is referred to as the problem of “fine-tuning” or the problem of Higgs mass stabilisation. It must also be stated that the absence of fine-tuning is not a consistency requirement, but based on the un-naturalness of such a fine cancellation when there is no symmetry that requires it.

The dominant corrections to the Higgs mass come from top loops. Therefore, models with scalar top partners (like Supersymmetry) can alleviate the problem since the loop contributions from these new particles will cancel contributions from the top loop. Alternately, the Higgs need not be a fundamental scalar, but can be a composite particle (e.g. in theories of Technicolour, Little Higgs etc.)

1.3.5 The flavour problem

The flavour problem refers to the unexplained structure of the fermionic sector of the SM. We have six flavours of quarks, each with a different mass and similarly six flavours of leptons. The masses of the SM fermions range from sub-eV for neutrinos to over hundred GeV for the top quark. There is no fundamental explanation for this large hierarchy in mass. The fermions also come in three “generations”, with higher generations having a higher masses.

The mixing in the quark sector is given by the CKM matrix which can be thought of as a unitary matrix parametrised by three angles and one phase. The mixing also shows a generational structure, i.e. the largest mixing is between the generations one and two, followed by mixing of two and three and finally the mixing between one and three.

Despite having this empirical data regarding the fermionic sector, there is no theory that explains the pattern. Since there are no consistency requirements that demand a more fundamental explanation of this pattern, it is again, an aesthetic question.

1.4 The Large Hadron Collider

In the previous section, we discussed some indications of anomalous behaviour — both experimental and theoretical, that require explanations from physics beyond the Standard Model (BSM). Many experiments around the world are probing the various questions outlined above. The discovery of new particles has been the domain of collision experiments. The latest of these are the Large Electron-Positron (LEP) collider which ran from 1989–2000 and the Tevatron which ran from 1983–2011. The LEP was an e^+e^- collider which probed the gauge structure to very high accuracy. It also searched for the SM Higgs boson and, at the end of its run put a limit of $M_h > 114$ GeV on its mass [23]. The Tevatron discovered the top quark in 1994 [24] and was the first to observe single top production [25, 26]. Both these experiments have looked for signatures of BSM physics and have placed limits on masses of new particles in various scenarios.

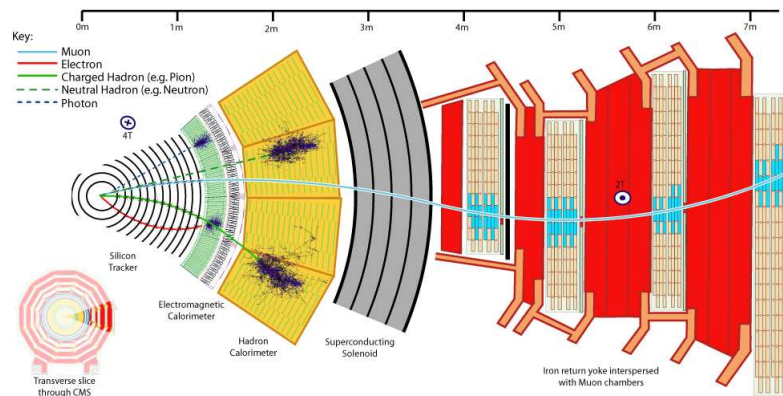


Figure 1.5: A schematic slice of the CMS detector. (Image by CMS Collaboration).

The LHC began operation at a center of mass energy of 7 TeV in 2010, becoming the highest energy accelerator to date and collected 5 fb^{-1} data till December 2011. As of writing this thesis, collision at 8 TeV have just begun. Four main experiments – ATLAS, CMS, ALICE and LHCb, are stationed at collision points along the LHC ring. Of these, ATLAS (which stands for A Toroidal LHC Apparatus) and CMS (which stands for Compact Muon Solenoid) are general purpose detectors for detecting signatures of the Higgs and any new physics signals. ALICE (which stands for A Large Ion Collider Experiment) is specialised for observing quark-gluon plasma. And finally, LHCb is an experiment specialising in physics of the b-hadrons. Since this thesis deals with searches for new physics and therefore needs to address the detectability of the proposed signals at actual experiments, we shall now describe the general features of detectors like ATLAS and CMS.

1.4.1 Detection of particles

Both ATLAS and CMS have four main sub-components — the tracker, the electromagnetic calorimeter, the hadronic calorimeter and the muon chambers. The components form concentric cylinders as is schematically illustrated in Figure 1.5. The collision occurs at the center of this assembly and each component performs measurements as the particles travel through it and interact with its material. The whole assembly is placed in a magnetic field which curves the tracks of the charged particles and thus provides a way of measuring their momentum.

The innermost detector sub-system is the tracker, which is finely grained enough to be able to reconstruct the tracks of charged particles. The electromagnetic calorimeter stops electrons and photons and measures the energy they deposit. The hadronic calorimeter measures the energy carried by hadrons (e.g. pions, protons and neutrons).

The muons escape the entire detector and their presence is inferred from the hits along its path in the muon chamber. The full technical specifications of the two detectors can be found in the official Technical Design Reports for both ATLAS [27] and CMS [28, 29].

The analyses in this thesis use Monte-Carlo event generators to simulate events at the LHC. Since the prediction of event rates and analysis variables depends crucially on the ability to detect particles, the analyses use some simple criteria to ensure a reasonable simulation of detection efficiency. These include cuts on momentum and rapidity of the particle. Besides this, we take care to apply cuts like lepton isolation which are crucial in a hadron collider environment. To further simulate the errors in the measurement of energy (or momentum) of the detected objects, we use a Gaussian smearing procedure. The exact acceptance cuts will be detailed in each of the analyses.

1.4.2 Physics goals of the LHC

The Large Hadron Collider will test the SM at very high energies and to look for any deviations from the its predictions. As has been mentioned before, its most important goal will be to determine the nature of electroweak symmetry breaking. Besides this, the LHC experiments will search for signatures from various theories of physics beyond the SM which have been postulated as solutions for the outstanding problems described in section 1.3.

Determining the mechanism of EWSB

The primary goal of the LHC to to probe the mechanism of spontaneous electroweak symmetry breaking. That we have a spontaneously broken $SU(2) \times U(1)$ theory has been verified to a very high accuracy at LEP. However, the mechanism of breaking has not been conclusively proven. If indeed, it is via the Higgs mechanism, we would expect to detect signatures of a Higgs boson. If the LHC does discover a resonance that might be a Higgs candidate, we need to determine the nature of its couplings to the gauge bosons to conclusive claim that it is the SM Higgs. We address the determination of the nature of the HWW coupling at the LHC in Chapter 6. It is also possible that the Higgs sector is not minimal (i.e. a single Higgs doublet) but has multiple Higgses. The Higgs production and decays depend crucially on this and therefore the measurement of these would be the first step in determining the nature of the Higgs sector.

In the absence of the Higgs mechanism, the SM becomes an effective theory which will be superseded by a more fundamental theory at the high scale. In this case, we would expect signatures of unitarity violating behaviour in WW scattering events.

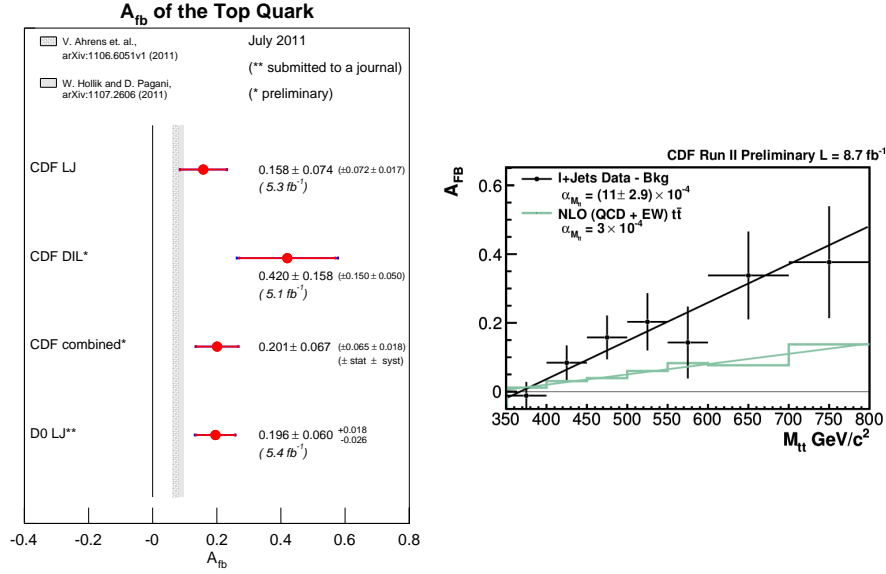


Figure 1.6: (Left) Summary of the $t\bar{t}$ asymmetry measured by CDF and DØ experiments and (right) the dependence of the asymmetry on the invariant mass of the $t\bar{t}$ pair ($M_{t\bar{t}}$).

Top physics

The large center-of-mass energy of the LHC enhances the $t\bar{t}$ production cross section by several orders of magnitude as compared to the Tevatron. The LHC therefore is uniquely placed to probe top physics in detail. The top quark is the only quark that decays before it hadronises and therefore its polarisation information is preserved in the angular distribution of its decay products. The top quark is also particularly interesting because its mass is so close to the EWSB scale and therefore it provides a hitherto unavailable probe for contributions of new physics that may be present at that scale.

The $t\bar{t}$ asymmetry

The Tevatron is a $p\bar{p}$ collider at Fermilab that has just finished its physics run in 2011. The production of $t\bar{t}$ at the Tevatron is dominated by strong production process $q\bar{q} \rightarrow t\bar{t}$. Therefore, the expected forward-backward asymmetry comes, not from the Z -mediated diagrams, but from the interference between the tree-level and one-loop diagrams and the expected value is very small. The CDF analysis defines the $t\bar{t}$ forward-backward asymmetry by

$$A_{FB} = \frac{\sigma(\Delta y > 0) - \sigma(\Delta y < 0)}{\sigma(\Delta y > 0) + \sigma(\Delta y < 0)} \quad (1.25)$$

where Δy is the difference of the rapidities of t and \bar{t} . Both experiments, CDF and DØ, measure a value of the inclusive asymmetry incompatible with the SM prediction [30, 31]. The summary of the latest measurements as well as the latest theoretical predictions [32, 33] can be seen from Figure 1.6. Another intriguing feature of the measured asymmetry is that it seems to increase with the invariant mass of the $t\bar{t}$ pair and therefore hints at some massive particle as its cause.

The added complexity in finding a satisfactory explanation for this anomaly, is that the measured total $t\bar{t}$ cross section ($\sigma_{t\bar{t}}^{\text{Obs.}} = 7.50 \pm 0.48$ pb for $M_t = 172.5$ GeV) [34] is in excellent agreement with the expected SM value ($\sigma_{t\bar{t}}^{\text{Theo.}} = 7.46_{-0.80}^{+0.66}$ pb) [35]. Therefore, even if the asymmetry is caused by some new physics contribution, it cannot contribute significantly to the total production cross section.

This measurement is doubly complicated at the LHC. First, since it is a symmetric collider, there is no natural z -direction around which the asymmetry can be measured. Secondly, $t\bar{t}$ production at the LHC is dominated by gluon-fusion (as opposed to quark-antiquark fusion at the Tevatron) which washes out the asymmetry. The measurement therefore is much more complicated at the LHC.

Signals of any new physics

Besides probing the mechanism of EWSB and top physics, the LHC also performs generic searches for new physics. This includes e.g. the search for compositeness in quarks, searches for lepto-quarks, extra gauge bosons and resonances in various final states etc. Some popular theoretical models (or classes of models) of new physics include Supersymmetry, Extra dimensional models, models of Technicolour etc. Each of these add many new particles to the SM spectrum and have been studied extensively. A large part of the work in this thesis (chapters 3-5) deals with the theory of Supersymmetry, or more accurately, the phenomenological models of the minimal supersymmetric extension of the SM. We shall discuss this in more detail in the next chapter.

CHAPTER

2

SUPERSYMMETRY

“Symmetry is a complexity-reducing concept [...]; seek it everywhere.

Alan Perlis

The Large Hadron Collider (LHC) at CERN is now running at an energy of $\sqrt{s} = 7$ TeV and the two experiments ATLAS and CMS are hard at work in constraining theories beyond standard model (BSM). Supersymmetry (SUSY) [36, 37] has long been one of the most popular BSM models, due to its ability to solve the hierarchy problem and to provide a dark matter candidate (in its R-parity conserving versions). In this chapter, we give a brief introduction to SUSY and its phenomenological consequences.

In 1967, Coleman and Mandula proved [38] that, demanding certain reasonable properties of scattering amplitudes restricts non-trivial mixing between space-time and internal symmetries. The extension to this theorem by Haag et. al. [39] showed that it is possible to add a fermionic (anti-commuting) symmetry that mixes with space-time symmetries but still satisfies all reasonable requirements. This kind of symmetry came to be called a “supersymmetry.”

The addition of fermionic symmetries requires the extension of normal space-time to include fermionic co-ordinates, thus forming a “superspace”. The fields defined on this superspace are called superfields. If one Taylor-expands these in terms of the fermionic co-ordinates, the anti-commuting nature the co-ordinates ensures that the highest term is at most linear with the coefficient of each power of the fermionic co-ordinate being a field in space-time (a component field of the superfield). Moreover, to maintain the

transformation properties of the superfield, the component fields are required to have spins that differ by a half.

The extension of the symmetries of the SM by adding supersymmetric generators requires that we replace each SM field by a superfield. This then naturally implies the presence of another component of the superfield that differs in spin from the SM field but has the same gauge quantum numbers, i.e. a ‘‘superpartner.’’ The work in this thesis deals with the phenomenological consequences of the minimal supersymmetric extension of the SM (MSSM) which is obtained by adding a single pair of SUSY generators to the SM. We outline here, the construction of the MSSM Lagrangian, its particle spectrum and some phenomenological parameterisations of it. For detailed reviews of the MSSM, see e.g. [40, 41].

2.1 The Minimal Supersymmetric Standard Model

In this section, we briefly outline the SUSY algebra, the properties of the superfields and the method of constructing a supersymmetric Lagrangian.

2.1.1 The SUSY algebra and superfields

The Supersymmetry algebra in the case of a minimal extension contains four momentum operators P_μ and two SUSY generators Q_α and $\bar{Q}_{\dot{\alpha}}$ and is then given by

$$\begin{aligned} [Q_\alpha, P_\mu] &= [\bar{Q}_{\dot{\alpha}}, P_\mu] = [P_\mu, P_\nu] = 0 \\ \{Q_\alpha, Q_\beta\} &= \{\bar{Q}_{\dot{\alpha}}, \bar{Q}_{\dot{\beta}}\} = 0 \\ \{Q_\alpha, \bar{Q}_{\dot{\beta}}\} &= 2\sigma^\mu_{\alpha\dot{\beta}} P_\mu \end{aligned} \quad (2.1)$$

Since the SUSY generators commute with P_μ , the mass of the particles $P_\mu P^\mu = m^2$ remains invariant under SUSY transformations.

The superspace is parametrised by the space-time co-ordinate x^μ and two spinor co-ordinates θ_α and $\bar{\theta}_{\dot{\alpha}}$. The dotted and un-dotted indices refer to the $SU(2)$ representation of the spinor. A general SUSY transformation with parameters $(a^\mu, \xi, \bar{\xi})$ acting on the co-ordinates $(x^\mu, \theta, \bar{\theta})$ corresponds to the following transformation.

$$\begin{aligned} x^\mu &\rightarrow x^\mu + a^\mu - i\xi\sigma^\mu\bar{\theta} + i\theta\sigma^\mu\bar{\xi} \\ \theta &\rightarrow \theta + \xi, \quad \bar{\theta} \rightarrow \bar{\theta} + \bar{\xi} \end{aligned} \quad (2.2)$$

The transformation of a superfield with parameters $(x^\mu, \theta, \bar{\theta})$ under a general SUSY transformation $G(a^\mu, \xi, \bar{\xi})$ is given by

$$S(x^\mu, \theta, \bar{\theta}) \rightarrow \exp\{i(\xi Q + \bar{\xi}\bar{Q} - a^\mu P_\mu)\}S(x^\mu, \theta, \bar{\theta}) \quad (2.3)$$

where the generators are

$$\begin{aligned}
P_\mu &= i\partial_\mu \\
Q_\alpha &= \frac{\partial}{\partial\theta^\alpha} - i\sigma_{\alpha\dot{\beta}}^\mu \bar{\theta}^{\dot{\beta}} \partial_\mu \\
\bar{Q}_{\dot{\alpha}} &= -\frac{\partial}{\partial\theta^{\dot{\alpha}}} + i\theta^\beta \sigma_{\beta\dot{\alpha}}^\mu \partial_\mu
\end{aligned} \tag{2.4}$$

The SUSY-covariant derivatives can be written as

$$\begin{aligned}
D_\alpha &= \frac{\partial}{\partial\theta^\alpha} + i\sigma_{\alpha\dot{\beta}}^\mu \bar{\theta}^{\dot{\beta}} \partial_\mu \\
\bar{D}_{\dot{\alpha}} &= -\frac{\partial}{\partial\theta^{\dot{\alpha}}} - i\theta^\beta \sigma_{\beta\dot{\alpha}}^\mu \partial_\mu
\end{aligned} \tag{2.5}$$

The superfields corresponding to left and right handed fermions are called left or right chiral superfields respectively, and are defined by

$$\bar{D}_L \Phi_L = 0, \quad D_R \Phi_R = 0 \tag{2.6}$$

where

$$(D_L)_\alpha = \frac{\partial}{\partial\theta^\alpha} + 2i\sigma_{\alpha\dot{\beta}}^\mu \bar{\theta}^{\dot{\beta}} \partial_\mu; \quad (\bar{D}_L)_{\dot{\alpha}} = -\frac{\partial}{\partial\theta^{\dot{\alpha}}} \tag{2.7}$$

$$(\bar{D}_R)_{\dot{\alpha}} = \frac{\partial}{\partial\theta^{\dot{\alpha}}} - 2i\sigma_{\alpha\dot{\beta}}^\mu \bar{\theta}^{\dot{\beta}} \partial_\mu; \quad (D_R)_\alpha = \frac{\partial}{\partial\theta^\alpha} \tag{2.8}$$

In this representation, the left-chiral superfield is independent of $\bar{\theta}$ whereas the right-chiral superfield is independent of θ . In the component notation, a left-chiral superfield can be written as

$$\Phi_L = \phi(x) + \sqrt{2}\theta^\alpha \psi_\alpha(x) + \theta^\alpha \theta^\beta \epsilon_{\alpha\beta} F(x) \tag{2.9}$$

The component $\phi(x)$ is a scalar field with a mass dimension of 1 and $\psi(x)$ is a fermionic field with mass dimension of 3/2. The last component $F(x)$ is an auxiliary field with mass dimension of 2.

The left and right handed fermions of the SM transform differently under $SU(2) \times U(1)$. Therefore, by using one chiral superfield corresponding to each fermionic field in the SM, we can elegantly extend the SM to its SUSY counterpart. In the component form, this corresponds to having a fermion (ψ) and its partner, the sfermion (ϕ).

We also define chiral superfields for each fundamental Higgs fields. In this case, it is the scalar part that is the Higgs and the extra fermionic degrees of freedom are called Higgsinos.

The final ingredient that would allow us to write the supersymmetric version of the SM is the SUSY equivalent of a vector field and its gauge transformation. The corresponding superfield is called a “vector superfield” which satisfies the self-conjugacy condition

$$V^\dagger(x^\mu, \theta, \bar{\theta}) = V(x^\mu, \theta, \bar{\theta}) \quad (2.10)$$

In the Wess-Zumino gauge, the expansion of the vector superfield in component notation is

$$V = i\theta\theta\bar{\theta}\bar{\lambda}(x) - i\bar{\theta}\bar{\theta}\theta\lambda(x) - \theta\sigma^\mu\bar{\theta}A_\mu(x) + \frac{1}{2}\theta\theta\bar{\theta}\bar{\theta}D(x) \quad (2.11)$$

where, A_μ is the gauge field (of mass dimension 1), λ is its superpartner — the gaugino (with mass dimension 3/2), and D is an auxiliary field (with mass dimension 2) that does not have any dynamics.

2.1.2 Constructing the Lagrangian

To construct the Lagrangian, we need to write all gauge-invariant terms with mass dimension four. The kinetic terms for the scalar and fermion fields come from terms of the form $\int d^2\theta d^2\bar{\theta}\Phi^\dagger\Phi$. In the SM Lagrangian, the fermion couplings to gauge bosons and the fermion kinetic terms can be obtained by replacing the standard derivative ∂_μ by the gauge-covariant derivative $D_\mu = \partial_\mu + igT^a A_\mu^a$. Similarly, the terms in the Lagrangian corresponding to the kinetic terms and gauge-interactions of fermions and scalars in the matter supermultiplet can be obtained from

$$\mathcal{L}_1 = \int d^2\theta d^2\bar{\theta}\Phi^\dagger e^{2gV}\Phi \quad (2.12)$$

This term contains the kinetic energy terms for fermions and sfermions, and the interactions of these with the gauge field and gauginos (fermion-fermion-gauge, sfermion-sfermion-gauge, and fermion-sfermion-gaugino).

All possible terms involving the interactions of chiral fermions can be written down in a convenient way in terms of a quantity called the superpotential which is defined as

$$\mathcal{W} = \sum_i k_i \Phi_i + \sum_{ij} m_{ij} \Phi_i \Phi_j + \sum_{ijk} g_{ijk} \Phi_i \Phi_j \Phi_k \quad (2.13)$$

which is a holomorphic function of the chiral superfields. The mass and Yukawa terms obtained from

$$\mathcal{L}_2 = \int d^2\theta \frac{\partial^2 \mathcal{W}}{\partial \phi_i \partial \phi_j} \psi_i \psi_j + \text{h.c.} \quad (2.14)$$

The gauge part of the Lagrangian is written in terms of the superfield W_α defined as

$$W_\alpha = \bar{D}_{\dot{\alpha}} \bar{D}_{\dot{\beta}} \epsilon^{\dot{\alpha}\dot{\beta}} D_\alpha V \quad (2.15)$$

The kinetic terms for the gauge fields and the gauginos along the interaction terms between them are obtained from

$$\mathcal{L}_3 = \int d^2\theta \frac{1}{32} W_\alpha W^\alpha \quad (2.16)$$

This expression also contains the term $D_a D^a$ which does not have any dynamical behaviour, as expected from an auxiliary field. After using the equations of motion for the F and D fields, the scalar potential is given by

$$V = F_i F_i^* + \frac{1}{2} D^a D^a = \left| \frac{\partial \mathcal{W}}{\partial \phi_i} \right|^2 + \frac{1}{2} \sum_a g_a \sum_{ij} (\phi_i^* (T^a)_{ij} \phi_j) \quad (2.17)$$

where the sum over a implies a sum over all generators of all gauge groups in question. The F -terms also ensure that the four-vertex containing scalars has the same Yukawa coupling as the corresponding fermion, thus ensuring the cancellation of divergences from the fermion loop by the divergences from the sfermion loop.

We can now enumerate the superfields required for the MSSM. The left-handed superfields containing quarks and their scalar partner squarks are called Q_i , those containing leptons (and sleptons) are called L_i (i runs over generations); and both are doublets under $SU(2)$. The corresponding right-handed chiral superfields are called U_i , D_i (for those containing up and down quarks respectively) and E_i for those containing the right handed charged lepton. Similar to the SM, there is no right-handed neutrino superfield. The gauge bosons (and the corresponding gauginos) are contained within the vector fields G for the gluon and gluino, W for the W-bosons and the Winos, and B for the B-boson and the Bino.

We start by writing down the MSSM superpotential which gives the Yukawa terms, SM fermion masses and Higgsino masses. Since the Higgsinos are chiral fermions charged under $U(1)_Y$, they contribute to the chiral anomaly. We therefore need two Higgs fields with opposite $U(1)_Y$ charges to maintain the consistency of the theory. This also ensures that masses for both up and down type quarks can be derived from the superpotential. The MSSM superpotential is given by

$$\mathcal{W}_{\text{MSSM}} = (\lambda_U)^{ij} Q_i U_j^c H_u + (\lambda_D)^{ij} Q_i D_j^c H_d + (\lambda_E)^{ij} L_i E_j^c H_u + \mu H_u H_d \quad (2.18)$$

Here, Q_i is the $SU(2)_L$ doublet quark superfield, L_i is the $SU(2)_L$ doublet lepton superfield, U_i and D_i are right handed quark superfields, E_i is the right handed superfield for charged leptons and H_u and H_d are Higgs superfields.

In principle, one can also add lepton and baryon-number violating terms to this superpotential. To avoid this, an extra parity, called R-parity, is defined as $R = (-1)^{3B-L+2S}$. However since they are not forbidden by gauge invariance, it is possible to study the effect of adding these extra terms to the superpotential. The R-parity violating terms are:

$$\mathcal{W}_{RPV} = \mu_i L_i H_u + \lambda_{ijk} L_i L_j E_k^c + \lambda'_{ijk} L_i Q_j D_k^c + \lambda''_{ijk} U_i^c D_j^c D_k^c \quad (2.19)$$

From the definition of R-parity, all SM fields are even under it while all superpartners are odd. The demand of R-parity invariance, therefore, has two consequences — first, the superpartners are always produced in pairs, and second, the lightest SUSY particle (LSP) is stable. We discuss a particular case of R-parity violation via the λ'' -type term in Chapter 5.

2.2 SUSY breaking and the sparticle spectrum

The presence of SUSY naturally implies the same mass for superpartners. Since we have not yet observed the superpartners of any of the SM particles, SUSY must obviously be broken. Since one of the prime motivations of SUSY is to restore the naturalness of the Higgs mass by cancelling the quadratic divergences, we need to break SUSY in a way that does not cause the reappearance of those quadratic divergences. It was shown [42] that this can be achieved by adding SUSY breaking “soft-terms” to the Lagrangian.

$$\mathcal{L}_{\text{soft}} = -(m^2)_{ij} \phi_i \phi_j - \left(\frac{1}{2} M_a \lambda^a \lambda^a + \frac{1}{6} A^{ijk} \phi_i \phi_j \phi_k + B^{ij} \phi_i \phi_j + C_i \phi_i \right) + c.c. \quad (2.20)$$

The first term corresponds to adding a mass term for each sfermion, and the second, a mass term for each gaugino. Besides these, we have scalar bilinear and trilinear terms. The term $C_i \phi_i$ is gauge invariant only for gauge singlet scalar fields and will be dropped in all other cases. Since we include mass terms for the sfermions and gauginos but not for the corresponding chiral fermions and gauge bosons, these terms explicitly break SUSY. The soft SUSY breaking terms for the MSSM are

$$\begin{aligned} -\mathcal{L}_{\text{MSSM-soft}} &= \frac{1}{2} M_1 \tilde{B} \tilde{B} + \frac{1}{2} M_2 \tilde{W} \tilde{W} + \frac{1}{2} M_3 \tilde{g} \tilde{g} \\ &+ M_{H_u}^2 |H_u|^2 + M_{H_d}^2 |H_d|^2 + (B\mu H_u H_d + c.c.) \\ &+ \sum_i M_{Q_i}^2 |\tilde{q}_{L_i}|^2 + \sum_i M_{U_i}^2 |\tilde{u}_{R_i}^c|^2 + \sum_i M_{D_i}^2 |\tilde{d}_{R_i}^c|^2 \\ &+ \sum_i M_{L_i}^2 |\tilde{\ell}_{L_i}|^2 + \sum_i M_{E_i}^2 |\tilde{e}_{R_i}^c|^2 \\ &+ \left((\lambda_E A_E)_{ij} H_u \tilde{\ell}_{L_i} \tilde{e}_{R_j}^c + c.c. \right) \\ &+ \left((\lambda_U A_U)_{ij} H_u \tilde{q}_{L_i} \tilde{u}_{R_j}^c + (\lambda_D A_D)_{ij} H_u \tilde{q}_{L_i} \tilde{d}_{R_j}^c + c.c. \right) \quad (2.21) \end{aligned}$$

The addition of these terms adds 105 more independent parameters (masses, mixing angles and phases) to those of the SM and it is this that make the full MSSM phenomenologically intractable. We will discuss ways of constraining this large parameter space based on theoretical and phenomenological arguments in the next section.

2.2.1 MSSM particle spectrum

The scalar potential for the Higgs field contains contributions from the F - and D -terms as well as from the terms in the soft Lagrangian. The Electro-weak symmetry breaking takes place, similar to the SM, when the two scalar Higgs fields acquire a vacuum expectation value. Out of the eight degrees of freedom available to us from the two scalar doublets, three become the longitudinal modes of the gauge bosons to give massive W^\pm and Z bosons. The remaining five degrees of freedom make up the five Higgs bosons — CP even h_0 and H_0 , CP-odd A_0 and the charged Higgses H^\pm . The ratio of the vevs of the two Higgs fields is denoted by $\tan \beta$. Analogous to equation (1.9) for the SM, the tree-level mass of the Z -boson can be written in terms of the two vevs v_u and v_d as

$$M_Z^2 = \frac{v^2}{2}(g^2 + g'^2) = \frac{v_u^2 + v_d^2}{2}(g^2 + g'^2) \quad (2.22)$$

The fermion masses are derived from the superpotential $\mathcal{W}_{\text{MSSM}}$. Thus, all up-type quarks get their mass from the vacuum expectation value of H_u i.e. v_u whereas the down-type quarks and charged leptons get their masses from v_d . The tree level masses are given by

$$m_{ui} = \lambda_{U_i} v \sin \beta ; m_{di} = \lambda_{D_i} v \sin \beta \quad (2.23)$$

2.2.2 Neutralinos and Charginos

The new fermionic particles in the MSSM come from two sources. First are the fermionic superpartners of the Higgs fields are the Higgsinos ($\tilde{H}_u^0, \tilde{H}_d^0, \tilde{H}_u^\pm, \tilde{H}_d^\pm$). Second are the superpartners of the gauge bosons — gauginos ($\tilde{g}, \tilde{W}^3, \tilde{B}, \tilde{W}^\pm$). Once the $SU(2)_L \times U(1)_Y$ is broken, the only unbroken symmetries are $SU(3)_c$ and $U(1)_{\text{EM}}$. Therefore, it is possible to write soft terms such that states with the same colour and electric charge mix with each other.

Since the gluino is the only colour-charged fermion, it does not mix with any of the others. It's mass is given by the soft mass M_3 .

The mixing matrix for the two neutral gauginos and two neutral Higgsinos (in the basis $(\tilde{B}, \tilde{W}^3, \tilde{H}_u^0, \tilde{H}_d^0)$) can be written as

$$M_{\mathcal{N}} = \begin{pmatrix} M_1 & 0 & -M_Z \cos \beta S_W & M_Z \cos \beta S_W \\ 0 & M_2 & M_Z \cos \beta C_W & -M_Z \sin \beta C_W \\ -M_Z \cos \beta C_W & M_Z \sin \beta C_W & 0 & \mu \\ M_Z \sin \beta S_W & -M_Z \cos \beta S_W & \mu & 0 \end{pmatrix} \quad (2.24)$$

where $S_W = \sin \theta_W$ and $C_W = \cos \theta_W$. The eigenstates in which this mass matrix is diagonal are called the ‘‘Neutralinos’’ and are denoted by $\tilde{\chi}_i^0$ with $i = 1 - 4$.

The charged gaugino-higgsino mixing is more complicated. The mass matrix for $(\tilde{W}^+, \tilde{H}_u^+, \tilde{W}^-, \tilde{H}_d^-)$ is given by

$$M_C = \begin{pmatrix} 0 & \mathbf{X}^T \\ \mathbf{X} & 0 \end{pmatrix} \quad (2.25)$$

$$\text{where } \mathbf{X} = \begin{pmatrix} M_2 & \sqrt{2}M_W \sin \beta \\ \sqrt{2}M_W \cos \beta & \mu \end{pmatrix} \quad (2.26)$$

The the matrix \mathbf{X} is diagonalised as $U^* \mathbf{X} V^{-1}$ where U and V are 2×2 unitary matrices given by

$$\begin{pmatrix} \tilde{\chi}_1^+ \\ \tilde{\chi}_2^+ \end{pmatrix} = U \begin{pmatrix} \tilde{W}^+ \\ \tilde{H}_u^+ \end{pmatrix}; \quad \begin{pmatrix} \tilde{\chi}_1^- \\ \tilde{\chi}_2^- \end{pmatrix} = V \begin{pmatrix} \tilde{W}^- \\ \tilde{H}_d^- \end{pmatrix} \quad (2.27)$$

This gives the charged mass eigenstates $\tilde{\chi}_1^\pm$ and $\tilde{\chi}_2^\pm$ called the ‘‘Charginos’’.

2.2.3 Squarks and sleptons

Finally, we come to the sfermion sector. As mentioned above, all sfermions with the same colour and electric charge can mix together when we allow all possible soft terms. This would result in three 6×6 mixing matrices — one for up-type squarks $(\tilde{u}_L, \tilde{c}_L, \tilde{t}_L, \tilde{u}_R, \tilde{c}_R, \tilde{t}_R)$, one for down-type squarks $(\tilde{d}_L, \tilde{s}_L, \tilde{b}_L, \tilde{d}_R, \tilde{s}_R, \tilde{b}_R)$ and one for charged leptons $(\tilde{e}_L, \tilde{\mu}_L, \tilde{\tau}_L, \tilde{e}_R, \tilde{\mu}_R, \tilde{\tau}_R)$. The sneutrino sector has only left-handed fields as the SM does not contain right handed neutrinos. We therefore also have a 3×3 sneutrino mixing matrix for $(\tilde{\nu}_{eL}, \tilde{\nu}_{\mu L}, \tilde{\nu}_{\tau L})$.

However, the presence of arbitrary mixings would cause very large flavour changing neutral current (FCNC) effects. Since we have very strong experimental bounds on the observables sensitive to FCNC, it is important to avoid these by explicit model requirements. The simplest is to demand alignment — i.e. that the squark mass eigenstates are completely aligned with the quark mass eigenstates. In this case, the only mixing terms that remain are between the left and right squarks of the same flavour, and which originate from the trilinear A -terms and from the Higgs-squark-squark interaction terms after the higgs takes a vev. For e.g. the stop mass matrix is given at tree level by

$$M_{\tilde{t}}^2 = \begin{pmatrix} M_{\tilde{t}_L}^2 & m_t(A_t - \mu \cot \beta) \\ m_t(A_t - \mu \cot \beta) & M_{\tilde{t}_R}^2 \end{pmatrix} \quad (2.28)$$

This matrix is diagonalised by 2×2 matrix that can be parametrised as a rotation in terms of a mixing angle $\theta_{\tilde{t}}$. The mass eigenstates are then denoted by \tilde{t}_1 and \tilde{t}_2 .

As the mixing term is proportional to the mass of the corresponding fermionic partner, it is only in the third generation squark mass matrices that mixing plays a significant role. Similarly, one can also write the mass matrix for sbottoms. It is given by

$$M_b^2 = \begin{pmatrix} M_{b_L}^2 & m_b(A_b - \mu \tan \beta) \\ m_b(A_b - \mu \tan \beta) & M_{b_R}^2 \end{pmatrix} \quad (2.29)$$

Even though the mass of the b -quark is two orders of magnitude smaller than the that of the top quark, a large $\tan \beta$ can lead to a large mixing. Similarly, mixing plays an important role in the $\tilde{\tau}$ mass matrix only for large $\tan \beta$. We discuss in detail the limits from LHC data on the masses of stop and sbottom squarks in Chapter 4.

2.3 Phenomenological Modelling of the MSSM

The minimal supersymmetric standard model (MSSM) extends the nineteen standard model parameters to over a hundred. However, the proposed mechanisms of SUSY breaking, together with the requirements of suppressing FCNC and obtaining the correct electroweak breaking scale often suggest a common origin of some of the parameters at high scale. This results in highly constrained models like the minimal supergravity model (mSUGRA) [43, 44] or the very similar constrained MSSM (cMSSM) [45], gauge mediated SUSY [46] and others. Alternately, the new parameters can be constrained by not putting any theoretical constraints beforehand, but only demanding only that all observed experimental constraints are obeyed, thus limiting the masses and mixing of SUSY parameters in such a way as to suppress FCNC processes to fall below observed bounds. This second method leads to a model called the phenomenological MSSM (pMSSM) [47]. In this section, we discuss in detail two models, viz. the cMSSM and the pMSSM models.

2.3.1 The constrained MSSM

The cMSSM model is inspired by the gravity mediated SUSY breaking model mSUGRA. However, it does not contain the graviton or its superpartner, the gravitino. One of the successes of supersymmetry is that in Grand Unified Theories (GUT) with SUSY, the gauge couplings are found to unify at the high GUT scale. A very simplifying idea emerges from this observation — is it possible to also have unified masses for sparticles at this high scale?

To begin, the model assumes that all soft gaugino mass terms are the same at a high scale (usually assumed to be same as the GUT scale i.e. approximately 10^{16} GeV). Their masses at EW scale are then calculated by running down the masses using RG

equations. The running mass at low scale is given by the relation

$$\frac{M_1}{g'^2} = \frac{M_2}{g^2} = \frac{M_3}{g_s^2} \quad (2.30)$$

This means that at the TeV scale, the ratio $M_1 : M_2 : M_3$ is approximately $1 : 2 : 6$, or, that the gluino mass is approximately six times larger than the mass of the bino. The unified gaugino mass parameter at high scale is commonly denoted by $M_{1/2}$.

Taking the idea further, the cMSSM model also assumes that the soft mass terms for all scalar particles (squarks, sleptons, sneutrinos and higgses) at the low scale can be derived from a single unified parameter at the high scale, denoted by M_0 . It should be noted that in these models, the electroweak symmetry breaking occurs via radiative spontaneous symmetry breaking which completely determines the magnitude of the Higgs parameter μ . Since the masses of the Higgs bosons will be completely determined from the RG running, the only other independent parameter in the higgs sector is $\tan \beta$. Finally, all trilinear terms are assumed to be unified at the high scale to a common parameter denoted by A_0 .

Thus we arrive at a very simple model of SUSY that has only five free parameters — unified sfermion mass (M_0), unified gaugino mass ($M_{1/2}$), unified trilinear couplings (A_0), ratio of higgs vevs ($\tan \beta$) and the sign of the parameter μ .

Since the RG equations for masses are fixed once we choose the gauge group and the particle spectrum, the mass spectrum is uniquely determined once the boundary values of the above five parameters are given. We have already seen one consequence of this — the fixed mass relation between the gauginos. In the sfermion sector, the fermion loop pulls the masses down as we evolve the RG equations to low scale. Therefore, the higher the mass of the partner fermion, the lower the mass of the corresponding sfermions. This means that the third generation squarks and sleptons have the lowest mass among the three generations. Moreover, the left handed sfermions interact also with $SU(2)$ gauge bosons which has the effect to raising the mass. Thus, the left handed sfermions are in general heavier than the right handed sfermions. The RG equations for the squarks can be found in [48].

The squarks have colour charges that the sleptons and sneutrinos do not. Therefore squarks couple to gluinos which, as we have seen, are the heaviest of the gauginos. The effect of this too, is to increase the mass of the squarks. Therefore, in the cMSSM, squarks are generally much heavier than the sleptons. In the third generation sector, the left and right handed squarks mix to form the mass eigenstates. Therefore, we have the lighter stop (typically with a large right-handed fraction) as the lightest squark and the lighter stau (again mostly right handed) as the lightest slepton. A typical spectrum (point SPS1A [49]) can be seen in Figure 2.1.

The simplicity of this model has made it, by far, the most popular model for SUSY. Most experimental searches have been designed with this particular model in mind and the small number of parameters makes it easy to constrain the parameter space based on

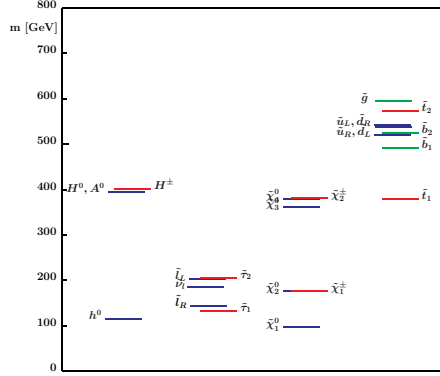


Figure 2.1: The SUSY benchmark point SPS1a generated with the input parameters $M_0 = 100$, $M_{1/2} = 250$, $A_0 = -100$, $\tan \beta = 10$, $\mu > 0$.

data. The LHC experiments have used cMSSM to put severe constraints on the masses of squarks and gluinos at the LHC. We shall show in Chapter 4 that these constraints are severely diluted when the requirement of universality in the sfermion sector is dropped and suggest alternate ways to interpret constraints on the third generation squarks.

2.3.2 The phenomenological MSSM

The pMSSM model reduces the 105 SUSY parameters to nineteen — the gaugino mass parameters M_1 , M_2 and M_3 ; the squark mass parameters for the first two generations M_Q , M_U and M_D , the third generation squarks M_{3Q} , M_{BR} , M_{TR} ; the corresponding slepton mass parameters M_L , M_R , $M_{\tau L}$, $M_{\tau R}$; the trilinear couplings A_t , A_b and A_τ ; and the higgs sector parameters μ , M_A and $\tan \beta$, the ratio of the vacuum expectation values of the two Higgs doublets.

The pMSSM model does not assume any high-scale unification. We therefore retain all three gaugino mass parameters. Similarly, all independent parameters of the Higgs sector are also retained. In the scalar sector, the parameters are grouped using phenomenological arguments. First, the sfermions that are the part of a left-handed doublet field are assumed to have the same soft mass term to avoid explicitly breaking $SU(2)_L$. Secondly, FCNC constraints require that the masses of the squarks of the first two generations cannot be very widely separated. This is similar to the GIM mechanism for the quark sector. This constraint is relaxed in the case of third generation squarks as the limits on FCNC processes involving the third generation are less stringent than in cases where only the first two generations come in. Therefore, the first two generation squarks (and similarly, the first two generation of sleptons) are assumed to have soft mass terms of the same magnitude whereas the third generation mass term can be different from these.

Next, we see that only the three trilinear couplings for third generation sfermions are retained. As we have seen earlier, trilinear couplings are responsible for mixing in the sfermion mass matrix and the term is proportional to the fermion mass. As the masses for all fermions except those of the third generation are very small, the presence of a trilinear coupling has negligible effect for the sfermions of the first two generations. Therefore, only those corresponding to the third generation are retained.

Given these parameters, the mass eigenstates of the Higgses, the gaugino, the neutralinos, charginos, squarks and sleptons can be calculated thus providing a complete spectrum. However, since the parameters here are completely arbitrary, it is important to verify that they are consistent with EWSB. Also, since the MSSM has coloured scalars, it is possible to reach a condition where one of the squark fields gets a vacuum expectation value, thereby breaking the colour vacuum. That this does not happen also has to be explicitly checked. Once the basic theoretical consistency requirements are satisfied, the constraints from data on the pMSSM model parameter space can be investigated.

2.4 Summary

In this chapter, we give a short outline of the construction of a supersymmetric theory for the SM. Due to the large number of possible soft terms in the MSSM, we turn to models that make simplifying assumptions to unify some of them. In this context, we discuss and two models and describe the resultant sparticle spectrum.

For the work done in this thesis, we have used both these models. In Chapter 3, we use a cMSSM-like model of high scale parameters with the sfermion unification condition relaxed. Using different scalar masses for the generations, we explore a situation where the third generation squarks may be much lighter than those of the first two generations (which are assumed to be decoupled) and discuss the signatures of such models at the LHC. In Chapter 4, we continue on the theme of light third generation squarks and use a low-scale pMSSM model to reinterpret the limits from LHC on third generation squark masses. In Chapter 5, we use the cMSSM model with R-parity violating terms to examine resonant production of top-squarks and gauge the potential of the LHC to constrain baryon number violating couplings at the LHC.

SIGNATURES OF SUPERSYMMETRY

CHAPTER

3

SIGNALS FOR SQUARKS OF THE THIRD GENERATION

“It is a capital mistake to theorise before one has data. Insensibly one begins to twist facts to suit theories, instead of theories to suit facts.”
– Sir Arthur Conan Doyle, *A Scandal in Bohemia*.

The LHC, being a pp -collision machine, is ideally suited to production of particles charged under $SU(3)_C$. The problem of looking for SUSY is therefore best addressed by looking for superpartners of the strongly interacting SM particles — the squarks and the gluino. The sparticle mass spectrum and hierarchy is often assumed to be determined by the (as yet unknown) high-scale SUSY breaking mechanism. Without the simplification afforded by such a mechanism, the large number of soft mass parameters in SUSY make the job of deducing model-independent signatures of SUSY nearly impossible. It is therefore highly desirable to reduce the number of parameters to a subset that is phenomenologically relevant.

This is partially achieved by the phenomenological MSSM (pMSSM) model (described in section 2.3.2) where the squark sector has degenerate masses for the first two generations and the third generation is parametrised by M_{3Q} , M_{tR} and M_{bR} corresponding to the soft mass parameters for the left-handed doublet, the right-handed stop mass and the right handed sbottom mass. The presence of coloured scalars in QCD is likely to give rise to flavour changing neutral currents (FCNC) that are strongly disfavoured by

all current data [50]. As the strongest constraints from FCNC pertain to the light quark sector, these can be avoided by requiring that the first two families of squarks are heavy enough to be decoupled [51, 52] from the third generation (which can still be at the TeV scale.) The solution to hierarchy problem of the Higgs mass depends crucially only on the contributions from the top squarks and therefore this arrangement does not hurt the arguments for motivation of SUSY as a solution to the hierarchy problem. On the other hand, it may be argued, that a squark sector with only the third generation accessible at the LHC, corresponds to a sort of “minimal” model that satisfies all experimental constraints and has the desirable theoretical properties.

One can think of, several theoretical schemes suggested to achieve the proposed scenario. It is possible, for example, to have a hidden sector such that it couples differently to the third generation squarks, leading to smaller soft SUSY breaking terms compared to those of the first two [53, 54]. Besides this, the existence of a “horizontal symmetry” under which the third generation is a singlet but the first two generations are doublets can also cause a mass splitting [55]. Thirdly, in SO(10) SUSY Grand Unified Theories (GUT), it is possible to adjust parameters to obtain suitable D-terms for the fields belonging to $\bar{5}$ and 10 of SU(5) leading to a mass hierarchy of the suggested type [56, 57]. Alternately, similar mass separation can also arise out of the D-terms of some additional (anomalous) U(1) gauge symmetry [58, 59]. Finally, certain regions in the parameter space of the minimal supergravity model (mSUGRA) or the similar constrained MSSM (cMSSM)[45], with a large universal scalar soft breaking mass, can lead to low values of only the third family sfermions due to the role of Yukawa couplings in the process of running down to the electroweak scale [60, 61].

The question of detecting new physics particles that couple exclusively to third generation quarks has garnered considerable interest in the recent years. It has been proposed, for example, that $t\bar{t}$ resonances can be indicative of (a) Kaluza-Klein Graviton or the heavy Z_H bosons from Little Higgs models[62, 63] (b) Color-Octet Scalars [64] (c) Or even a completely new particle (of spin 0, 1 or 2) that couples to the top [65]. Recent studies of collider phenomenology include both non-SUSY [66, 67] and SUSY scenarios [65, 68, 69, 70, 71].

The distinctive feature of the scenario where only the third generation squarks are accessible at the LHC is that it results in final states with multiple tops and bottoms. Moreover, if the particles in question are near the kinematical reach of the LHC, the resultant tops and bottoms are expected to have very large transverse momenta (p_T). In such situations, b-tagging efficiencies may not be optimum due to the highly collimated decay products of the b-hadron. The decay products of the top too, are likely to be collimated enough to form only one “fat” jet. This situation has received much attention by the development of top-tagging techniques using jet-substructure methods. We shall address these problems in an orthogonal channel — by dropping the requirement of top-identification and requiring energetic leptons instead. We shall also estimate whether the

traditional b-tagging searches can be used for isolating the signal over the background, taking into account that b-tagging efficiency is optimum only for transverse momentum in the range of 50 - 100 GeV[27].

3.1 Choice of parameters and benchmarks

Of the nineteen parameters that describe the pMSSM, we choose the following as the most significant for our study. First, the left and right-handed sfermion mass parameters for the first two generations, collective denoted as $M_0^{(1,2)}$, are all set to 5 TeV at the GUT scale. Second, the left and right handed parameters for the third generation sfermions are denoted as $M_0^{(3)}$ and will be varied to probe the reach of the LHC. The two higgs mass parameters are also set to this value at high-scale. Third, we retain the gaugino mass pattern (at EW scale) from the gravity mediated breaking schemes viz. $M_1 : M_2 : M_3 = 1 : 2 : 6$. Also, taking the notation from the gravity mediated models, we use $M_{1/2}$ to mean the unified gaugino mass at the GUT scale. Fourth, the three trilinear coupling parameters for the third generation are all set to be the same and will be denoted by $A^{(3)}$. We demand consistent radiative symmetry breaking which means the magnitude of the higgsino mass parameter μ is fixed and therefore, $\text{sign}(\mu)$ and $\tan \beta$, where β is the angle between the VEVs of the two Higgs doublets, complete our list of independent parameters. We fix $\text{sign}(\mu)$ to be positive as the favoured value from $(g - 2)_\mu$ data. To summarise, the independently varying parameters in our study are: $(M_0^{(3)}, M_{1/2}, A^{(3)}, \tan \beta)$ viz. scalar mass for the third generation of sfermions, unified gaugino mass, the trilinear coupling for the third generation and $\tan \beta$.

We focus specifically on $\tilde{g}\tilde{g}$ production with each gluino decaying via either $\tilde{t}_1 t$ or $\tilde{b}_1 b$ followed by decays of the \tilde{t}_1 or \tilde{b}_1 . There is also a contribution from $\tilde{t}_i \tilde{t}_i^*$ and $\tilde{b}_i \tilde{b}_i^*$ production. However t-channel squark-gluino type contributions are much suppressed. We also choose to look at regions where the gluino mass is greater than a TeV and stop mass is greater than 500 GeV as an illustration of the region where the b-identification becomes difficult.

With this in mind, high scale value of $M_0^{(1,2)}$ is set to 5 TeV for the first two families, while the high-scale mass for the third family ($M_0^{(3)}$) is set so as to obtain third generation squark masses of the order of 1 TeV. The trilinear coupling $A^{(3)}$ is set to zero. We find that non-zero values of $A^{(3)}$ serve to lower the stop and sbottom masses for fixed $M_0^{(3)}$ and $M_{1/2}$. We wish to also probe the change in detection efficiency for the entire range of $\tan \beta$. We therefore sample benchmarks with $\tan \beta = 5, 10$ and 40 to see if any major differences are indicated. The Higgs mass parameters M_{H_u} and M_{H_d} are set to the value of the third family M_0 at the high scale.

The particle spectrum has been generated using SuSpect 2.34 [72] using high scale inputs in the pMSSM (phenomenological MSSM). The squark and gluino masses for

| Point | $\tan \beta$ | $m_{\frac{1}{2}}$ | $m_0^{(3)}$ | $m_{\tilde{g}}$ | $m_{\tilde{t}_1(\tilde{t}_2)}$ | $m_{\tilde{b}_1(\tilde{b}_2)}$ |
|--------------|--------------|-------------------|-------------|-----------------|--------------------------------|--------------------------------|
| 1A | 10 | 800 | 800 | 1918 | 1124 (1403) | 1376 (1502) |
| 1B | 10 | 600 | 1000 | 1496 | 856 (1130) | 1100(1283) |
| 1C | 10 | 400 | 1200 | 1063 | 623 (916) | 892 (1153) |
| 2A | 5 | 600 | 1000 | 1496 | 842 (1130) | 1100(1290) |
| 2B | 5 | 400 | 1200 | 1063 | 603 (916) | 890(1160) |
| 3A | 40 | 600 | 1000 | 1493 | 856 (1065) | 1024(1157) |
| 3B | 40 | 400 | 1200 | 1058 | 619 (819) | 783(982) |

Table 3.1: Third generation squark and gluino masses in GeV for the benchmark points considered.

| Point | $m_{\chi_1^+}$ | $m_{\chi_2^+}$ | $m_{\chi_1^0}$ | $m_{\chi_2^0}$ | $m_{\chi_3^0}$ | $m_{\chi_4^0}$ |
|--------------|----------------|----------------|----------------|----------------|----------------|----------------|
| 1A | 660 | 881 | 348 | 660 | 864 | 881 |
| 1B | 484 | 648 | 258 | 484 | 622 | 649 |
| 1C | 288 | 409 | 167 | 290 | 356 | 410 |
| 2A | 487 | 707 | 258 | 488 | 686 | 701 |
| 2B | 313 | 492 | 168 | 315 | 465 | 492 |
| 3A | 482 | 619 | 259 | 482 | 590 | 619 |
| 3B | 261 | 384 | 166 | 265 | 302 | 383 |

Table 3.2: Chargino and Neutralino masses in GeV for all the benchmark points.

the various benchmark points are given in Table 3.1. The masses for charginos and neutralinos are given in Table 3.2. We explore regions of the parameter space where squarks are lighter than the gluino and of the order of ~ 1 TeV. Cases where the gluino is considerably lighter than all squarks, which corresponds to the “focus-point” scenarios has been investigated in [70].

Thus our chosen benchmark points elicit a number of features of the signals of SUSY with only the third family of sfermions accessible. We use these in our study of the suggested signals in the next section.

3.2 Signals and Backgrounds

We are concerned primarily with observing final states with a large number of top and bottom quarks. Signal events have been generated using Pythia v6.409¹ [73] by al-

¹A new C++ version of this program (PYTHIA 8) is now available and as of v 8.160 includes all SUSY processes including R-parity violating resonant production. For details on this version and my contributions to the code, see Appendix A.

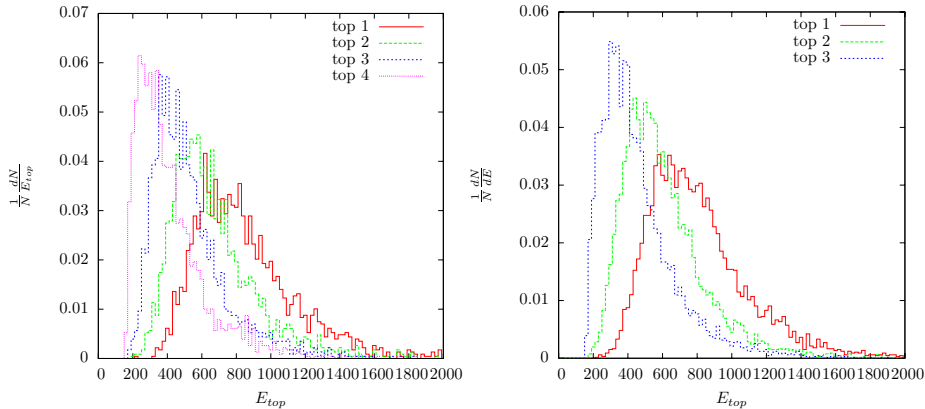


Figure 3.1: Energy(E) distribution of tops for four- and three-t events for benchmark point 1A.

lowing the squark-squark, gluino-gluino and squark-gluino production channels. The heaviness of the first two generations of squarks implies that only stop and sbottom are produced with a cross section large enough to be relevant. We have used CTEQ5L parton distribution functions. The factorisation and renormalisation scales have been set to $\mu_R = \mu_F = \sqrt{p_\perp^2 + (P_1^2 + P_2^2 + M_3^2 + M_4^2)/2}$ where P_1, P_2 are the virtualities of the incoming particles, p_\perp is the transverse momentum of the scattering process and M_3, M_4 are the masses of the outgoing particles in the initial hard scattering process.

We concentrate on three and four-top events in particular. The \tilde{g} can decay into $t\tilde{t}_{1,2}$ or $b\tilde{b}_{1,2}$. Whenever it is kinematically allowed, the squarks can then decay via $\tilde{t}_{1,2} \rightarrow t\tilde{\chi}_i^0$ (with $i = 1 - 4$), $\tilde{t}_{1,2} \rightarrow b\tilde{\chi}_{1,2}^+$, $\tilde{b}_{1,2} \rightarrow b\tilde{\chi}_i^0$ and, $\tilde{b}_{1,2} \rightarrow t\tilde{\chi}_{1,2}^+$. Thus, $\tilde{g}\tilde{g}$ production can give four-top final states via $\tilde{g}\tilde{g} \rightarrow t\tilde{t}_{1,2}t\tilde{t}_{1,2}$ and each $\tilde{t}_{1,2} \rightarrow t\tilde{\chi}_i^0$. Three-top final states can be obtained when $\tilde{g}\tilde{g} \rightarrow t\tilde{t}_{1,2}b\tilde{b}_{1,2}$ with $b_{1,2} \rightarrow t\tilde{\chi}_{1,2}^+$.

Figures 3.1 and 3.2 give the energy distribution of the top quarks in four-top and three-top events for benchmark points 1A (highest squark/gluino masses) and 1C (lowest squark/gluino masses). Irrespective of the decay chain of the gluino, the resultant final state always has four b-quarks. Final states with only three b-quarks are possible via sbottom-gluino production driven by the b-quark distribution in the proton. Due to the small b-quark distribution in the proton, the number of 3b events is expected to be much smaller than 4b events (less than a few percent). We therefore present the transverse momentum (p_T) distribution of the b-quarks in 4b events in Figure 3.3.

We now come to the question of what the realistic b-tagging efficiencies in such a scenario are. A b-tagging efficiency of 50% with a rejection of QCD jets at more than 99% is well established for b-hadrons with the transverse momentum (p_T) between 50 to 80 GeV [27]. But in our case, it can be seen that the p_T of b-hadrons very often exceeds this. It is not clear how the efficiency goes down as p_T increases above 100

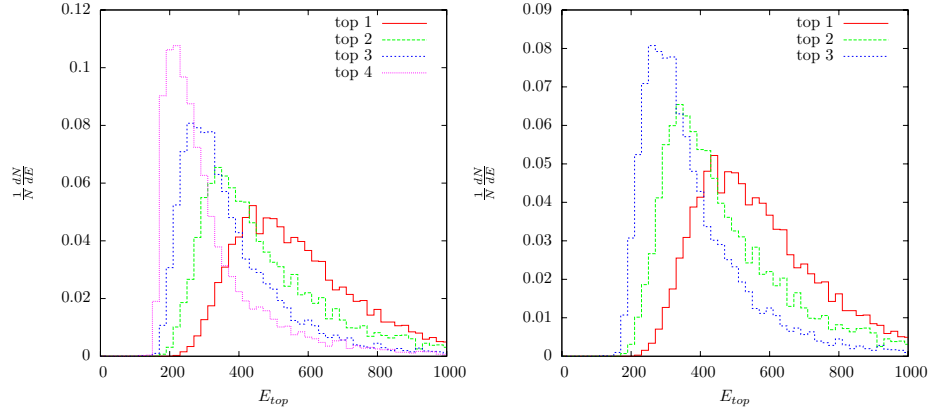


Figure 3.2: Same as in Figure 1, for benchmark point 1C.

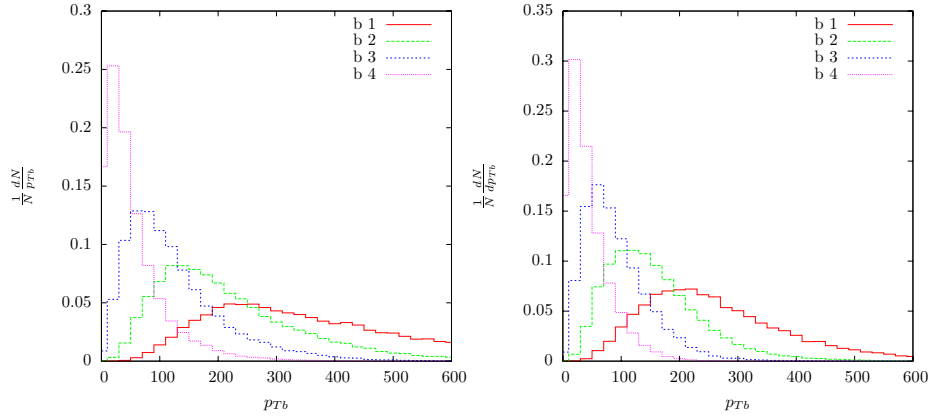


Figure 3.3: Transverse momentum p_T of b-quarks for points 1A and 1C.

GeV. The p_T -distribution of b's in four-b events can be seen in Figure 3.3.

Top quarks can be identified by a combination of a b-jet and a W , which give an invariant mass within a window of the top mass. The candidate W s are obtained from jet-pairs having invariant mass in the range $M_W \pm 15$ GeV. Besides the aforementioned b-tagging difficulty, this top reconstruction is complicated by two other factors in our situation.

First, at very high boosts, the jets from decay of the top can be highly collimated. However, very high energy QCD jets can also develop an invariant mass up to 15 - 20% of the jet energy, and thus, a top depositing a large energy in the hadron calorimeter can be faked by a similarly energetic jet whose 'effective' invariant mass may be of the same order as the top mass. In such cases, one has to resort to special techniques, such as specific kinematics, energetic leptons contained in jets, and using jet-substructure.

Such techniques have been studied recently by various groups [74, 75].

An extra complication, is Higgs production through the cascade $\chi_2^0 \rightarrow h\chi_1^0$. The χ_2^0 is produced in about 50% of the events we generate, and at low $\tan\beta$ its decay into a Higgs has a large branching ratio. The Higgs largely decays into a pair of b-quarks. The mass of the Higgs in all our benchmark points lies at $\lesssim 120$ GeV. In cases where either of the b-jets from Higgs decay are not tagged, they contribute to the large combinatorial background that is found to completely wash out the W-peak from invariant mass of jet-pairs. Thus our benchmark points highlight one additional difficulty in selecting the final states via traditional top identification.

To ameliorate these difficulties, we do not emphasise the reconstruction of the top. We also supplement b-tagging by identifying hard leptons from the decay of energetic top quarks. We find that looking for leptons of various multiplicity can compensate for the potentially low tagging efficiencies for very high energy b's.

We are looking at very high masses for squarks and gluinos and consequently rather low production cross sections. Thus, it will require a large integrated luminosity at the LHC to achieve the required statistical significance. By that time, we assume that the lightest neutral SUSY Higgs has already been identified. An additional handle for our benchmark points is thus provided by the possibility of looking for final states with leptons/b-quarks, together with not only large missing energy but also a Higgs in the final state, identified by a mass peak.

To isolate the signal, we examine final states with various combinations of b's and leptons. We comment first on certain generic features of signal identification, before the numerical results for each signal are presented. These features also help us in evolving the event selection criteria for this scenario.

3.2.1 Identification of physics objects:

- **Leptons** (e, μ) : We are interested in identifying leptons coming from top decay. Since the parent W of the lepton is on-shell, we expect that the lepton to be well isolated from the nearest jet². We first identify leptons with the following cuts:

1. $p_T^l > 10$ GeV (trigger)
2. Separation from each jet $\Delta R_{lj} > 0.4$
3. Sum of hadronic deposits $\Delta R < 0.2$ should have energy less than 10 GeV.

Lepton momenta are smeared according to the prescription $\sigma(E) = a\sqrt{E} + bE$ where $\sigma(E)$ is the resolution, with $a = 0.055(0.02)$ and $b = 0.005(0.037)$ for electrons (muons) and energy measured in GeV.

²Although the boost of the tops may give rise to the question of whether these leptons would indeed be isolated, we have found by actual simulation that the number of events with isolated leptons is significant enough for discovery.

We subsequently apply further cuts for each channel to restrict to leptons coming from tops.

- **Jets:** Jets are formed using the routine PYCELL built into PYTHIA. We demand $p_T \geq 20 \text{ GeV}$ and $|\eta| < 2.5$ as requisites for identification. The jet energy is smeared using $\sigma(E) = \sqrt{E}$. The parton-level processes that lead to the final states of interest to us have usually a large jet multiplicity. Using PYTHIA, the multiplicity peaks at 6 when both initial and final state radiation are taken into account. With this in view, we have always demanded a minimum of four jets in the final state.
- **b-Tagging:** In the absence of any clear guideline on the tagging efficiency for very high- p_T b-hadrons, we take a conservative approach and restrict our b-tagging capabilities to b-hadrons with p_T between 50 and 100 GeV. A jet is assumed b-tagged with an efficiency of 0.50 if:
 1. A b-hadron lies within a cone of $\Delta R < 0.5$ of the jet-axis
 2. The b-hadron has a $50 \text{ GeV} \leq p_T \leq 100 \text{ GeV}$.
- **Missing transverse energy (\cancel{E}_T) and the effective mass (M_{eff}):** The conservation of R-parity means the lightest supersymmetric particle (LSP) is stable. In our case, the lightest neutralino is the LSP and since it is uncharged, it escapes detection. This gives a very large missing- E_T which gives us the first handle for discriminating supersymmetric events. Also, since the masses of the supersymmetric particles are very high for the scenarios investigated here, the effective mass of the event, defined by $M_{\text{eff}} = \sum_{jets} |p_T^j| + \sum_{leptons} |p_T^l| + \cancel{E}_T$ also takes a very high value compared to what is expected of standard model processes. The \cancel{E}_T and M_{eff} distributions for two benchmark points are shown in Figure 3.4, along with the corresponding distribution for standard model backgrounds.

The calculation of \cancel{E}_T has to take into account not only the ‘‘visible’’ \mathbf{p}_T due to jets, leptons and photons that satisfy the requisite triggers but also objects with $p_T > 0.5 \text{ GeV}$ and $|\eta| < 5$ which are not identified as leptons or do not fall within any jet cone. The contribution from this extra part is summed up as the ‘soft- p_T ’ component. This is smeared according to the prescription $\sigma(p_T) = \alpha\sqrt{p_T}$ with $\alpha = 0.55$. The total visible transverse momentum is given by $\mathbf{p}_T^{vis} = \sum_{jets} \mathbf{p}_T^j + \sum_{leptons} \mathbf{p}_T^l + \mathbf{p}_T^{soft}$. Missing E_T is then the magnitude $|\mathbf{p}_T^{vis}|$.

In gluino decay, the production of the $\tilde{\chi}_2^0$ occurs in about 50% of all events. For the benchmark points with $\tan\beta = 5, 10$, the difference between masses of the second and the first neutralino is more than the mass of the lightest neutral Higgs (M_{h^0}). The most common decay channel $\tilde{\chi}_2^0 \rightarrow h\tilde{\chi}_1^0$ yields a neutral Higgs in the final state which then

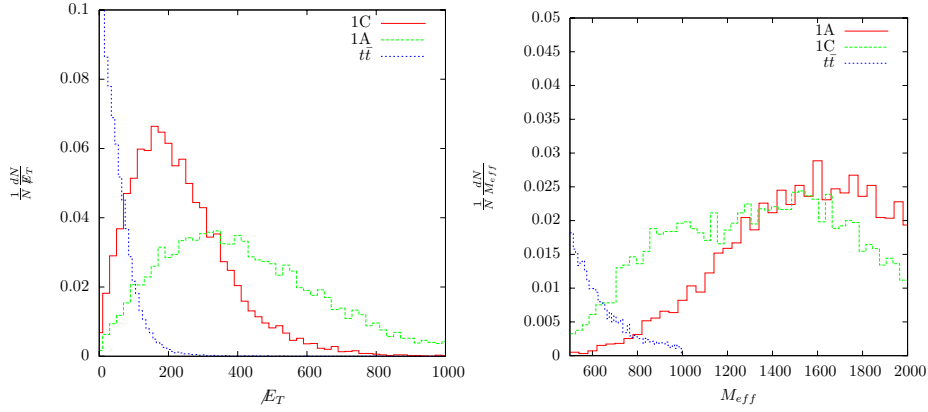


Figure 3.4: Missing transverse energy (E_T) and effective mass M_{eff} distribution for benchmark points 1A, 1C and the dominant standard model background ($t\bar{t}$).

decays into a pair of b-quarks. This is because there are two primary two-body decays of the $\tilde{\chi}_2^0$, namely, $\tilde{\chi}_2^0 \rightarrow h\tilde{\chi}_1^0$, $\tilde{\chi}_2^0 \rightarrow Z\tilde{\chi}_1^0$. The decay into a Z is suppressed by the product of Higgsino components of both $\tilde{\chi}_2^0$ and $\tilde{\chi}_1^0$. The decay into a Higgs requires the Higgsino component of any one neutralino and it therefore wins when kinematics are favourable. For the case with $\tan\beta = 40$, the mass difference $M_{\tilde{\chi}_2^0} - M_{\tilde{\chi}_1^0}$ is smaller than M_{h^0} . As a result, $\tilde{\chi}_2^0 \rightarrow Z\tilde{\chi}_1^0$ is the dominant decay. The identification of Higgs can therefore give us information on the value of $\tan\beta$.

Based on the above observations, we now list the basic cuts that have to be satisfied by all events:

1. $E_T \geq 300 \text{ GeV}$
2. $M_{\text{eff}} = (\sum |\vec{p}_T| + E_T) \geq 1000 \text{ GeV}$
3. Jet multiplicity $n_{\text{jet}} \geq 4$
4. $p_T(j_1) > 100 \text{ GeV}$
5. $p_T(j_2) > 80 \text{ GeV}$
6. $p_T(j_3) > 40 \text{ GeV}$

The inclusive cross sections for ‘all events’ satisfying the basic cuts for our benchmark points are summarised in Table 3.3.

We now discuss signals in various channels. The cuts or extra identification criteria applied henceforward will be over and above the basic cuts enumerated above.

| Point | 1A | 1B | 1C | 2A | 2B | 3A | 3B |
|-----------------------|------|-------|--------|-------|--------|---------|--------|
| $\sigma_{nocuts}(fb)$ | 4.51 | 32.47 | 308.00 | 37.07 | 352.01 | 34.62.0 | 337.51 |
| $\sigma_{basic}(fb)$ | 3.89 | 15.09 | 83.87 | 17.21 | 98.31 | 16.62 | 93.767 |

Table 3.3: Total $\tilde{g}\tilde{g}$, $\tilde{g}\tilde{q}$ and $\tilde{q}\tilde{q}$ production cross sections for all the benchmark points before and after basic cuts.

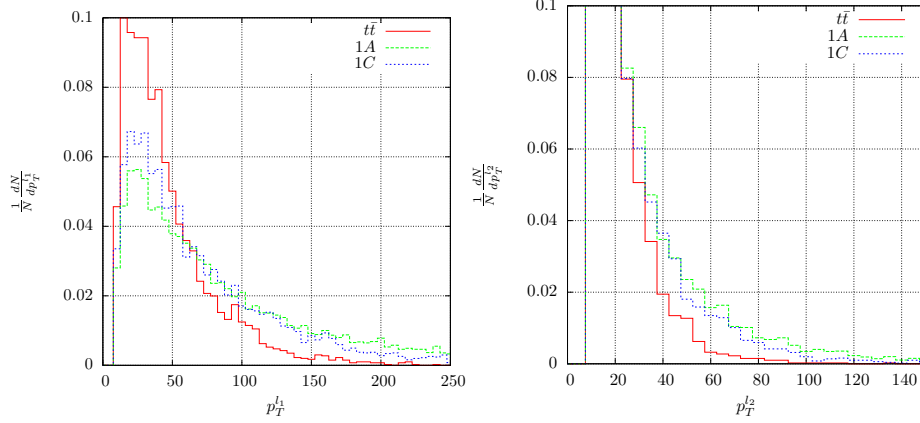


Figure 3.5: Magnitudes of p_T for the two hardest leptons for points 1A, 1C and standard model $t\bar{t}$ production.

3.2.2 Dilepton Channels: $1b + 2l$, $1b + 2l_{(SSD)}$ and $2l_{(SSD)}$

As mentioned earlier, the tops produced from the decay of heavy squarks and gluinos are highly energetic. Even in three-top (four-top) events which would give three (four) b-quarks, it is not always possible to tag all of them. However, we expect that leptons arising out of the decay of the tops to be very energetic. Therefore, we look at two energetic leptons with and without additional b-tags.

The backgrounds are calculated including the processes $t\bar{t} + jets$, $Wb\bar{b} + jets$, $Wt\bar{t} + jets$, $Zt\bar{t} + jets$, $Zb\bar{b} + jets$, $4t$, $4b$ and $2t2b$ generated with the help of ALPGEN [76]. Most of the background comes from the $t\bar{t}$ channel. The p_T distributions for leptons for benchmark points 1A and 1C along with $t\bar{t}$ are given in Figure 3.5. We therefore apply the following cuts to select leptons over those from standard model backgrounds.

The final cuts on the leptons are:

1. $p_T(l_1) \geq 80$ GeV
2. $p_T(l_2) \geq 30$ GeV

To suppress the $t\bar{t}$ background even further, we demand that the leptons be of the same sign. We also look at the inclusive same-sign dilepton channel (without any b-tags).

| Point | $1b + 2l$ | $1b + 2l_{(\text{SSD})}$ | $2l_{(\text{SSD})}$ | $2b + l$ | $3b$ |
|----------------------|-----------|--------------------------|---------------------|----------|------|
| 1A | 15 | 6 | 25 | 4 | 2 |
| 1B | 83 | 35 | 117 | 27 | 24 |
| 1C | 478 | 221 | 626 | 147 | 175 |
| 2A | 72 | 36 | 119 | 23 | 27 |
| 2B | 486 | 166 | 568 | 181 | 161 |
| 3A | 84 | 35 | 143 | 19 | 20 |
| 3B | 13(5) | 109 | 592 | 243 | 712 |
| SM Background | 10 | 4 | 4 | 1514 | 5 |

Table 3.4: Signal and background events for different channels for an integrated luminosity of 300 fb^{-1} .

The signals and backgrounds for such dilepton events, with and without a tagged b-jet, are seen in Table 3.4. We have calculated the the number of events, for both signals and backgrounds, corresponding to an integrated luminosity of 300 fb^{-1} . Although the $1b + 2l$ channel seems to give worse statistics for discovery as compared to the inclusive $2l_{(\text{SSD})}$, the presence of associated b-tagged jets is a sure indication of the involvement of particles coupling to the third generation of quarks. The presence of an excess in both these channels simultaneously can therefore be used to discriminate against other models of new physics which do not predict new particles decaying to top or bottom quarks.

3.2.3 Multi-b Channels: $2b + l$ and $3b$

The first consequence of having only third family squarks accessible is that all SUSY processes involving the production of strongly interacting superparticles lead to a multiplicity of b's in the final state. As we have mentioned already, most of these have too high p_T to be reliably tagged. However, there will still be sufficient number of events with two or three b-tags. There one has to compromise on number of tagged leptons to retain a significant number of events. On the whole, this reflects a tug-of-war between the loss in rate due to leptonic branching ratios and that due to our demand that only b's in a specific p_T -range be identified. Thus for identifying events with high squark and gluino masses, where the cross section is already very low, we recommend looking at only single-lepton events when more than one b's are tagged.

For two b-tagged events, we find a very large background from $t\bar{t}$ processes. We suppress this by demanding the presence of a high- p_T , isolated lepton, satisfying $p_T(l_1) \geq 80 \text{ GeV}$. The requirement of leptons has to be given up for $3b$ events, for otherwise the overall rates will be far too small.

The primary backgrounds for $2b + l$ channel are same as $1b + l$, viz. $t\bar{t} + jets, Wb\bar{b} +$

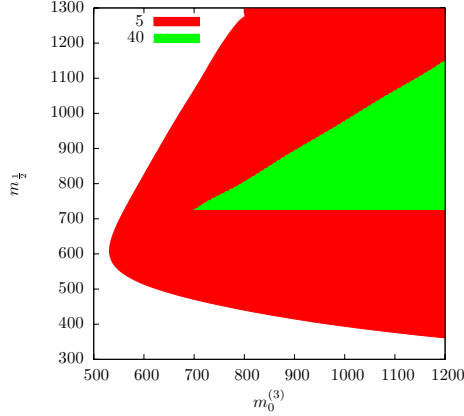


Figure 3.6: Regions in parameter space corresponding to the branching fraction $BF(\tilde{\chi}_2^0 \rightarrow h\tilde{\chi}_1^0) > 0.9$ for $\tan\beta = 5$ and 40 .

$jets, Wt\bar{t}+jets, Zt\bar{t}+jets, Zb\bar{b}+jets, 4t, 4b$ and $2t2b$. Again, we have used ALPGEN to compute the background rates.

Since the $3b$ cannot result from tree-level standard model processes (excepting those suppressed by weak mixing), the backgrounds are only due to $4t, 2t2b$ and $4b$. However, the $4b$ processes do not have a source of high \cancel{E}_T , so the highest contribution comes from $2t2b$ production processes.

The results are presented in Table 3.4. For the channel $2b + l$, we see that although the significance s/\sqrt{b} is large for points 1C, 2B and 2C, the very small s/b makes it highly sensitive to systematics of the background. Therefore, it may be used at best as a supplementary channel.

3.2.4 Channels with reconstructed Higgs

In this study, we wish to emphasise situations where the gluino mass is $\gtrsim 1$ TeV. This roughly corresponds the region of the parameter space with $M_{1/2} \geq 400$ GeV. As can be seen from Figure 3.6, decay $\tilde{\chi}_2^0 \rightarrow h\tilde{\chi}_1^0$ has a branching ratio greater than 90% over most of the region of parameter space for $\tan\beta = 5$. The decay $\tilde{\chi}_2^0 \rightarrow Z\tilde{\chi}_1^0$ is suppressed in these regions, and the lightest neutral Higgs occurs in a significant number of events in this scenario. As mentioned before, this is because, the decay into a Z requires significant Higgsino fractions in both neutralinos $\tilde{\chi}_2^0$ and $\tilde{\chi}_1^0$ whereas the decay into a Higgs requires significant Higgsino component in either neutralino. For $\tan\beta = 40$, this region is much reduced and the decay into a Higgs is appreciable only in the region $M_{1/2} > 700$ GeV where the gluino mass is close to the upper limit of accessibility. The dominant decay then is $\tilde{\chi}_2^0 \rightarrow Z\tilde{\chi}_1^0$.

We assume a situation where the lightest neutral Higgs has already been discovered

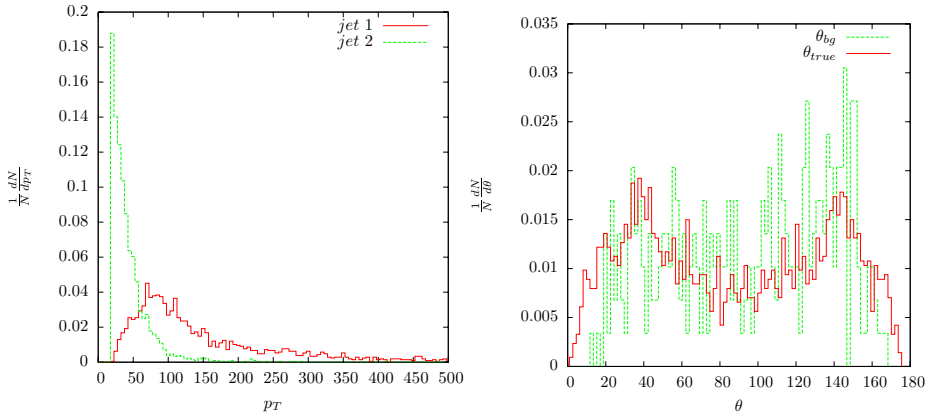


Figure 3.7: The transverse momentum (p_T) of jets from Higgs decay and the opening angle θ between the jets for signal events (“ θ_{true} ”) and the combinatorial background (“ θ_{bg} ”).

and it’s mass is known. Ideally, one would like to identify the Higgs by picking a b-jet pair with it’s invariant mass near the mass of the Higgs. However, in most events, both b’s from the Higgs cannot be identified (as seen from Figure 3.7). And demanding only one b-tagged jet instead of two leads to a combinatorial background much higher than actual number of signal events. To be able to reduce this, we compare the p_T distribution of jets from Higgs decay and the opening angle between the jets for true Higgs events and the combinatorial background. The distributions are shown in Figure 3.7.

We then select events with the following cuts which are designed to suppress events which do not have a Higgs:

1. $|M_{j_1 j_2} - M_h| < 15.0$ GeV where $M_{j_1 j_2}$ is the invariant mass of the jet pair.
2. The second (less energetic) jet has $p_T < 80$ GeV.
3. *At least one of the two jets is b-tagged.*
4. The opening angle between the jets is less than $\pi/2$.

These cuts reduce the combinatorial background to about half that of the signal. Identifying the Higgs means at least one b-tag. Therefore, we study the channels $2l + h$, $2l_{(SSD)} + h$, $1b + l + h$ and $2b + h$ with exactly the same hard-lepton cuts. The signals and backgrounds for all Higgs channels are summarised in Table 3.5. The combinatorial background is mentioned in the parenthesis accompanying each number of signal events.

We find that for points with gluino mass $\gtrsim 1.5$ TeV, the event rates are not significant enough to make a distinction between the region favouring Higgs production

| Point | $2l + h$ | $2l_{(\text{SSD})} + h$ | $1b + l + h$ | $2b + h$ |
|----------------------|----------|-------------------------|--------------|----------|
| 1A | 3(1) | 1(0) | 1(0) | 0(0) |
| 1B | 13(5) | 5(2) | 3(2) | 3(0) |
| 1C | 110(60) | 28(14) | 32(9) | 37(9) |
| 2A | 12(3) | 4(1) | 5(1) | 8(1) |
| 2B | 96(55) | 40(25) | 30(10) | 46(5) |
| 3A | 13(5) | 6(2) | 5(2) | 3(0) |
| 3B | 132(121) | 69(69) | 0(0) | 5(5) |
| SM Background | 5 | 3 | 7 | 3 |

Table 3.5: Signal and background events for different channels with Higgs identification for an integrated luminosity of 300 fb^{-1} . The irreducible combinatorial background for each channel is given the the parentheses.

and the region where it is suppressed. However, for points 1C, 2B and 3B (which correspond to the same $M_0^{(3)}$ and $M_{1/2}$), we can see a clear distinction in the number of Higgs events in Table 3.5. Thus, one can use this information to infer whether the situation corresponds to low or high $\tan \beta$. In particular, the $1b + l + h$ and $2b + h$ channels have the added advantage of a low combinatorial background. These channels show a significant excess even after taking the combinatorial background into consideration. However, for the two di-leptonic channels, the combinatorial background rejection efficiency of these cuts is insufficient which makes them unreliable for making definite statements about Higgs production with the identification criteria stated above.

3.3 Distinction from cMSSM scenarios

While signals have been suggested above for discovering SUSY with only the third family light, it is also instructive to ask whether such a scenario can be distinguished from the more frequently discussed case where all three families are obtained from a unified high-scale mass and therefore are all typically within the reach of the LHC. We take up such a discussion in this section, showing that this can be done by (a) considering the ‘effective mass’ distribution of events, and (b) taking event ratios for different channels. For illustration, we choose the benchmark point 1C from our previous analysis and choose two points generated in the cMSSM scenario (i.e. all sfermion masses now arise from the same M_0) as representatives of the case when all three sfermion families are accessible. In this situation too, the renormalisation group running renders the third generation squarks to be the lightest and therefore, there is a realistic possibility that gluino production would give rise to similar signatures.

As the variable M_{eff} has long been considered as a good indicator of the SUSY

| Point | $M_{1/2}$ | $M_0^{(3)}$ | $M_{\tilde{g}}$ | $M_{\tilde{t}_1(\tilde{t}_2)}$ | $M_{\tilde{b}_1(\tilde{b}_2)}$ | $M_{\tilde{u}_1(\tilde{u}_2)}$ |
|--------------|-----------|-------------|-----------------|--------------------------------|--------------------------------|--------------------------------|
| 1C | 400 | 1200 | 1063 | 623 (916) | 892 (1153) | 5015(5023) |
| S1 | 400 | 100 | 998 | 697 (895) | 847 (879) | 914 (883) |
| S2 | 570 | 1200 | 1362 | 1163 (1468) | 1453(1616) | 1654 (1628) |

Table 3.6: Third generation squark and gluino masses in GeV for two cMSSM points and point 1C. The value $\tan \beta = 10$ is used for illustration.

| Point | $\sigma_{basic}(fb)$ | $1b + 2l$ | $1b + 2l_{(SSD)}$ | $2l_{(SSD)}$ | $2b + l$ | $3b$ |
|-------------------|----------------------|-----------|-------------------|--------------|----------|------|
| 1C | 83.87 | 478 | 221 | 626 | 147 | 175 |
| S1 | 1160 | 1619 | 298 | 3239 | 255 | 213 |
| S2 | 74.63 | 446 | 195 | 622 | 117 | 123 |
| Background | | 10 | 4 | 4 | 1514 | 5 |

Table 3.7: Number of events at $300 fb^{-1}$ for the cMSSM points S1 and S2. We have repeated the numbers for point 1C and background for comparison.

scale (or the mass of the lightest strongly charged SUSY particle) [77], the first cMSSM point (S1) is generated so as to have low-scale stop and gluino masses as close to 1C as possible. As one can see from Figure 3.8, this corresponds to a nearly identical M_{eff} distribution. The second point (S2) was generated to give a similar event rate at $300 fb^{-1}$ in several channels. Since in our previous analysis, we have found SSD to be the best channel for discovery, it has been used here for illustration. The low-scale masses for third-generation squarks and gluinos for the two cMSSM points corresponding to the point 1C are given, along with the high-scale values of $(M_0, M_{1/2})$, in Table 3.6. The values of $\tan \beta$ and $sign(\mu)$ are chosen to be 10 and positive respectively. The trilinear soft breaking parameter A_0 is set to zero at high scale.

We calculate the event rates for the same channels ($1b + 2l$, $1b + 2l_{(SSD)}$, $2l_{(SSD)}$, $2b + l$, $3b$) as before. The basic cuts as well as any extra cuts applied are same as in section 3. The event rates are given in Table 3.7.

In R-parity conserving SUSY, only even number of superparticles can be produced. Therefore, the peak of the M_{eff} distribution corresponds roughly to twice the mass of the lightest superparticle pair-produced through hard scattering. This gives us an indication of the mass scale of SUSY particles. As the the third family sfermions are usually the lightest squarks in most of the cMSSM parameter space (though the first two are not necessarily decoupled), the masses of the gluino and/or the third family squarks will be indicated by the peak of the M_{eff} distribution. The M_{eff} distributions for points 1C, S1 and S2 are shown in Figure 3.8.

Based on the information from the M_{eff} distribution and the event rates, we can draw

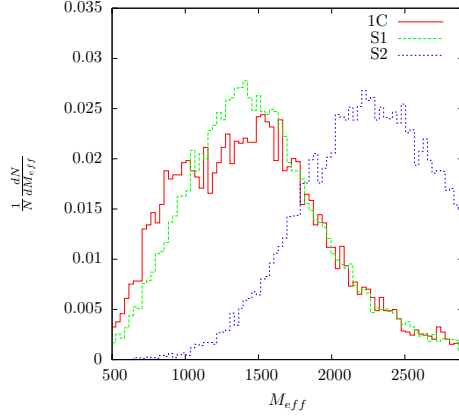


Figure 3.8: Comparison of M_{eff} distributions for points 1C, S1 and S2.

the following inferences:

1. Case of identical M_{eff} spectrum:

- (a) The points 1C and S1 have a very similar spectrum for third generation squarks and gluino masses. They are not distinguishable by looking at the M_{eff} distribution alone.
- (b) The cross section for squark and gluino production for S1 is very high since all the squarks are accessible. Note, in particular, that the ratio $3b_{1C} : 3b_{S1} = 0.82$ is close to one whereas the ratio $\text{SSD}_{1C} : \text{SSD}_{S1} = 0.19$ is much smaller. The $3b$ final state which comes only from $\tilde{b}\tilde{g}$ production shows a similar event rate due to similar gluino mass.
- (c) Rates for the channels $1b + 2l$ and SSD are highly enhanced for the points S1. Since $\tilde{q}\tilde{q}, (q = u, d, s, c)$ is allowed, their cascades into charginos yield larger number of dileptons. This also explains why on demanding one b-tag ($1b + 2l(\text{SSD})$ channel), the increase in the number of events is not so dramatic.

2. Case of identical SSD rates:

- (a) The M_{eff} distribution for the two points is very different and easily distinguishable.
- (b) As intended, the number of events in the SSD channel are nearly same $3b_{1C} : 3b_{S2} = 1.01$ for points 1C and S2. The $3b$ channel however, shows more events in the case of 1C ($\text{SSD}_{1C} : \text{SSD}_{S2} = 1.42$.) This is to be expected since the mass of the gluino is higher for S2 and therefore, the cross section

of $\tilde{g}\tilde{g}$ is lower. Also, the masses of $\tilde{t}_{1,2}$ and $\tilde{b}_{1,2}$ are higher resulting in higher p_T of b's in the final state and hence lower identification efficiency.

Thus we find the total cross sections for sparticle production are much lower for the case where only third family sfermions are accessible, making detection more challenging than the case where all three generations have masses ~ 1 TeV. However, the points in parameter space of cMSSM which mimic the scenario are characterised either by a very different effective mass distribution or very different rates in the leptonic channels. We can conclude that this scenario can be distinguished from a universal scenario with all three generations are accessible.

3.4 Summary

We investigate the signals of supersymmetry where only the third generation of squarks is accessible at the LHC, focussing on the special case when the gluino is heavier than a TeV and decays via on-shell squarks.

We show that same-sign dilepton signatures are particularly useful in probing the scenario in question, and complementary measurements in channels with multiple b-tagged jets can serve as an indicator of light third generation squarks. We also specifically study signatures with Higgs produced in cascade decays of the neutralinos and find that this particular branching fraction is highly correlated with the value of $\tan\beta$. Finally, we show that such scenarios can be easily distinguished from the universal cMSSM scenarios.

It should be noted that none of the benchmarks we probe lead to signals that can be currently ruled out at the LHC after collecting 1.04 fb^{-1} data (as it stands when this thesis is being written). The full impact of LHC data on the sector of third-generation squarks is obviously an important question to address. A low-scale analysis of the ATLAS data based on the phenomenological MSSM is presented in the next chapter.

CHAPTER

4

CONSTRAINTS ON THIRD GENERATION SQUARKS FROM LHC DATA

*“Captain, sensors show nothing out there. Absolutely nothing.”
– Data (Star Trek: The Next Generation)*

After the first year of running at a center-of-mass energy of $\sqrt{s} = 7$ TeV, the data for the first femtobarn-inverse data was released at the Lepton Photon 2011 conference. The supersymmetry search interpretations fall into two categories — the limits on cMSSM models and on “Simplified Models”. The first of these have the obvious limitation of relying on a very constrained model. The analysis based on Simplified Models relies on having a fixed hierarchy of particles and only one decay channel open at a time. Although, this does present a freedom from high-scale assumptions that are common in SUSY phenomenology, we find it ignores the complexity that arises from opening of new decay modes as sparticle masses increase. We therefore present a re-interpretation of the limits on SUSY particle masses in the jets+MET channels in terms of third generation squarks in the pMSSM model.

The best reach in superparticle masses at the LHC is expected in the channel with two or more hard jets and missing energy [27] which is the characteristic signature from $\tilde{g}\tilde{g}$ and $\tilde{q}\tilde{q}$ production. In particular, the simplest decays of the gluino and the squark,

viz. $\tilde{g} \rightarrow qq\tilde{\chi}_1^0$ and $\tilde{q} \rightarrow q\tilde{\chi}_1^0$ result in four and three-jet states (at parton-level) with large missing energy for the two production processes respectively. Similarly, the subdominant $\tilde{q}\tilde{q}^*$ and $\tilde{q}\tilde{q}$ production processes would result in two-jet final states. This parton-level prediction is not significantly altered even after initial and final state radiation. Therefore, looking for 2-4 jets with missing energy is known to be the best channel for SUSY searches. However, in the case that the first two generations of squarks are not accessible at the LHC (as can indeed be motivated from suppression of flavour changing neutral currents)[51, 52], the power of these searches would be dramatically reduced. Since the limits on the mass of third generation squarks in a cMSSM-based analysis follow simply from limits obtained from production and gluinos and squarks of the first two families, they cannot be considered truly indicative of the limit on stop and sbottom masses. We therefore reinterpret the ATLAS limits in the pMSSM model where the first two generations of squarks and all sleptons are decoupled (thereby also suppressing the three-body decays of the gluino mediated by these squarks).

Considerable interest has also grown in recent times in SUGRA with non-universal high-scale masses. A high-scale parametrisation has the advantage that the masses of several particles are obtained naturally through renormalisation group (RG) running. Here too, we focus of situations where the third family sfermions are within the reach of the LHC, while the first two families are heavy. This, among other things, helps in a natural suppression of FCNC. The advantage of this scenario will be to allow us to investigate the effect of a low-mass slepton sector without requiring its full pMSSM parametrisation. The phenomenology of third generation squarks has also been studied in various scenarios by [68, 78, 79, 80, 81, 82, 83, 84, 85, 86, 87, 88, 89, 90, 91, 92]. Naturalness of the higgs mass from SUSY has also been investigated in [93].

We base our study on the data from the ATLAS experiment for signatures with jets and missing energy with and without b-tagged jets [94, 95, 96, 97, 98]. These ATLAS analyses assumes an mSUGRA-type unification for the interpretation of its data. As mentioned above, the limits from this analysis cannot be applied to the third generation squarks in a model independent way. The results have been interpreted in terms of a high-scale non-universal model in [99]. However, its dependence on mSUGRA based mass hierarchies (e.g. the lighter stop \tilde{t}_1 is always right-handed, the lightest neutralino is mostly bino-like etc.) hampers full understanding of the implication of the experimental data on the third generation squark sector. We therefore perform a more detailed study by performing a low-scale pMSSM analysis with a scan over the physical stop/sbottom masses. We also include the case of stop decay via the flavour-violating decay $\tilde{t} \rightarrow c\tilde{\chi}_1^0$ [100, 101, 102] when all other decays are forbidden by kinematics.

4.1 Simulation of the signal and ATLAS exclusion curves in cMSSM

We simulate the signal using PYTHIA 6.4 [73] and all strong production cross sections are normalised to their next-to-leading order (NLO) values as obtained from Prospino 2.1 [103]. The renormalisation and factorisation scales are set to the average of masses in the final state of the hard scattering process. We follow the detector acceptance region for all reconstructed objects and apply all the cuts as described in the ATLAS papers.

The full set of identification and acceptance cuts is as follows:

- **Electrons:** (1) $p_T > 20$ GeV (2) $|\eta| < 2.47$ (3) Sum of p_T of particles within $\Delta R = \sqrt{(\Delta\eta)^2 + (\Delta\phi)^2} < 0.2$ should be less than 10 GeV (4) Event vetoed if electron found in $1.37 < |\eta| < 1.52$.
- **Muons:** (1) $p_T > 20$ GeV (2) $|\eta| < 2.4$ (3) Sum of p_T of charged tracks within $\Delta R = \sqrt{(\Delta\eta)^2 + (\Delta\phi)^2} < 0.2$ should be less than 1.8 GeV.
- **Jets:** (1) Formed using Anti-kt algorithm from Fastjet with parameter $R = 0.4$ (2) $p_T > 20$ GeV.
- **b-tagged jets:** A jet is b-tagged if a b-hadron falls within a cone of radius R from a jet. We have checked that this reproduced the 50 % tagging efficiency for $t\bar{t}$ samples as mentioned in [96].
- **Missing transverse energy** is calculated by summing over the p_T of all objects and all stable visible particles not belonging to any reconstructed objects but falling within $|\eta| < 4.9$ with $p_T > 0.5$ GeV.

To account for detector effects, we smear the momenta of leptons and jets obtained from the Monte Carlo generator according to

$$\frac{\sigma(E)}{E} = \frac{a}{\sqrt{E}} \oplus b \quad (4.1)$$

The values of a and b are (0.11, 0.007) for electrons, (0.03, 0.06) for muons and (1.0, 0.05) for jets¹. After smearing, we apply cuts used in each ATLAS analysis under consideration.

A cross-check of our analysis is the correct reproduction of the missing transverse energy (MET) and effective mass (M_{eff}) distributions and consequently the reproduction of the ATLAS exclusion curves [97, 96] in the context of mSUGRA. The online resources for the jets+MET analysis for 35 pb^{-1} [94] provide both the benchmark points

¹B. Mellado, private communication.

used in the scan as well as the efficiencies and cross sections at each of the points. We use this information to verify the correctness of our simulation. We present in Fig. 4.1, the final exclusion curves for the jets+MET analysis at 165 pb^{-1} which are obtained using the same acceptance and smearing parameters. We find that the “true” ATLAS curve lies in between our leading order (LO) and NLO curves in all cases.

Since we aim to determine the limits on third generation squarks, the limits on b-tagged events are of particular importance and are expected to provide much stronger limits. Therefore, reliable modelling of b-tagging is of prime importance in looking at these signals. The work reporting the analysis of b-jet+MET describes the performance of the b-tagging algorithm as having an efficiency factor of 50% for a $t\bar{t}$ sample. We reproduce this number by this simple algorithm: we first form jets using the anti- k_T algorithm using FASTJET 2.4 with the radius parameter $R = 0.4$ (for a definition of the parameter and the jet algorithm, please see [104]). A jet is assumed to be b-tagged if a b-hadron is found within a distance R from its axis. Since the correct reproduction of MET and M_{eff} has been verified from the non-b-tagged samples, we can see that this algorithm gives a reasonably correct b-jet tagging by looking at the bottom-right panel in Fig. 4.1. Here too, we find that the LO and NLO curves encapsulate the ATLAS curve reliably.

In all the above cases, we find that the LO curve only slightly underestimates the ATLAS limits. In the worst case, the difference between the LO limits and the ATLAS curve is within 20%. We therefore mostly present the LO mass limits in the subsequent study. Our LO results with simplistic detector simulation do not differ by more than 20% from what a full re-analysis of the data, including detector responses, would give. Our cross-checks on the mSUGRA results convince us such limits are adequate for putting across our main point, given the uncertainty of detector effects.

We use the results on jets+MET for 1.04 fb^{-1} and b-jets+MET results for 0.83 fb^{-1} for our analysis. As mentioned above, our simulation includes all the cuts in each of the channels under consideration. The benchmark points for our analyses are obtained using SUSPECT 2.41 [72]. To obtain the exclusion curves, we use the value of cross section times acceptance provided by the ATLAS analysis. The values corresponding to different channels taken from these ATLAS analyses are summarised in Table 4.1. The names of the signal regions are the same as those used in the respective ATLAS analyses.

We concentrate here only on signals without leptons in the final state. The primary reason for this is that we wish to investigate the third generation squark sector in as model independent a way as possible. Leptonic states generally result from decays on gauginos into gauge bosons or into sleptons which then decay into leptons. For a pMSSM study based on leptonic signatures, it would therefore be imperative to also include a completely general gaugino sector as well as a low-mass slepton sector. Since adding a completely phenomenological slepton sector means adding five new parame-

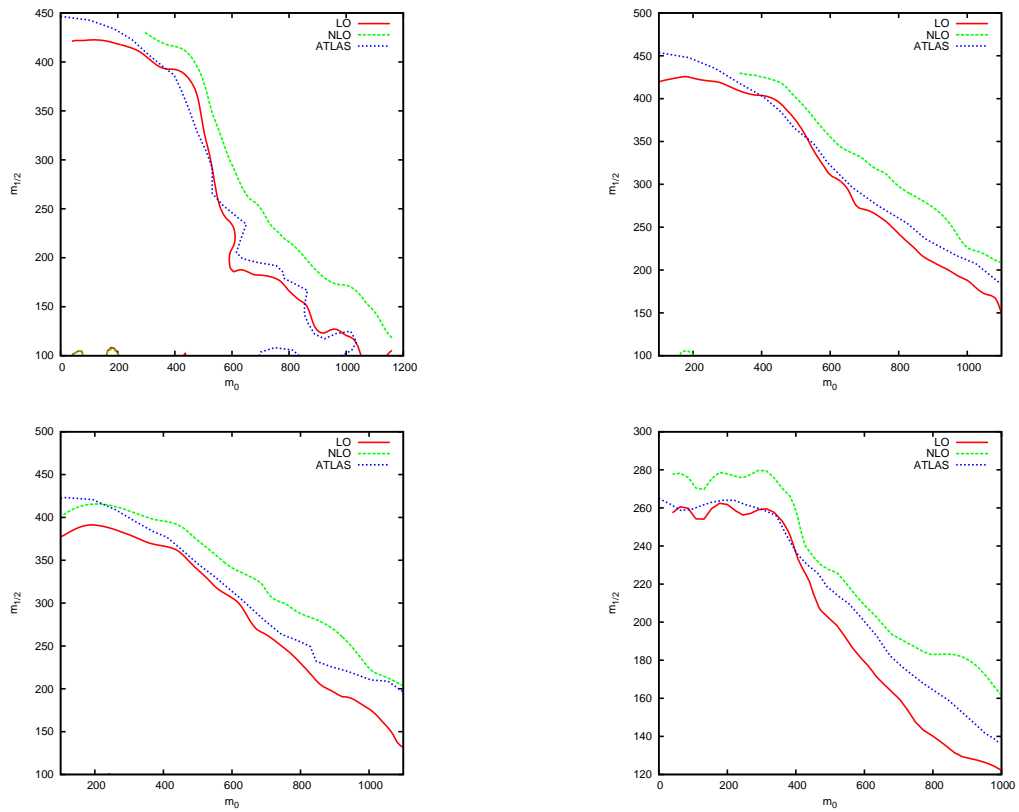


Figure 4.1: Comparison of our exclusion curves with the ATLAS exclusion curves. The panels represent: 2-jet with 165 pb^{-1} (top-left), 3-jet with 165 pb^{-1} (top-right), 4-jet with 165 pb^{-1} (bottom-left) and b-jet with 0-leptons with 35 pb^{-1} (bottom-right). The true ATLAS curve lies between our LO and NLO contours in all cases.

ters which complicate the analysis beyond too much, our low-scale analysis deals with a decoupled sleptonic sector. It is, in principle, possible that the limits obtained in the decoupled slepton limit are diluted when decays into sleptons (and hence leptons) are possible. We include the possibility of a low-mass slepton sector in section 4.4, where we use high-scale parametrisation and allow the RG running to determine the masses in the slepton sector. However, we shall see that allowing low-mass sleptons do not make significant difference to the limits for signatures based on jets and missing energy.

We perform our analysis retaining the cMSSM-like gaugino mass pattern $M_1 : M_2 : M_3 \simeq 1 : 2 : 6$. In general, for most gaugino mass patterns, we expect our results to remain fairly unchanged since our signal does not depend strongly on particles obtained from intermediate decays in SUSY cascades. However, we explicitly comment at the end of the paper on the extreme cases of gaugino mass patterns that would be likely yield results drastically different from ours.

It is also possible to ask what fraction of the pMSSM phase space is ruled out by current data. For the effect of the experimental limits on the full pMSSM space, we refer the reader to [105]. The effects on the cMSSM parameter space are addressed in, for example, [106, 107, 108, 109] whereas other interpretations of the recent LHC data on SUSY have been discussed in [110, 111, 112, 113].

| Channel | $\sigma \times acc$ (fb) |
|--|--------------------------|
| 2 jets + MET | 24 |
| 3 jets + MET | 30 |
| 4 jets + MET ($M_{\text{eff}} = 1$ TeV) | 32 |
| 1 btag + $M_{\text{eff}} > 500$ (3JA) | 288 |
| 1 btag + $M_{\text{eff}} > 700$ (3JB) | 61 |
| 2 btag + $M_{\text{eff}} > 500$ (3JC) | 78 |
| 2 btag + $M_{\text{eff}} > 700$ (3JD) | 17 |

Table 4.1: The values of cross section times acceptance from ATLAS analysis used for applying exclusion limits. The first set uses 1.0 fb^{-1} of data whereas the second uses 0.833 fb^{-1} of data. The names “3JA” etc. are the corresponding signal regions as defined in [98].

4.2 Parameterisation of the third generation sector

As mentioned earlier, we work in the pMSSM framework where the parameters are assigned at the low-scale. The program SUSPECT is used to ensure that electroweak symmetry breaking has correctly taken place and the spectrum is consistent. To start with, we retain the cMSSM-like gaugino mass ratios, correspond to $M_1 : M_2 : M_3 \simeq 1 :$

2 : 6 among the U(1), SU(2) and SU(3) gaugino masses. We discuss the effect of lifting this assumption in detail in section 4.5. The squark masses of the first two generations and all the slepton masses are set to 2 TeV which is beyond the reach of the 7 TeV LHC run. The stop and sbottom sector can each be described by three parameters – the two mass eigenstates and the mixing angle. We use these as the input parameters for the scan and use the diagonalisation to determine the left and right handed mass parameters of the pMSSM. The stop sector requires three parameters — the masses $M_{\tilde{t}_1}$ and $M_{\tilde{t}_2}$ and the stop mixing angle $\theta_{\tilde{t}}$. Using the stop mass-squared matrix diagonalisation condition

$$\begin{pmatrix} M_{\tilde{t}_1}^2 & 0 \\ 0 & M_{\tilde{t}_2}^2 \end{pmatrix} = \mathcal{R} \begin{pmatrix} M_{3Q}^2 & m_t X_t \\ m_t X_t & M_{TR}^2 \end{pmatrix} \mathcal{R}^{-1}; \quad \mathcal{R} = \begin{pmatrix} \cos \theta_{\tilde{t}} & \sin \theta_{\tilde{t}} \\ -\sin \theta_{\tilde{t}} & \cos \theta_{\tilde{t}} \end{pmatrix} \quad (4.2)$$

where $X_t = A_t - \mu \cot \beta$, we can use the low-scale masses $M_{\tilde{t}_1}$, $M_{\tilde{t}_2}$ and $\theta_{\tilde{t}}$ as the input parameters which uniquely determine A_t given μ and $\tan \beta$. The left handed sbottom mass is expected to be close to the left handed stop mass since they are derived from the same parameter (M_{3Q}) in the low-scale pMSSM model. The right handed sbottom mass and A_b can then be set depending on the requirement of $M_{\tilde{b}_1}$, $M_{\tilde{b}_2}$ and $\theta_{\tilde{b}}$.

Assuming that the third generation squarks and the gluino are the only strongly charged superparticles accessible at the LHC, we investigate in particular, the following cases:

- Case A: $\sin \theta_{\tilde{t}} = 0.99$ i.e. $\tilde{t}_1 \simeq \tilde{t}_R$ is the lightest squark. This is commonly the case in cMSSM models. We also set $M_{\tilde{b}_1} \simeq M_{\tilde{t}_2} \simeq M_{\tilde{b}_2} = M_{\tilde{t}_1} + 500$ GeV, which makes the sbottom sector somewhat heavier than the lighter stop. We scan the parameter space in $M = M_{\tilde{t}_1}$.
- Case B: $\sin \theta_{\tilde{t}} = 0.01$ i.e. $\tilde{t}_1 \simeq t_L, \simeq \tilde{b}_1 \simeq \tilde{b}_L$. The lightest stop and sbottom are nearly degenerate and mostly left handed. $M_{\tilde{t}_2} \simeq M_{\tilde{b}_2} = M_{\tilde{t}_1} + 500$ GeV. We scan the parameter space in $M = M_{\tilde{t}_1} = M_{\tilde{b}_1}$.
- Case C: $\tilde{b}_1 \simeq \tilde{b}_R$ is the lightest squark. $M_{\tilde{b}_2} \simeq M_{\tilde{t}_1} \simeq M_{\tilde{t}_2} = M_{\tilde{b}_1} + 500$ GeV with $\sin \theta_{\tilde{t}} = 0.70$ and $\sin \theta_{\tilde{b}} = 0.99$. We scan the parameter space in $M = M_{\tilde{b}_1}$.
- Case D: $M_{\tilde{t}_1} \simeq M_{\tilde{b}_1} \simeq M_{\tilde{t}_2} \simeq M_{\tilde{b}_2}$. This is the case of maximal mixing in both stop and sbottom sectors. The most stringent limits on the light third family scenario will arise for this particular case, as it allows all four squarks to be produced with similar cross sections. The scan in this case is over the common mass of all the third generation squarks.

In each case, we are now able to perform a scan over the $M - M_2$ plane, where M is the mass of \tilde{t}_1 in cases A, B and D and \tilde{b}_1 in the case C. The Tevatron reach for searches in the $\tilde{t}_1 \rightarrow c\tilde{\chi}_1^0$ rule out stop masses up to 180 GeV [114]. We therefore start our search at $M_{\tilde{t}_1} = 200$ GeV and scan up to 2 TeV. Also, since we assume gaugino

| Parameter | Scan range |
|-------------------|--------------------------|
| $M_{\tilde{t}_1}$ | 100 - 2000 GeV |
| M_2 | 150 - 600 GeV |
| $\tan \beta$ | 5, 10, 40 |
| μ | -200, 200, 500, 1000 GeV |

Table 4.2: The parameters of the scan in $M_{\tilde{t}_1}$ - M_2 space.

mass unification, we use the chargino mass limits from Tevatron ($M_{\tilde{\chi}_1^\pm} > 164$ GeV) to start our scan at $M_2 = 150$ GeV and vary M_2 up to a value of 600 GeV which would correspond to gluino mass of 1.8 TeV and therefore cover the entire range of masses reachable at the 7 TeV run of the LHC. We fix $M_A = 400$ GeV and perform this scan for 12 combinations of 3 values of $\tan \beta$ and 4 values of μ , which are listed in Table 4.2.

4.3 Results

The hierarchy among M_1 , M_2 and μ determines the composition of the neutralino and chargino sector and therefore has strong effects on the limits. In particular, for cases with low values of μ , the lightest neutralino has a significant higgsino fraction. When M_2 becomes large enough, the states $\tilde{\chi}_1^0$ and $\tilde{\chi}_1^\pm$ become higgsino dominated and their masses remain close to the value of μ . In this case, the masses and compositions of $\tilde{\chi}_1^0$, $\tilde{\chi}_1^\pm$, $\tilde{\chi}_2^0$ are not affected by changes in the value of M_2 , so long it is considerably larger than μ . For large μ , on the other hand, the allowed decays of the squark will depend strongly on M_2 up to very large values. Therefore, we expect that for low squark masses and μ low with respect to M_2 , the exclusion contour is relatively insensitive to M_2 . This can clearly be seen in figure 4.2 and best illustrated in the fourth panel corresponding to Case-D. Here, the production cross section is high because all four third generation squarks are degenerate. Moreover, it can clearly be seen that $\mu = -200$ and 200 both lead to large exclusion in M_2 for small masses. The effect is similar also in the panel corresponding to Case-B. The third panel, corresponding to sbottom being the lightest shows minimal change with changing μ . This is mostly because the decay $\tilde{b}_1 \rightarrow b\tilde{\chi}_1^0$ is always open irrespective of μ due to the small mass of the b-quark. Thus, the sensitivity to μ is reduced.

To estimate the effect of enhancement due to NLO corrections in the production cross section, we present the comparison of LO and NLO curves for each case with $\tan \beta = 10$ and $\mu = 500$ GeV in Fig. 4.3. The large k-factors (~ 2.5) in most of the parameter space result in much stronger limits from the NLO curves. However, taking note of the results of our cMSSM limits in Section 4.1, where the LO limits are closer

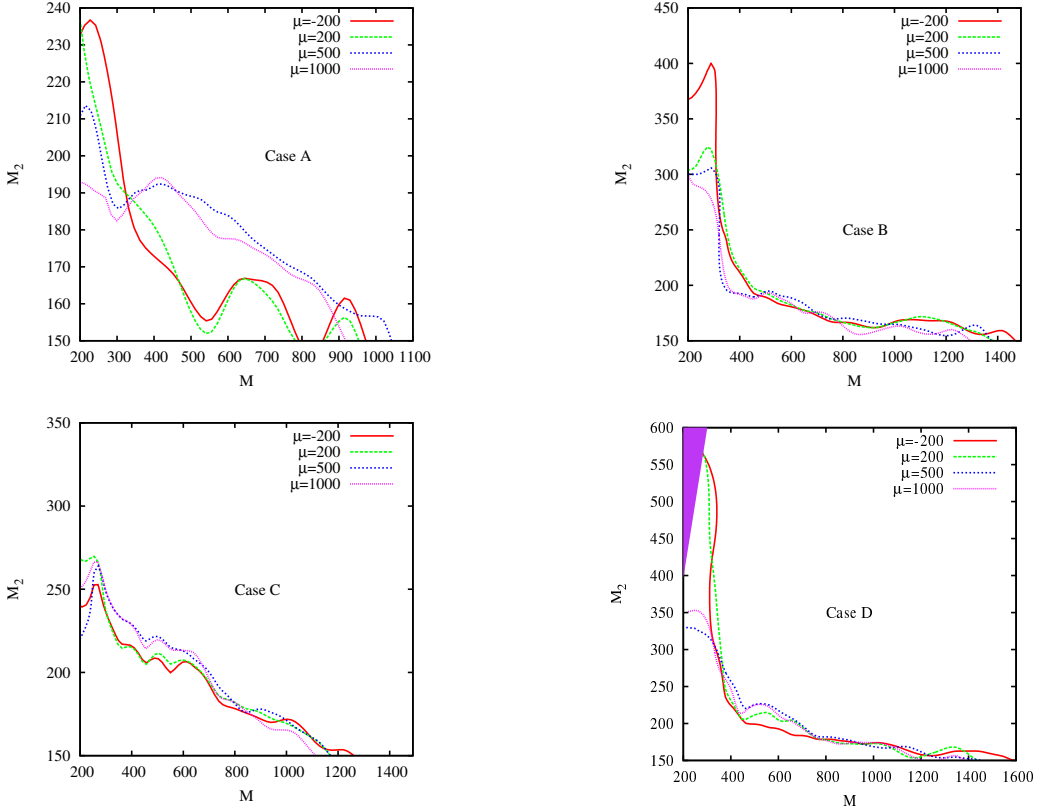


Figure 4.2: The dependence of the exclusion curves on different values of μ for $\tan\beta = 10$. The least dependence is for the case where the sbottom is the lighter squark. The shaded region at the top in the fourth panel corresponds to stop LSP and is therefore ruled out. The x-axis refers to $M_{\tilde{t}_1}$ for Cases A, B and D and $M_{\tilde{b}_1}$ for Case C.

to actual ATLAS limits, we take the conservative approach of presenting LO limits for most of our study.

4.3.1 Case A

This is the case closest to mSUGRA-type models where \tilde{t}_1 is the lightest squark. The primary production processes in this case are $\tilde{g}\tilde{g}$ and $\tilde{t}_1\tilde{t}_1^*$. Since our scan starts with $M_2 = 150$ GeV, i.e. a gluino mass of 450 GeV, the decay $\tilde{g} \rightarrow t\bar{t}\tilde{\chi}_1^0$ is always open and forms the dominant decay mode. In the low mass regions which are probed by the LHC data, the dominant decay mode of the \tilde{t}_1 depends on the mass hierarchy of \tilde{t}_1 , $\tilde{\chi}_1^0$ and $\tilde{\chi}_1^+$. Since we are working in R-parity conserving models, we disallow the region where the lighter stop is the lightest supersymmetric particle (LSP) i.e. the region where $M_{\tilde{t}_1} < M_{\tilde{\chi}_1^0}$. Following this, the hierarchy $M_{\tilde{\chi}_1^0} < M_{\tilde{t}_1} < M_{\tilde{\chi}_1^+}$ results in the case of

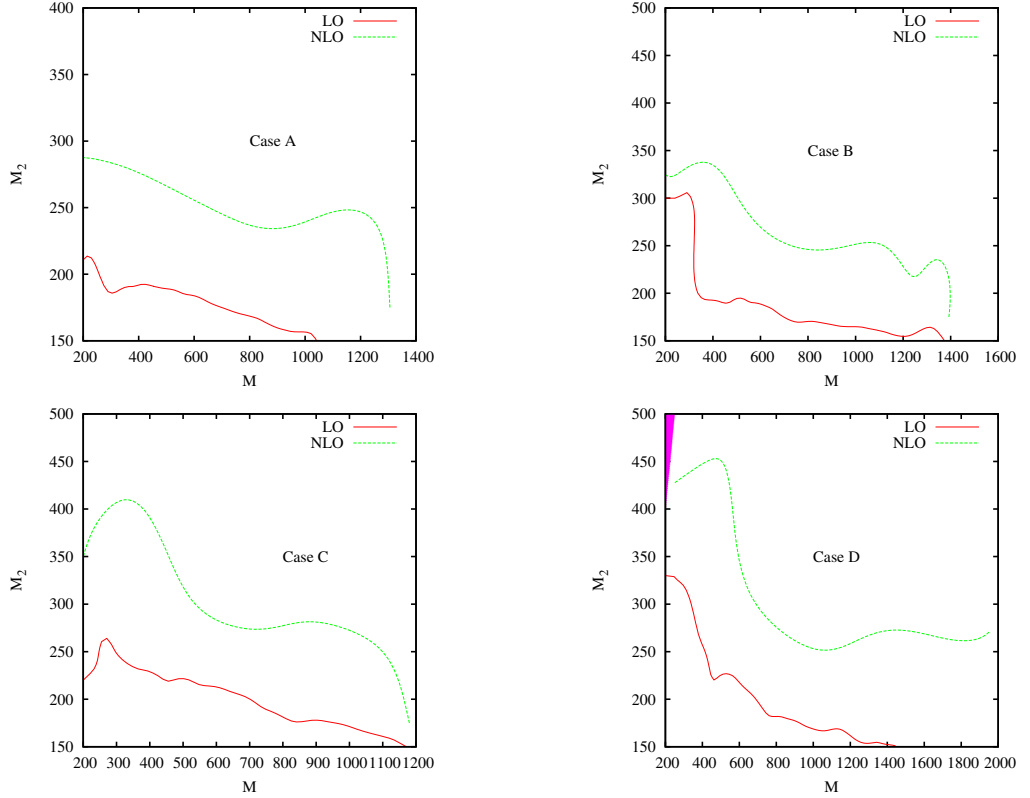


Figure 4.3: Comparison of LO and NLO exclusion curves for Cases A, B, C and D, illustrated for values $\tan\beta = 10$ and $\mu = 500$ GeV. The x-axis refers to mass of the lightest third generation quark in each case, as discussed in the text.

stop NLSP (next-to-LSP). The dominant mode is $\tilde{t}_1 \rightarrow t\tilde{\chi}_1^0$ if $M_{\tilde{t}_1} > M_t + M_{\tilde{\chi}_1^0}$. In the remaining region which satisfies $M_{\tilde{t}_1} < M_t + M_{\tilde{\chi}_1^0}$ and $M_{\tilde{t}_1} < M_b + M_{\tilde{\chi}_1^+}$, we expect \tilde{t}_1 to decay via three- or four-body decays or via the mode $\tilde{t}_1 \rightarrow c\tilde{\chi}_1^0$. For this work, we assume that this last mode dominates over the three or four body decays. Finally, in the case where $M_{\tilde{t}_1} > M_b + M_{\tilde{\chi}_1^+}$, the decay into $b\tilde{\chi}_1^+$ is also open. For larger stop masses, decays into other neutralinos, second chargino or gluino may also open.

The effect of various values of $\tan\beta$ for two values of μ are shown in Fig. 4.4. The exclusion curves show minor dependence on $\tan\beta$. We find that for low values of μ , low $\tan\beta$ results in a larger reach in M_2 whereas high $\tan\beta$ results in a larger reach in $M_{\tilde{t}}$. This trend is reversed for large values of μ , as can be seen in the panel corresponding to $\mu = 500$ GeV of Fig. 4.4. However, it must be reiterated, that this variation cannot be considered experimentally significant due to the uncertainties on the exclusion curves in our analysis.

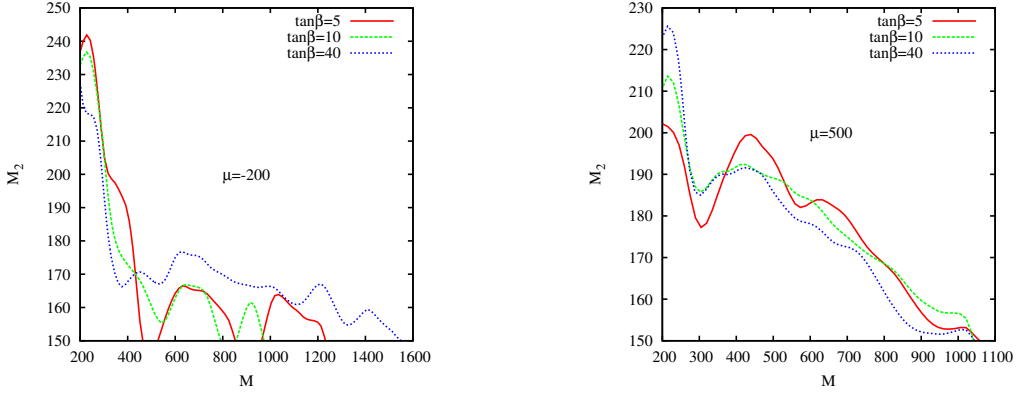


Figure 4.4: Exclusion curves for Case-A (stop lightest scenario). The x-axis refers to the mass of \tilde{t}_1 squark.

4.3.2 Case B

In this case, the \tilde{t}_1 and \tilde{b}_1 form a degenerate pair of lightest squarks. They are both primarily left handed and therefore have an enhanced coupling to wino-like states. Again, due to the requirement of neutral dark matter candidate, we disallow any region with stop or sbottom LSP. The decays of the lighter stop are similar to those in case A. The decay of the lighter sbottom into $b\tilde{\chi}_1^0$ is almost always allowed and will form the dominant decay for most of the low mass region. In cases of large μ , where $M_{\tilde{\chi}_2^0} \simeq M_2$, the decay $\tilde{b}_1 \rightarrow b\tilde{\chi}_2^0$ will dominate over $\tilde{b}_1 \rightarrow b\tilde{\chi}_1^0$ and similarly for stop decays. The decay $\tilde{b}_1 \rightarrow t\tilde{\chi}_1^+$ is relatively disfavoured due to large top mass. The gluino decays dominantly to $b\bar{b}\tilde{\chi}_1^0$ in the region $M_{\tilde{g}} < M_{\tilde{b}_1}$ and to $b\tilde{b}_1$ otherwise. The decays to corresponding top-sector are again disfavoured due to large top mass.

The dependence of the exclusion curves on $\tan\beta$ is shown in Fig. 4.5. For the case of $\mu = -200$ GeV and $\tan\beta = 5$, we find that \tilde{t}_1 and \tilde{b}_1 up to 300 GeV are ruled out for gluino masses up to 700 GeV. The region just below the \tilde{t}_1 or \tilde{b}_1 -LSP region is still allowed, as the near-degeneracy of their mass and the mass of the LSP results in a low missing energy and M_{eff} spectrum which does not satisfy the hardness cuts imposed.

4.3.3 Case C

This case considers the situation where both the stop states are heavier than the lightest sbottom state. The primary production processes are $\tilde{g}\tilde{g}$ and $\tilde{b}_1\tilde{b}_1^*$. As before, we disallow the region $M_{\tilde{b}_1} < M_{\tilde{\chi}_1^0}$. The region $M_{\tilde{\chi}_1^0} < M_{\tilde{b}_1} < M_{\tilde{\chi}_1^+}$ corresponds to a \tilde{b}_1 -NLSP with the dominant decay $\tilde{b}_1 \rightarrow b\tilde{\chi}_1^0$. The gluino dominantly decays via $b\bar{b}\tilde{\chi}_1^0$ in the region $M_{\tilde{g}} < M_{\tilde{b}_1}$ and to $b\tilde{b}_1$ otherwise. This case is the closest to the scenarios considered by the ATLAS collaboration for the interpretation of their b-jet and missing

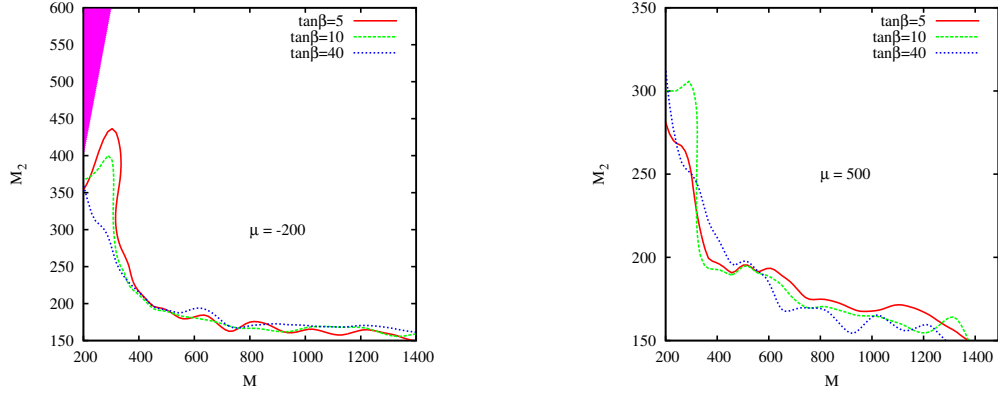


Figure 4.5: Exclusion curves for Case-B (left-handed degenerate stop and sbottom scenario). The x-axis refers to the common mass of \tilde{b}_1 and \tilde{t}_1 squarks. The shaded region at the top in the fourth panel corresponds to stop/sbottom LSP and is therefore ruled out.

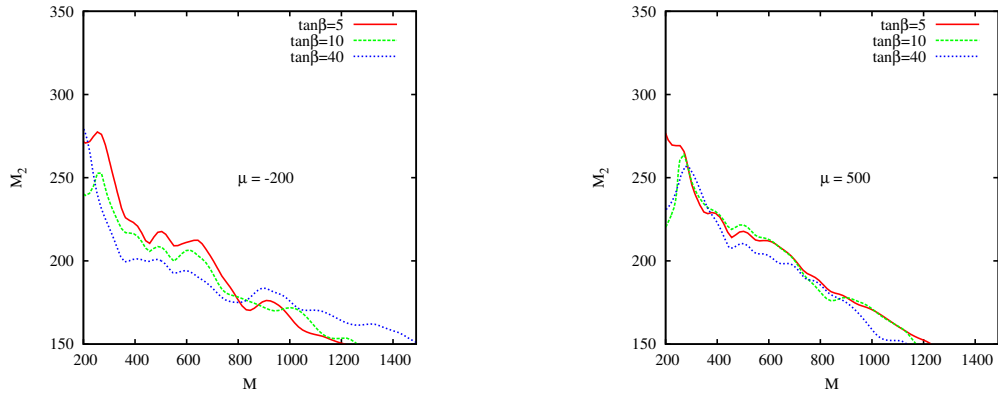


Figure 4.6: Exclusion curves for Case-C (sbottom lightest scenario). The x-axis refers to the mass of \tilde{b}_1 squark.

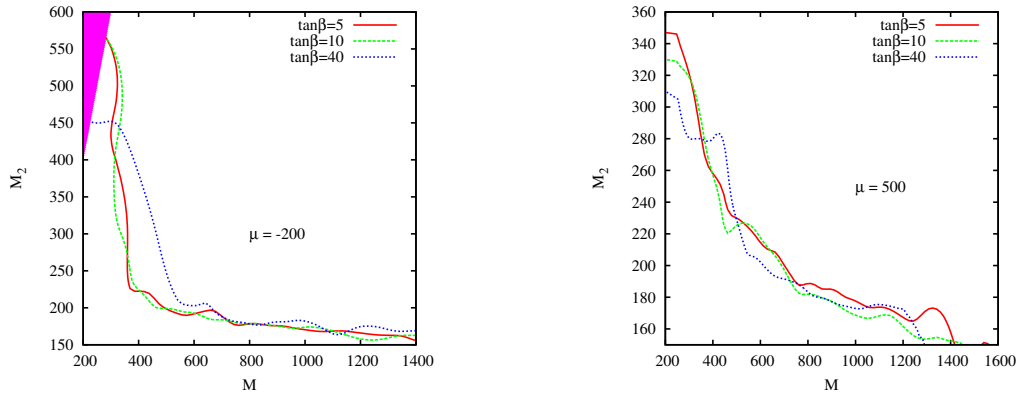


Figure 4.7: Exclusion curves for Case-D (maximal mixing scenario). The x-axis refers to the common mass of all the third generation squarks. The shaded region at the top corresponds to stop LSP and is therefore ruled out.

energy searches [98]. They split their analysis into a case where they disallow any three body decays of the gluino via $\tilde{g} \rightarrow b\bar{b}\tilde{\chi}_1^0$ and the case of a simplified model where there are no two-body decays but all decays are via this channel. According to the first case, they rule out gluino masses up to 720 GeV for \tilde{b}_1 masses up to 600 GeV [98]. As can be seen from Fig. 4.6, for $\tilde{b}_1 = 600$ GeV, we rule out $M_{\tilde{g}} < 570-660$ GeV for $\mu = -200$ and $M_{\tilde{g}} < 600-660$ GeV for $\mu = 500$ GeV.

4.3.4 Case D

In the maximal mixing scenario in both the stop and sbottom sector, all four squarks of the third generation have nearly degenerate masses. Therefore the production cross section is maximum for this scenario and the limits are strongest. The decay scheme for the sbottom is same as in Case B whereas for the stop, it is the same as in Case A. The gluino can now decay both via stops or sbottoms, but the large mass of the top means it decays preferentially via $b\bar{b}_i$ channels. As expected, low μ results in large exclusion in M_2 for low squark masses. The dependence of the limits on $\tan\beta$ is shown in Fig. 4.7. The case for $\mu = -200$ GeV (and similarly $\mu = 200$ GeV) result in an exclusion of third generation squark masses of 280 GeV for all allowed values of M_2 . This case is similar to the one considered in [91], where, for naturalness requirements they require \tilde{t}_R, \tilde{t}_L and \tilde{b}_L to be degenerate and assume a Higgsino LSP. Their limits on the mass of the third generation squarks lie between 200-300 GeV.

The exclusion limits for the case of $\mu = 500$ GeV does not show any exclusions that are independent of gaugino (and hence gluino) masses. The third-generation squark masses are completely un-constrained for $M_{\tilde{g}} > 1$ TeV. Whereas, the approximate requirement for naturalness that $M_{\tilde{t}_1} < 500$ GeV would translate into $M_{\tilde{g}} > 600$ GeV.

In conclusion, among the four cases discussed above, only the case with degenerate third-generation squarks and low- μ leads to mass limits independent of gluino mass – that of 280 GeV. In most other cases, we find that limits depend strongly on the composition of the neutralinos and charginos. The case where only \tilde{t}_1 is accessible is the least constraining, mainly due to low production cross sections compared to the other cases. For the case where the LSP is almost a pure Bino (high- μ), $M_{\tilde{t}_1} = 200$ GeV is ruled out for a gluino mass less than 570 GeV. Taking into account all values of μ and $\tan\beta$, $M_{\tilde{t}_1} = 200$ GeV is ruled out for gluino masses in the range 570 – 720 GeV.

The case of lightest third generation squark being \tilde{b}_1 is the most insensitive to variations of both μ and $\tan\beta$. For this case, our limits are consistent with ATLAS's own interpretations within 10%. $M_{\tilde{b}_1} = 200$ GeV is ruled out for gluino masses between 680 – 820 GeV. The case of degenerate left-handed squarks rules out $M_{\tilde{t}_1} = M_{\tilde{b}_1} = 200$ GeV for gluino masses in the range 900 – 1050 GeV. And finally, the case with all squarks degenerate rules out $M_{\tilde{t},\tilde{b}} = 200$ for $M_{\tilde{g}} < 900$ GeV in the worst case, and for all gluino masses in the best case.

4.4 High-scale non-universal scalar scenarios

Besides the low-scale study done in the previous section, it is also possible to perform a scan over high-scale parameters. The advantage of a high-scale analysis is that the hierarchy of the particles is uniquely and consistently determined from the renormalisation group (RG) running of masses to low scale from given high-scale parameters. We use the simplification afforded by this model to include the effects of slepton sector in our analysis.

It is possible that the limits described in the previous section are diluted if slepton masses are allowed to be light. This is because the gauginos would then decay predominantly to sleptons resulting in leptonic final states which would be discarded since all the analyses considered here have a lepton veto. Including the full lepton sector in the low-scale pMSSM requires five more parameters and makes a general study far more complicated. We therefore leave a fully model independent investigation of interpreting the ATLAS limits involving a low mass slepton sector to a future work. However, we partially answer the question as to whether the limits are diluted by studying some illustrative cases, as described below.

Even though the soft-scalar masses may in principle take separate values, the constraints from flavour changing neutral currents (FCNC) from meson decays dictate that the first two generation squarks remain degenerate. Similarly, absence of decays like $\mu \rightarrow \gamma e$ means that the masses of first two generations of sleptons also have to degenerate. Therefore we can consider three schemes of non-universality:

- **Case HA:** Third generation squarks are lighter than all other sfermions. This will

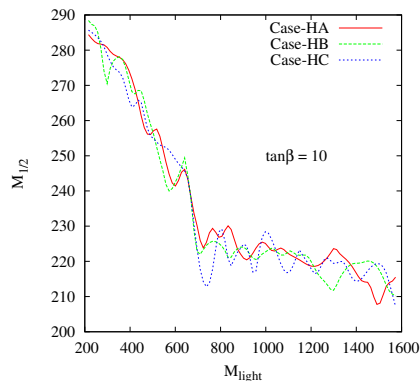


Figure 4.8: Comparison of exclusion curves from three high-scale non-universal scenarios. All cases agree with each other within statistical uncertainties.

lead to a hierarchy similar to Case A in the preceding analysis.

- **Case HB:** Third generation squarks and sleptons are lighter than all other sfermions. This leads to light staus and tau-sneutrinos. Possibly, this would lead to $b\tau$ final states which have been studied in [115].
- **Case HC:** Third generation squarks and all sleptons are light. Comparing the limits in this case to those in Case HA will answer the question of dilution of limits due to leptonic signatures.

As in the previous analysis, we retain the cMSSM-like gaugino masses. We now have two mass scales in the scalar sector – the scale of heavy, decoupled particles ($M_{\text{heavy}} = 2 \text{ TeV}$) and the scale of light scalars (M_{light}). We once again assume that the gaugino sector follows the universal structure and we set the higgs mass parameters for the two higgs doublets to be same as M_{light} . The parameters are all set at the grand unified theory (GUT) scale and the TeV-scale values are determined by RG running using the program SUSpect. The exclusion curves obtained for the three cases are shown in Fig. 4.8 for a value of $\tan\beta = 10$. The results for values of $\tan\beta = 5, 40$ are similar. We do not see any significant difference among the exclusion curves for the various high-scale cases. This can be interpreted as the robustness of the 0-lepton signals against different slepton masses and justifies the assumption of decoupled slepton masses made in the previous section.

4.5 Caveat: Non-universality in the gaugino sector

One may also question the assumption of the gaugino mass pattern of $M_1 : M_2 : M_3 \simeq 1 : 2 : 6$. We can expect the case of right-handed sbottom being the lightest of the third generation to be fairly independent of the assumption of gaugino mass pattern since the only dominant decays are $\tilde{b}_1 \rightarrow b\tilde{\chi}_1^0$ and $\tilde{g} \rightarrow b\bar{b}\tilde{\chi}_1^0$, and both are always allowed (except for very compressed spectra). We would expect significant deviations from the stop limits when, for example, the decay $\tilde{t}_1 \rightarrow b\tilde{\chi}_1^+$ is largely inaccessible because both M_2 and μ are so high that the charginos are generally heavier than the stop. In this case, the dominant decay for most of the parameter space would be $\tilde{t}_1 \rightarrow t\tilde{\chi}_1^0$. In the current study, regions where the $t\tilde{\chi}_1^0$ decay was kinematically disallowed was still largely covered by the $b\tilde{\chi}_1^+$ decay, thus leaving only a small region of parameter space corresponding to the flavour violating decay. However, in the absence of the decay into a chargino, one would need to examine in detail, the relative strengths of the (highly model-dependent) flavour-violating decay $\tilde{t}_1 \rightarrow c\tilde{\chi}_1^0$ and the three-body decay of the stop. In other cases, where the stop still decays via standard channels, we do not expect significant deviations from our limits.

4.6 Summary

We have investigated the consequences of the recent ATLAS data in channels with (b-) jets and missing energy on the limits on the mass of the third generation squarks. We work in the pMSSM framework, with TeV-scale parameters, without requiring a high-scale breaking scheme. For obtaining relatively model independent limits on the third generation squark masses, we decouple the first two squark generations as well as all sleptons. We also explicitly show that decoupling of sleptons is not likely to affect the limits as long as we work with 0-lepton signatures. We find that a stop of mass 200 GeV can be ruled out for a gluino mass of 570 GeV in the least constraining case whereas a stop of mass 500 GeV is allowed for gluino masses upward of 450-880 GeV depending on the structure of the third-generation squark sector, and the parameters μ and $\tan\beta$. In the case where all third generation squarks are degenerate, we can rule out masses less than 280 GeV for $|\mu| \leq 200$ GeV, independent of the gluino mass.

CHAPTER

5

R-PARITY VIOLATING RESONANT TOP SQUARK PRODUCTION

It is better to be alone than in bad company.
– George Washington

In the two previous chapters, we have considered SUSY models with conserved R-parity. The consequence of this is that (a) sparticles are always produced in pairs — which means we require a larger CM energy to produce them in significantly large number of events, and (b) the lightest of SUSY particles is always stable — which makes it a component of dark matter; thus requiring it to be charge-neutral and leads to signatures with large missing momentum at the LHC. The relaxation of R-parity requirements would in turn mean that single sparticles can be produced resonantly and moreover, there would be no stable sparticles and no massive, invisible momentum carriers. In this chapter, we investigate the detection of top squarks in such a scenario.

The current structure of the standard model, with gauge invariance and renormalisability built in, implies automatic lepton and baryon number conservation. This is no longer true in the supersymmetric extension of the SM [36, 37], where scalars carrying baryon or lepton number are present. Thus the MSSM superpotential, namely

$$\mathcal{W}_{MSSM} = h_{ij}^d Q_i D_j^c H_d + h_{ij}^u Q_i U_j^c H_u + h_{ij}^l L_i E_j^c H_d + \mu H_u H_d \quad (5.1)$$

can in principle be augmented to include

$$\mathcal{W}_{RPV} = \mu_i L_i H_u + \lambda_{ijk} L_i L_j E_k^c + \lambda'_{ijk} L_i Q_j D_k^c + \lambda''_{ijk} U_i^c D_j^c D_k^c \quad (5.2)$$

which contain terms that are gauge invariant and renormalisable but explicitly violate lepton or baryon number. Here, $L(E)$ is an $SU(2)$ doublet (singlet) lepton superfield and $Q(U,D)$ is (are) an $SU(2)$ doublet (singlet) quark superfield(s). H_u and H_d are the two Higgs doublet superfields, μ is the Higgsino parameter and (i, j, k) are flavour indices. Each term in equation (5.2) violates R-parity, defined as $R = (-1)^{3(B-L)-2S}$ (where B is baryon number, L is lepton number and S is spin), against which all SM particles are even whereas all superpartners are odd. The consequence of violating R-parity is that superpartners need not be produced in pairs anymore, and that the lightest superparticle (LSP) can now decay. The strongest argument for studying R-parity violation is that it does not arise as an essential symmetry of MSSM. However, the requirement of suppressing proton decay prompts one to allow *only one* of B and L to be violated at a time.

The collider phenomenology in the absence of R-parity may be very different from that of the usual R-parity conserving MSSM. In particular, if the R-parity violating (RPV) couplings are large enough, the LSP will decay within the detector and one can no longer assume a large missing- E_T (from heavy invisible particles) as a convenient discriminator. Although studies have taken place on such signals, closer looks at them are often quite relevant in the wake of the LHC. In particular, it is crucial to know the consequences of broken R-parity in the production of sparticles. Here we perform a detailed simulation in the context of the LHC, highlighting one possible consequence of the B-violating term(s), namely, the resonant production of a squark—in this case, the stop.

Many of the RPV couplings have been indirectly constrained from various decay processes, including rare and flavour-violating decays and violation of weak universality. The constraints derived are of two general kinds—those on individual RPV couplings, assuming the existence of a single RPV term; and those on the products of couplings when at least two terms are present, which contribute to some (usually rare) process. The constraints obtained so far are well-listed in the literature[116].

The L-violating terms are relatively well-studied, partly because of their potential role in generating neutrino masses and are constrained by indirect limits. In comparison, the baryon-number violating couplings are relatively unconstrained. $\lambda''_{112,113}$ are constrained from double nucleon decay and neutron-antineutron oscillations[117, 118, 119]. The rest of the couplings are constrained only by the requirement that they remain perturbative till the GUT scale. Limits on λ''_{3ij} type of couplings due to the ratio of Z-boson decay widths for hadronic versus leptonic final states have been calculated for a stop mass of 100 GeV [120]. However, the results do not restrict the couplings for high

stop masses of concern here. The coupling λ''_{3jk} is thus practically unconstrained for large stop masses. It is also known that mixing in the quark sector causes generation of couplings of different flavour structures and can therefore be constrained by data from flavour changing neutral currents(FCNC)[121]. Such effects arising from mixing in the quark and squark sector can affect the contribution of R-parity violation to physical process and alter the limits[122]. However these effects are model dependent and have not been taken into account here.

It has been already noticed that such large values of λ' -type couplings as are still allowed, not only cause the LSP to decay, but also lead to resonant production of squarks via quark fusion at the LHC. The rate of such fusion can in fact far exceed that of the canonically studied squark-pair production. One would therefore like to know how detectable the resonant process is at the LHC. Furthermore, one needs to know the search limits in different phases of the LHC, and how best to handle the backgrounds, both from the SM and the R-conserving SUSY processes. These are some of the questions addressed in this paper.

Single stop production, mostly in the context of the Tevatron, was studied in detail in [123, 124, 125, 126]. A full one-loop production cross section can be found in [127]. A study of SUSY with the LSP decaying through baryon-number violating couplings and therefore giving no missing energy was done in [128]. Further studies on determining the flavour structure of baryon number violating couplings and possible mass reconstruction following specific decay chains can be found in [129, 130]. There have also been recent studies on possible LSPs [131] and identification of R-parity violating decays of the LSP using jet substructure methods [132]. A recent study on identification of stop-pair production via top-tagging using jet-substructure can be found in [133].

We find, however, that the earlier studies on resonant stop production are inadequate in the context of the LHC. We improve upon them in the following respects:

- In the work done for the Tevatron, the sparticle masses were required to be less than 500 GeV to be within reach. Thus, the gluino was also required to be much lighter than a TeV to avoid large radiative corrections to squark masses. This implied that in the constrained MSSM (cMSSM) [45] scenario, the LSP, assumed to be the lightest neutralino ($\tilde{\chi}_1^0$), had to have mass less than 100 GeV. If we allow only the term proportional to λ''_{3ij} , the only three-body decay of $\tilde{\chi}_1^0$ is $\tilde{\chi}_1^0 \rightarrow \bar{t}\bar{d}_i\bar{d}_j(tds)$. Since the neutralino is much lighter than the top, it can decay only via a 4-body decay and therefore has long lifetime and decays outside the detector for all allowed values of λ''_{3ij} [134]. Thus, one still has the canonical missing- E_T signature. This was one of the main assumptions in[124]. However, if the stop mass is beyond the Tevatron reach but within the reach of the LHC, we may indeed have lightest-neutralino mass high enough to allow decay within the detector.
- For a light stop, the only available R-parity conserving decay modes are into the lightest neutralino($\tilde{\chi}_1^0$) and lighter chargino($\tilde{\chi}_1^\pm$) i.e. $\tilde{t} \rightarrow t\tilde{\chi}_1^0, b\tilde{\chi}_1^\pm$. For stop mass

near a TeV, the decay modes into higher neutralinos and the heavier chargino may open up, leading to different final states. We have found that this drastically improves the detectability of the signature over the SM backgrounds.

- We have taken into account all the potential backgrounds at the LHC, including those from $t\bar{t} + jets$, $Wt\bar{t} + jets$, $Zt\bar{t} + jets$, which pose little problem at the Tevatron. A detailed investigation towards reducing these backgrounds has been reported in the present study.

5.1 Resonant stop production and decays

5.1.1 Stop production

The resonant stop production process depends on B-violating couplings proportional to λ''_{3ij} , and also on fraction of the right-chiral eigenstate (\tilde{t}_R) in the mass eigenstate concerned. The corresponding term in the lagrangian is

$$\begin{aligned}\mathcal{L} &= -2\epsilon^{lmn}\lambda''_{3ij}\{\tilde{t}_{Rl}\bar{d}_{im}^c P_R d_{jn} + \text{h.c.}\} \\ &= -2\epsilon^{lmn}\lambda''_{3ij}\{(\sin\theta_{\tilde{t}}\tilde{t}_{1l} + \cos\theta_{\tilde{t}}\tilde{t}_{2l})\bar{d}_{im}^c P_R d_{jn} + \text{h.c.}\}\end{aligned}\quad (5.3)$$

We concentrate on the production of \tilde{t}_1 since the lighter stop eigenstate usually has a higher fraction of \tilde{t}_R . The resonant production cross section is given by

$$\begin{aligned}\sigma_{\tilde{t}_1} &= \frac{2\pi\sin^2\theta_{\tilde{t}}}{3m_{\tilde{t}}^2} \times \\ &\sum_{i,j} |\lambda''_{3ij}|^2 \int dx_1 dx_2 [f_i(x_1)f_j(x_2) + f_i(x_2)f_j(x_1)] \delta(1 - \frac{m_{\tilde{t}_1}}{\sqrt{\hat{s}}})\end{aligned}\quad (5.4)$$

where $\sin\theta_{\tilde{t}}$ is the amplitude of finding a \tilde{t}_R in \tilde{t}_1 , f_i is the proton parton distribution function for a parton of species i and $x_{(1,2)}$ are the momentum fractions carried by the respective partons. Out of the three possible λ'' couplings, contributions via λ''_{313} and λ''_{323} are suppressed due to the small fraction of b quarks in the proton. We therefore look at the production of top (anti) squark through the fusion of the d and s (anti)quarks, via the coupling λ''_{312} . Since the actual cross section for production of the lightest stop depends on the mixing angle via $\sin^2\theta_{\tilde{t}}$, it is useful to define the cross section in terms

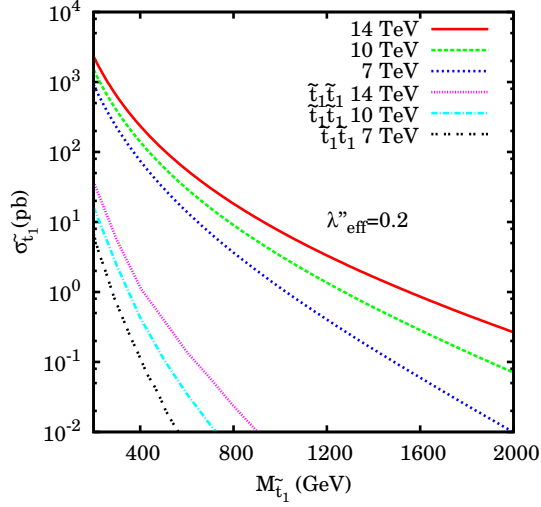


Figure 5.1: Production cross section at the LHC for $\sqrt{s} = 7, 10$ and 14 TeV with $\lambda''_{eff} = 0.2$. The corresponding cross sections for R-conserving \tilde{t}_1 pair production are also shown.

of an effective coupling $\lambda''_{eff} = \sin \theta_{\tilde{t}} \lambda''_{312}$.

$$\begin{aligned} \sigma_{\tilde{t}_1} = & \frac{2\pi}{3m_{\tilde{t}_1}^2} |\lambda''_{eff}|^2 \times \\ & 2 \int dx_1 dx_2 [f_d(x_1) f_s(x_2) + f_d(x_2) f_s(x_1) \\ & + f_{\bar{d}}(x_1) f_{\bar{s}}(x_2) + f_{\bar{d}}(x_2) f_{\bar{s}}(x_1)] \delta(1 - \frac{m_{\tilde{t}_1}}{\sqrt{\hat{s}}}) \end{aligned} \quad (5.5)$$

The production cross section at the LHC with centre-of-mass energies of 7, 10 and 14 TeV is given in Figure 5.1. As an illustration, we have chosen the value $\lambda''_{eff} = 0.2$ which is consistent with the existing limit on λ''_{312} . In general, both \tilde{t}_1 and \tilde{t}_2 will be produced. However, due to larger mass and smaller fraction of \tilde{t}_R , \tilde{t}_2 is rarely produced. For comparison, we also present the \tilde{t}_1 -pair production cross-section via strong interaction. For $m_{\tilde{t}_1} > 500$ GeV, the resonant production dominates over pair-production for $\lambda''_{eff} > 0.01$ at 14 TeV. Resonant production can therefore hold the key to heavy stop signals if baryon number is violated.

At next-to-leading order, the production cross section at $\sqrt{s} = 14$ TeV is modified by a k-factor of about 1.4[127]. The uncertainty due to renormalisation and factorisation scales at lowest order is about 10% and drops to 5% when NLO corrections are taken into account.

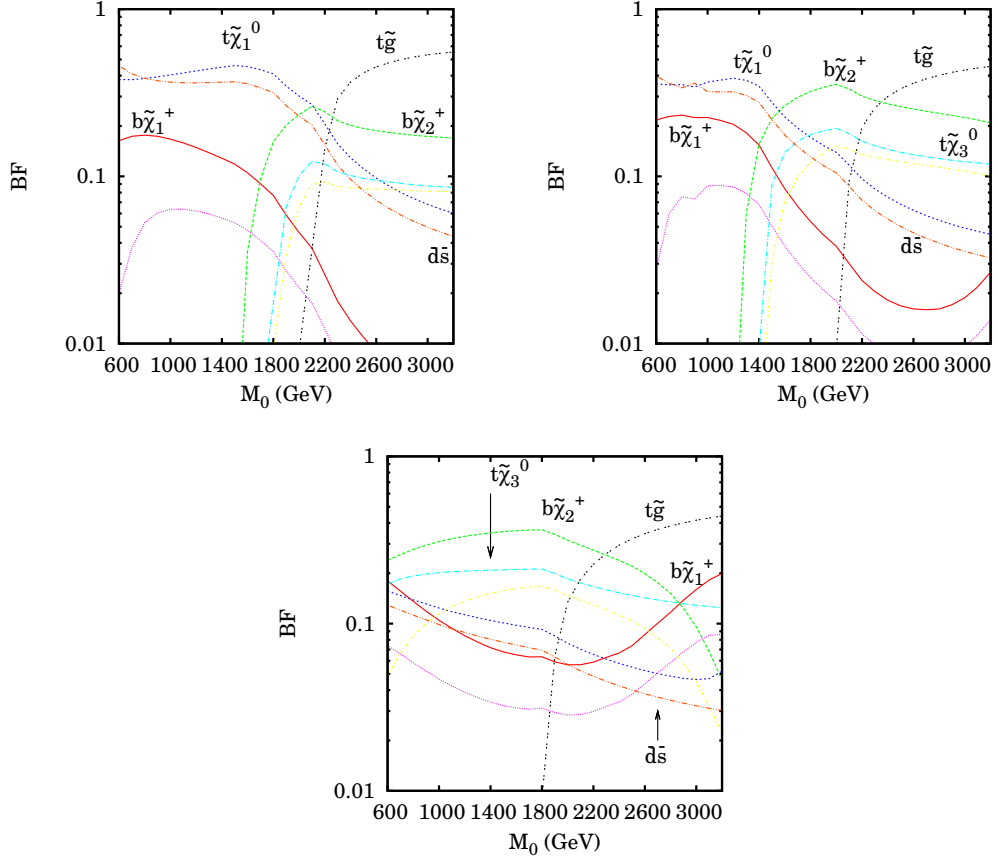


Figure 5.2: Lighter stop decay branching fractions in different modes for $\tan \beta = 5$, $A_0 = -1500$ (top left) ; $\tan \beta = 40$, $A_0 = -1500$ (top right) and $\tan \beta = 10$, $A_0 = 0$ (bottom). $\lambda''_{312} = 0.2$, $\mu > 0$ and $m_{1/2} = 450$ GeV in all cases.

5.1.2 Stop decays and choice of benchmark points

We wish to make our conclusions apply broadly to a general SUSY scenario and to include all possible final states arising from stop decay. However, the multitude of free parameters in the MSSM often encourages one to look for some organising principle. A common practice in this regard is to embed SUSY in high-scale breaking scheme. Following this practice, we have based our calculation on the minimal supergravity (mSUGRA) model[135], mainly for illustrating our claims in a less cumbersome manner. The high scale parameters in this model are: m_0 , the unified scalar parameter, $m_{1/2}$, the unified gaugino parameter, $sign(\mu)$, where μ is the Higgsino mass parameter, A_0 , the unified trilinear coupling and $\tan \beta$, the ratio of the two Higgs vacuum expectation values.

Although the production cross section of the stop depends only on the mass and mixing angle of the stop, any strategy developed for seeing the ensuing signals has to take note of the decay channels. We have tried to make our analysis comprehensive by including all possible decay chains of the stop. Thus we have included decays into $t\tilde{\chi}_i^0$, $b\tilde{\chi}_i^\pm$, $t\tilde{g}$ and ds , of whom the first three are R-conserving decays while the last one is R-violating. The charginos, neutralinos or the gluino produced out of stop-decay have their usual cascades until the LSP (here χ_1^0 , the lightest neutralino) is reached. The χ_1^0 thereafter undergoes three-body RPV decays driven by λ''_{312} , to give rise to final states consisting leptons and jets of various multiplicities.

We observe that for the same values of $(m_0, m_{1/2})$, the mass and branching fractions of the stop may vary drastically with different values of $(\tan\beta, A_0)$. We shall choose $\mu > 0$ for all the benchmark points as it is favoured by the constraint from the muon anomalous magnetic moment[136].

Since we explicitly want to study the situation in which the neutralino decays within the detector, the only available decay mode is $\tilde{\chi}_1^0 \rightarrow tds(\bar{t}\bar{d}\bar{s})$. We therefore require that the neutralino mass be greater than the top mass to allow for a three-body decay. We fix $m_{1/2} = 450$ GeV which gives $M_{\tilde{\chi}_1^0} \sim 180$ GeV. We also choose the high scale value of $\lambda''_{312} \sim 0.065$ such that it gives a value of 0.2 at the electroweak scale.

Figure 5.2 shows the branching fractions into various final states for three different choices of $(\tan\beta, A_0)$, namely, $(5, -1500)$, $(40, -1500)$ and $(10, 0)$ for different stop masses, obtained by varying m_0 . We notice that, for low m_0 , the dominant decay mode is $b\tilde{\chi}_2^+$ in the third case of Figure 5.2, while it is $t\tilde{\chi}_1^0$ in the first two cases. We also notice that the decays into higher neutralinos and charginos open up earlier for $\tan\beta = 40$ and compared to $\tan\beta = 5$. Choosing $\tan\beta < 5$ does not significantly alter the decay scheme and therefore we have chosen $\tan\beta = 5$ to be representative of low $\tan\beta$ values.

The Tevatron reach for single stop production is about 450 GeV. We therefore start with a benchmark point with stop mass of 500 GeV, just beyond this reach (Point A). The major decay channels in this case are $t\tilde{\chi}_1^0, b\tilde{\chi}_1^+$. A stop mass of a TeV at the electroweak scale may be obtained by various configurations in the high-scale parameter space. However, from the above plots, one expects its decays to change significantly with different parameters. Our objective is to determine whether signal of resonant production of a stop of mass near a TeV can be probed irrespective of what the high-scale parameters are. For this, we fix $M_{\tilde{t}_1} \sim 1$ TeV. We first look at the case with $A_0 = -1500$. We construct two benchmark points with $\tan\beta = 5$ (Point B) and 40(Point C) which represent the opposite ends of the allowed range in $\tan\beta$. We see that for a stop mass of 1 TeV, the decays into the higgsino-like $\tilde{\chi}_2^+$ and $\tilde{\chi}_3^0$ become dominant goes to high $\tan\beta$.

Similarly, we also look at a point with $A_0 = 0$ $\tan\beta = 10$ (Point D). In this case, we find that the Higgsino channels open up fairly early and the dominant decay is $b\tilde{\chi}_2^+$

followed by $t\tilde{\chi}_3^0$. As we shall see in the next section, this plays a crucial role in enhancing multi-lepton signals of a resonantly produced stop. Finally, since the decay into a top and a gluino does not open up until much higher stop masses, we also construct one point in which the stop decays dominantly into $t\tilde{g}$ (Point E).

Points A, B and E correspond to the same value of $(\tan\beta, A_0) = (5, -1500)$ and therefore provide a description of how the signal changes when only m_0 is varied. This choice of parameters also corresponds to the most conservative case in terms of signal since the decay modes into the higher gauginos does not open for a large region in the parameter space. We will therefore use these points to obtain limits on λ_{eff}'' .

We have tabulated the parameters and significant decay modes in Table 5.1. The benchmark points were generated with RPV renormalisation group running of couplings and masses using SOFTSUSY 3.0.2[137] and the RPV decays were calculated with the ISAWIG interface to Isajet[138].

| Point | $(m_0, \tan\beta, A_0)$ | $M_{\tilde{t}_1}$ | $\sin^2\theta_{\tilde{t}}$ | Dominant decay modes |
|-------|-------------------------|-------------------|----------------------------|---|
| A | (600,5,-1500) | 508 | 0.88 | $t\tilde{\chi}_1^0$ (0.35); $b\tilde{\chi}_1^+$ (0.19); $d\bar{s}$ (0.48) |
| B | (1650,5,-1500) | 1002 | 0.97 | $t\tilde{\chi}_1^0$ (0.48); $t\tilde{\chi}_2^0$ (0.04); $b\tilde{\chi}_1^+$ (0.10); $d\bar{s}$ (0.38) |
| C | (1570,40,-1500) | 1002 | 0.95 | $t\tilde{\chi}_1^0$ (0.35); $t\tilde{\chi}_2^0$ (0.05); $b\tilde{\chi}_1^+$ (0.12); $b\tilde{\chi}_2^+$ (0.21); $d\bar{s}$ (0.27) |
| D | (1250,10,0) | 1008 | 0.97 | $t\tilde{\chi}_1^0$ (0.13); $t\tilde{\chi}_2^0$ (0.04); $t\tilde{\chi}_3^0$ (0.20); $t\tilde{\chi}_4^0$ (0.13); $b\tilde{\chi}_1^+$ (0.08); $b\tilde{\chi}_2^+$ (0.33); $d\bar{s}$ (0.10) |
| E | (2450,5,-1500) | 1404 | 0.99 | $t\tilde{g}$ (0.39); $t\tilde{\chi}_1^0$ (0.15); $t\tilde{\chi}_2^0$ (0.02); $t\tilde{\chi}_3^0$ (0.08); $t\tilde{\chi}_4^0$ (0.07); $b\tilde{\chi}_1^+$ (0.02); $b\tilde{\chi}_2^+$ (0.17); $d\bar{s}$ (0.11) |

Table 5.1: Benchmark points and the dominant decay modes of the lighter stop. $\lambda_{312}'' = 0.2$, $\mu > 0$ and $m_{1/2} = 450$ GeV for all benchmark points.

The decay width of the stop in the R-parity violating channel ds depends only on λ_{eff}'' and the stop mass. Therefore, the branching ratio into this channel for same values of λ_{eff}'' and stop mass depends only on the decay widths of the other channels open at the same time. For the benchmarks under consideration, $\tilde{\chi}_{1,2}^0$ and $\tilde{\chi}_1^\pm$ have large gaugino fractions whereas $\tilde{\chi}_{3,4}^0$ and $\tilde{\chi}_2^\pm$ have large higgsino fractions. The large top mass means that stop coupling to higgsino-like chargino and neutralinos is large. Thus as soon as these decays become kinematically allowed, they quickly dominate over the decays into gaugino-like chargino and neutralinos. This can be seen for points B, C and D which have nearly identical stop masses and $\sin^2\theta_{\tilde{t}}$ ($\lambda_{312}'' = 0.2$ at electroweak scale for all points). Large $\tan\beta$ opens up the $b\tilde{\chi}_2^+$ mode early in point C as compared to point B and makes the branching fraction into ds for point C much lower. For point D, the branching fraction into higgsino-like chargino and neutralinos is larger than 60% and the RPV decay fraction is only about 10%. The $\tilde{t} - t - \tilde{g}$ coupling comes from strong interactions and therefore the $t\tilde{g}$ channel dominates whenever it becomes kinematically

allowed (as in point E).

5.2 Event generation and selection

5.2.1 Event generation

Signal events have been generated using HERWIG 6.510[139], and jets have been formed using anti- k_T algorithm[104] from FastJet 2.4.1. SM backgrounds have been calculated using Alpgen 2.13[76] showered through Pythia [73] with MLM matching. We have used CTEQ6L1 parton distribution functions[140]. The renormalisation and factorisation scales have been set at the lighter stop mass ($M_{\tilde{t}_1}$) for signal, while the corresponding default options in ALPGEN has been used for the backgrounds.

In R-parity conserving MSSM, the production of two heavy superparticles requires a large centre-of-mass energy at the parton level. This allows us to further suppress the SM background by applying cuts on global variables like the “effective mass” (M_{eff}). Since we no longer have a large missing- E_T and the energy scale of the resonant production process is not very high, the SM background cannot be suppressed so easily. We therefore concentrate on leptonic signals with or without b-tags to identify the signal over the background.

5.2.2 Event selection

Decay of the lighter stop in this scenario can lead to a variety of final states. Out of them, we have chosen the following ones:

- Same-sign dileptons: SSD
- Same-sign dileptons with one b-tagged jet: SSD + b
- Trileptons: $3l$

We do not consider the RPV dijet channel as a viable signature due to the enormous background from QCD processes. Similarly, we also omit opposite-sign dileptons due to large backgrounds from Drell-Yan, W^+W^- , $t\bar{t}$ etc.

We have imposed the following identification requirements on leptons and jets:

- **Leptons:** A lepton (l) is considered isolated if (a) It is well separated from each jet (j): $\Delta R_{lj} > 0.4$, (b) The total hadronic deposit within $\Delta R < 0.35$ is less than 10 GeV. We consider only those leptons which fall within $|\eta| < 2.5$ with $p_T > 10$ GeV. Here, $\Delta R = \sqrt{\Delta\eta^2 + \Delta\phi^2}$ where η is the pseudo-rapidity and ϕ is the azimuthal angle.

- **Jets:** Jets have been formed using the anti- k_T algorithm with parameter $R = 0.7$. We only retain jets with $p_T > 20$ GeV and $|\eta| < 2.5$.
- **B-tagged jets:** A jet is b-tagged with probability of 0.5 if a b-hadron with $50 < p_T < 100$ GeV lies within a cone of 0.7 from the jet axis. We have set the identification efficiency to be zero outside this window, in order to make our estimates conservative.

We also apply the following extra cuts on various final states to enhance the signal over background:

- **Cut 1: Lepton- p_T :** We demand that the p_T of the leptons be greater than (40, 30) GeV for dilepton and (30, 30, 20) for trilepton channels. This cut removes the background from semileptonic decays of b quarks. It strongly suppresses the $b\bar{b} + jets$, $Wb\bar{b} + jets$ and $t\bar{t} + jets$ background in the SSD-channel coming from semileptonic b-decays.
- **Cut 2: Missing E_T :** At least one lepton in the signal always comes from the decay of a W boson and is accompanied by a neutrino. We demand a missing- E_T greater than 30 GeV from all events. This helps in reducing the probability of jets faking leptons. Missing- E_T has been defined as $|\vec{p}_{T,visible}|$.
- **Cut 3: Jet p_T :** We demand that the number of jets, $n_j \geq 2$ with $p_T(j_1) > 100$ GeV and $p_T(j_2) > 50.0$ GeV for SSD and SSD + b. This cut is useful when high stop mass is very high and the production cross section is very low.
- **Cut 4: Dilepton invariant mass:** We also apply a cut on dilepton invariant mass (M_{l_1, l_2}) around Z-mass window ($|M_{l_1, l_2} - M_Z| < 15.0$ GeV) for opposite sign dileptons of same flavour in trilepton events. This serves to suppress contribution from $Zb\bar{b} + jets$ and $WZ + jets$ background to trileptons.

Due to the Majorana nature of neutralinos, λ'' -type interactions result in equal rates for $t\bar{d}s$ and $\bar{t}d\bar{s}$ -type final states. Therefore, the most promising signals are those involving same-sign dileptons (SSD). This not only applies to $\tilde{\chi}_1^0$ but also to the higher neutralinos produced in stop decay, whose cascades can give rise to W's. SSD have previously been used extensively for studying signals of supersymmetry [141, 142]. The most copious backgrounds to SSD processes come from the processes $t\bar{t}$ and $Wb\bar{b}$ due to one lepton from W and another from semileptonic decays of the b-quark. There is also a potentially large contribution from $b\bar{b}$ due to $B^0 - \bar{B}^0$ oscillations along with semileptonic decays of both B-mesons. The effect of oscillations is simulated in the Pythia program. The p_T -cuts on leptons have been selected to minimise the background from heavy flavour decays [143]. We find that after the isolation and p_T cuts on leptons, $Wb\bar{b}$ and $b\bar{b}$ cross sections fall to sub-femtobarn levels.

We simulate the $t\bar{t} + jets$ background up to two jets. The trilepton channel has another source of backgrounds in $WZ + jets$; however, we have checked and found them to be negligibly small after applying all the cuts. We also generate $Wt\bar{t} + jets$ and $Zt\bar{t} + jets$ up to one jet.

It should be mentioned here that the dilepton and trilepton final states can also arise in the same scenario from the pair-production of superparticles. These include, for example, pair production of gluinos and electroweak production of chargino-neutralino pairs. Such contributions have been explicitly shown in the plots in section 4.

We also expect that the p_T distribution of the \tilde{t}_1 becomes significantly harder if the NLO corrections are taken into account[127]. Our cuts on leptons have been designed to cut off the background from semileptonic b-decays by requiring the p_T to be about half the mass of the W . Therefore, if only the lepton cuts are used, we do not expect a decrease in the efficiency of the cuts quoted in the next section.

5.3 Results

We present results using $\lambda''_{312} = 0.2$; the predictions for other values of this coupling can be obtained through scaling arguments. If λ''_{312} is scaled by a factor of n then the production cross section as well as the decay width of the RPV channel scale by n^2 . All other decay widths remain unchanged. If f is the branching fraction of $\tilde{t} \rightarrow \bar{d}\bar{s}$ before scaling, then the signal rates in any other channel are scaled by a factor of

$$\frac{R_{new}}{R_{old}} = \frac{n^2}{(n^2 - 1)f + 1} \quad (5.6)$$

5.3.1 Limits at $\sqrt{s} = 14, 10$ TeV

The numerical results for various signals corresponding to the five benchmark points for LHC running energy $\sqrt{s} = 14, 10$ TeV are presented in Tables 5.2(for the SSD channel), 5.3 (for SSD + b) and 5.4 (for $3l$).

We can make the following observations from the numerical results:

- The final states SSD and SSD + b consistently have substantial event rates at both 14 and 10 TeV. Furthermore, the simultaneous observation of excesses in the SSD and SSD + b channel can serve as definite pointer to the production of a third generation squark.
- For point A, which is just above the Tevatron reach, we can achieve more than 5σ significance in the SSD channel with just 100 pb^{-1} data at both 14 and 10 TeV. For point E, which has $M_{\tilde{t}} = 1500 \text{ GeV}$, we can reach 3σ with $1(3) \text{ fb}^{-1}$ and 5σ

| SSD Point | 14 TeV | | | | 10 TeV | | | |
|------------------|--------|-------|--------------|-------------|--------|-------|--------------|------------|
| | Cut 0 | Cut 1 | Cut 2 | Cut 3 | Cut 0 | Cut 1 | Cut 2 | Cut 3 |
| A | 884.8 | 496.8 | 459.4 | 41.0 | 540.1 | 312.7 | 287.0 | 15.1 |
| B | 64.7 | 43.7 | 41.4 | 19.3 | 30.6 | 21.0 | 19.8 | 9.6 |
| C | 83.0 | 51.5 | 49.2 | 25.8 | 40.1 | 25.6 | 24.6 | 12.5 |
| D | 145.4 | 71.9 | 68.9 | 41.1 | 65.1 | 32.3 | 31.0 | 19.0 |
| E | 29.8 | 16.5 | 15.9 | 13.6 | 10.7 | 5.8 | 5.6 | 4.6 |
| $t\bar{t} + nj$ | 687.9 | 26.3 | 24.7 | 10.0 | 307.0 | 8.7 | 7.0 | 3.6 |
| $Wt\bar{t} + nj$ | 17.0 | 9.2 | 8.7 | 5.2 | 7.6 | 3.9 | 3.7 | 2.0 |
| $Zt\bar{t} + nj$ | 12.7 | 6.7 | 6.7 | 4.1 | 4.9 | 2.3 | 2.2 | 1.4 |
| Total BG | 717.6 | 42.2 | 40.1 | 19.3 | 319.5 | 14.9 | 12.9 | 7.0 |

Table 5.2: Effect of cuts on signal and SM background cross sections (in fb) in the SSD channel at $\sqrt{s} = 14, 10$ TeV. Cut 0 refers to all events passing the identification cuts. Cuts 1-3 are described in the text. The numbers corresponding to best significance (s/\sqrt{b}) of the signal (s) with respect to the background (b) are highlighted in bold.

with 3(9) fb^{-1} at 14(10) TeV. Therefore, we can conclude that the entire range from 500-1500 GeV can be successfully probed at the LHC for $\lambda''_{312} = 0.2$.

- Stops decaying into higher neutralinos and charginos make the total rates distinctly better. This is governed by Higgsino couplings and is therefore most prominent for high $\tan\beta$ and low A_0 . This effect is evident from the large event rates for point D. We can successfully probe this point in the SSD channel at 5σ with less than 1 fb^{-1} data at both 10 and 14 TeV runs.
- The trilepton final state occurs when the stop can decay into χ_2^+ , $\chi_{3,4}^0$ or \tilde{g} . Therefore, points A and B show almost no signal and Point D has the largest signal in this channel. This advantage is largely lost for benchmark point E due to the kinematic suppression in the stop production process.
- Reach for the LHC: Assuming the conservative case of ($\tan\beta = 5$, $A_0 = 0$), with 10 fb^{-1} luminosity, one can rule out λ''_{eff} greater than 0.007–0.045 (0.007–0.062) for stop masses between 500 and 1500 GeV at 95 % CL at $\sqrt{s} = 14$ (10) TeV. A 5σ discovery can be made in the same mass range for λ''_{eff} greater than 0.012–0.084 (0.012–0.12). However, we observe that the reach in stop mass does not decrease monotonously with stop mass. The opening of new decay channels can improve detection considerably. The statements about minimum value of λ''_{eff} that can be probed are therefore dependent on the particular decays of the stop. We therefore tabulate the minimum values of λ''_{eff} for each benchmark point at 10 fb^{-1} for both 10 and 14 TeV in Table 5.5.

| SSD + b Point | 14 TeV | | | | 10 TeV | | | |
|--------------------|--------|-------|--------------|------------|--------|-------|-------------|------------|
| | Cut 0 | Cut 1 | Cut 2 | Cut 3 | Cut 0 | Cut 1 | Cut 2 | Cut 3 |
| A | 243.2 | 134.7 | 121.2 | 14.1 | 158.7 | 67.5 | 61.8 | 6.6 |
| B | 13.8 | 9.6 | 9.2 | 4.7 | 8.3 | 6.0 | 5.6 | 2.8 |
| C | 25.3 | 15.2 | 14.6 | 8.0 | 12.7 | 7.8 | 7.4 | 4.1 |
| D | 47.9 | 23.9 | 23.0 | 15.2 | 21.2 | 9.9 | 9.5 | 6.3 |
| E | 11.3 | 6.2 | 6.0 | 5.3 | 4.1 | 2.2 | 2.1 | 1.8 |
| $t\bar{t} + nj$ | 173.0 | 7.6 | 7.1 | 2.3 | 80.9 | 4.2 | 1.4 | 1.3 |
| $Wt\bar{t} + nj$ | 6.7 | 0.8 | 0.8 | 0.6 | 4.0 | 2.1 | 1.9 | 1.3 |
| $Zt\bar{t} + nj$ | 5.6 | 2.6 | 2.6 | 1.8 | 2.3 | 1.1 | 1.1 | 0.7 |
| Total | 185.3 | 11.0 | 10.5 | 4.7 | 87.2 | 7.4 | 4.4 | 3.3 |

Table 5.3: Same as Table 5.2, but for the SSD + b channel.

In Figure 5.3, we present the effective mass distributions in SSD channel for all the benchmark points. Effective mass is defined as

$$M_{\text{eff}} = \sum_{jets} |\vec{p}_T| + \sum_{leptons} |\vec{p}_T| + \cancel{E}_T \quad (5.7)$$

The contributions from resonant stop production is superposed in the figures on the SM backgrounds and also RPC superparticle production processes. The RPC contributions are much smaller and therefore do not provide a serious background to our signals.

5.3.2 Observability at the early run of 7 TeV

The initial LHC run at $\sqrt{s} = 7$ TeV will collect up to 1 fb^{-1} data. It will be difficult to observe RPV production of a 1 TeV stop at this energy. However, we can make useful comments for lower stop masses by looking at the SSD channel. We therefore look two benchmark points with low stop masses: the first is the ‘Point A’ described earlier and the second is similar to ‘Point D’ (with $\tan \beta = 10$ and $A_0 = 0$). Since the $t\bar{t}$ backgrounds are much smaller at 7 TeV, we relax the jet- p_T cuts. The high scale parameters, stop mass at electroweak scale and cut-flow table for signal as well as background are given in Table 5.6.

We conclude that we can rule out up to $\lambda''_{eff} = 0.025$ at 95% confidence level for a stop mass of 500 GeV at 7 TeV with 1 fb^{-1} data and a 5σ discovery can be made at stop mass 500 GeV for $\lambda''_{eff} \geq 0.043$. For the case $\tan \beta = 10$ and $A_0 = 0$, the lowest possible theoretically allowed stop mass (with $m_{1/2} = 450$ GeV) is 775 GeV and we can rule out up to $\lambda''_{eff} = 0.054$ with 1 fb^{-1} data.

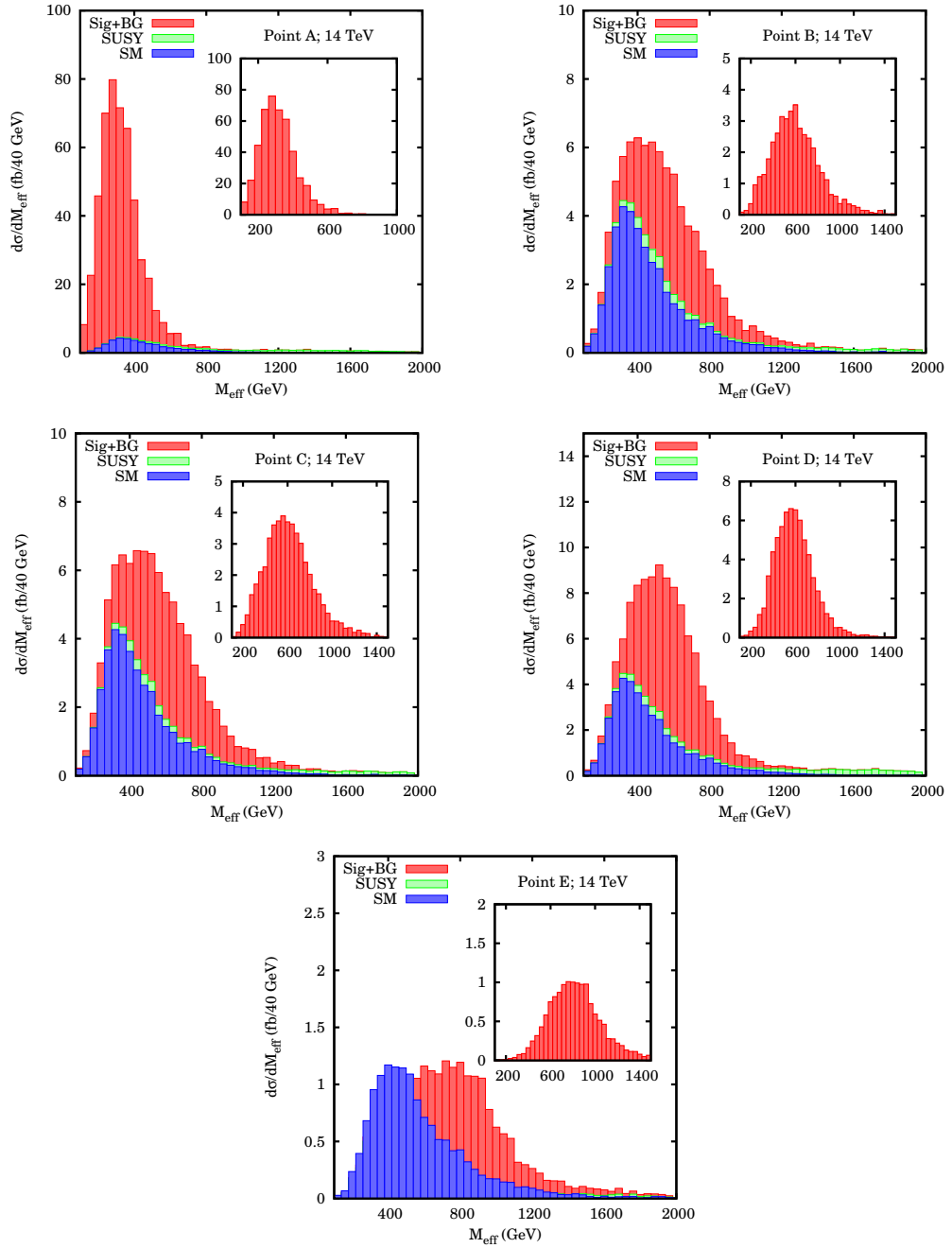


Figure 5.3: M_{eff} distributions at $\sqrt{s} = 14$ TeV. “SM” is the contribution to the background from Standard Model processes. “SUSY” refers to the contribution from R-conserving production processes. The inset in each figure contains the distribution for the signal alone.

| $3l$ Point | 14 TeV | | | | 10 TeV | | | |
|------------------|--------|-------|-------|-------|--------|-------|-------|-------|
| | Cut 0 | Cut 1 | Cut 2 | Cut 4 | Cut 0 | Cut 1 | Cut 2 | Cut 4 |
| A | 49.1 | 2.8 | 2.8 | 0.0 | 18.0 | 1.1 | 1.1 | 0.0 |
| B | 2.0 | 0.6 | 0.6 | 0.1 | 1.1 | 0.2 | 0.2 | 0.0 |
| C | 13.7 | 9.1 | 9.1 | 1.1 | 6.5 | 3.7 | 3.7 | 0.6 |
| D | 48.2 | 29.6 | 29.0 | 8.6 | 24.1 | 14.5 | 14.1 | 4.5 |
| E | 9.3 | 5.7 | 5.5 | 3.0 | 3.4 | 2.1 | 2.1 | 1.2 |
| $t\bar{t} + nj$ | 2.1 | 0.0 | 0.0 | 0.0 | 1.8 | 0.0 | 0.0 | 0.0 |
| $Wt\bar{t} + nj$ | 4.1 | 2.5 | 2.4 | 1.0 | 2.2 | 1.4 | 1.4 | 0.6 |
| $Zt\bar{t} + nj$ | 30.8 | 20.7 | 19.7 | 2.7 | 11.3 | 7.3 | 4.7 | 1.1 |
| Total BG | 37.0 | 23.2 | 22.1 | 3.7 | 15.3 | 8.7 | 6.1 | 1.7 |

Table 5.4: Effect of cuts on signal and SM background cross sections (in fb) in the trilepton ($3l$) channel at $\sqrt{s} = 14, 10$ TeV. Cut 0 refers to all events passing the identification cuts. Cuts 1, 2 and 4 are described in the text. Cut 4 is necessary to eliminate background from $WZ + jets$.

| Point | 14 TeV | | | 10 TeV | | |
|-------|--------|-----------|-----------|--------|-----------|-----------|
| | 95% CL | 3σ | 5σ | 95% CL | 3σ | 5σ |
| A | 0.007 | 0.009 | 0.012 | 0.007 | 0.009 | 0.012 |
| B | 0.027 | 0.037 | 0.052 | 0.029 | 0.041 | 0.059 |
| C | 0.026 | 0.035 | 0.048 | 0.028 | 0.038 | 0.052 |
| D | 0.024 | 0.032 | 0.042 | 0.027 | 0.036 | 0.047 |
| E | 0.045 | 0.062 | 0.084 | 0.062 | 0.087 | 0.12 |

Table 5.5: Values of minimum λ''_{eff} that can be ruled out at 95% CL, probed at 3σ or 5σ with $10 fb^{-1}$ of data at $\sqrt{s} = 10, 14$ for each of the benchmark points. The significance used is s/\sqrt{b} where s is the signal and b is the background. $s/b > 0.2$ in all cases.

5.3.3 Differentiating from R-conserving signals

We now address the question whether the signals we suggest can be faked by an R-parity conserving scenario in some other region(s) of the parameter space. One possible way that our signal may be mimicked is if a point in the mSUGRA parameter space (without RPV) gives similar kinematic distributions to any our benchmark points. More specifically, one may have a peak in the same region for the variable M_{eff} , defined in equation 5.7.

For each of our benchmark points A-D, an M_{eff} peak in the same region requires the strongly interacting sparticles to have masses in the range already ruled out by the Tevatron data[144]. In particular, they require the gluino mass $M_{\tilde{g}} < 390$ GeV. Thus the question of faking arises only for benchmark point E, which represents the highest

| Point | $(\tan \beta, A_0, m_0)$ | $M_{\tilde{t}_1}$ | Cut 0 | Cut 1 | Cut 2 |
|------------------|--------------------------|-------------------|-------|-------|-------|
| A | $(5, -1500, 600)$ | 508 | 283.3 | 158.6 | 147.5 |
| D' | $(10, 0, 100)$ | 775 | 70.0 | 33.9 | 32.0 |
| $t\bar{t} + nj$ | | | 116.0 | 3.7 | 3.5 |
| $Wt\bar{t} + nj$ | | | 4.3 | 2.3 | 2.1 |
| $Zt\bar{t} + nj$ | | | 1.8 | 0.9 | 0.8 |
| Total BG | | | 122.1 | 6.9 | 6.4 |

Table 5.6: The benchmark points for studying RPV stop production and the effect of cuts on signal and SM background cross sections (in fb) in the SSD channel at $\sqrt{s} = 7$ TeV. Cut 0 refers to all events passing the identification cuts. All other cuts are described in the text, we do not apply Cut 3.

mass where the signals rates are appreciable.

We generate such a point (Point RC) with the parameters $m_0 = 300$, $m_{1/2} = 180$, $A_0 = 0$, $\tan \beta = 10$, $\mu > 0$ and the resultant sparticle masses for coloured particles are $M_{\tilde{g}} = 465$, $M_{\tilde{q}} \sim 500$ GeV. The M_{eff} distributions for point E and point RC is shown in Figure 5.4. We present the following results at 14 TeV as an illustration. Distributions at 10 TeV are almost identical.

The missing E_T distribution is also not a good discriminator under such circumstances, as can be seen from Figure 5.4. This is because the neutrinos that contribute to missing- E_T in the RPV case are highly boosted due to the large masses of the particles produced in the initial hard scattering. Thus, the E_T spectrum is actually harder for the RPV case even though the RPC case has a stable massive LSP. However, as the resultant spectrum is quite light, the RPC production cross section (~ 40 pb) is about two orders of magnitude greater than the RPV case with $\lambda''_{312} = 0.2$ (~ 480 fb). Consequently, the rate of the SSD signals, for example, are much higher in the R-conserving scenario (~ 34 fb) as compared to those from point E (~ 14 fb). For values of $\lambda''_{312} < 0.2$, we can therefore make a reliable distinction simply based on the number of events expected in the SSD channel.

Another possible discriminator is the charge asymmetry. In the SSD channel, one can look at the ratio of negative to positive SSD $\frac{N_{--}}{N_{++}}$. The fraction of $ds \rightarrow \tilde{t}_1^*$ is more than the charge conjugate process $\bar{d}\bar{s} \rightarrow \tilde{t}_1$ due to the difference in parton distributions of d and \bar{d} in the proton. Therefore, one expects extra negative sign leptons than positive ones. Whereas in the RPC case, since most of the SSD contribution comes from $\tilde{g}\tilde{g}$ production, we do not expect a large asymmetry. In our illustration, we see that this ratio is 2.7 (1.4) for the RPV (RPC) case.

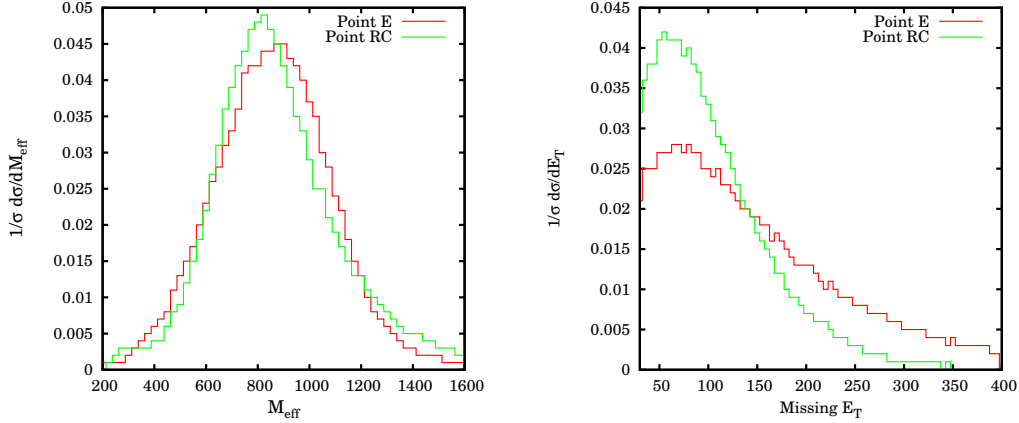


Figure 5.4: The normalised effective mass (M_{eff}) and missing energy (\cancel{E}_T) distributions in the SSD channel for Point E and an Point RC. Point RC has been generated using $m_0 = 300, m_{1/2} = 180; A_0 = 0, \tan\beta = 10$ and $\mu > 0$. The gluino mass is 465 GeV.

5.4 Non- $\tilde{\chi}_1^0$ LSPs

For RPV models, the restriction of having an uncharged LSP no longer exists. A significant region of the mSUGRA parameter space with low m_0 corresponds to a stau ($\tilde{\tau}$) LSP. With only λ''_{312} -type couplings present, the stau can only decay via off-shell $\tilde{\chi}_1^0$ and \tilde{t} propagators into the four body decay ($\tilde{\tau} \rightarrow \tau t d s$) if its mass, $m_{\tilde{\tau}} > m_{\text{top}}$ or via the five body decay ($\tilde{\tau} \rightarrow \tau b W d s$) if $m_{\tilde{\tau}} < m_{\text{top}}$ where the top propagator is also off-shell. The four-body decays of the stau in lepton-number violating scenarios was calculated in [145]. Since the intermediate $\tilde{\chi}_1^0$ is of Majorana character, we can always have one lepton of either sign from LSP decay via the W from an on-shell or off-shell top. Thus, for various types of \tilde{t} decays, the following situations may arise:

- For decays of $t\tilde{\chi}_i^0$ -type, we can still have same-sign dileptons with one lepton from top decay and the other from the decay of the LSP.
- For decays of type $b\tilde{\chi}_i^\pm$ with $\chi_i^\pm \rightarrow W^\pm\tilde{\chi}_1^0 + X$, we have $\tilde{\chi}_1^0 \rightarrow \tau\tilde{\tau}$ and the SSD come from W^\pm and LSP decay respectively.
- For decays of the type $\tilde{t} \rightarrow b\tilde{\chi}_i^+$ with $\tilde{\chi}_i^+ \rightarrow \nu_\tau\tilde{\tau} + X$, we may still get SSD from leptonic decay of the τ in the $\tilde{\tau}$ decay. If τ -identification is used, final states of the type same-sign ($\tau + e/\mu$) may be considered.
- Since the stau has to decay via four- or five-body processes, it is possible that the lifetime of the $\tilde{\tau}$ is large and it is stable over the length scale of the detector. In this case, it will leave a charged track like a muon and one can look at same-sign

leptons with this “muon” as one of the leptons. It is also possible that the lifetime is large but the stau still decays within the detector. In this case, a displaced vertex can be observed in the detector.

We leave the detailed simulation of all scenarios of resonant stop production with stau LSP to a future study.

Another possibility that arises with a large λ''_{312} is of having a stop LSP. In this case however, the decay will be almost entirely via the RPV $\bar{d}\bar{s}$ di-jet channel. The overwhelmingly large dijet backgrounds at the LHC would most likely make this situation unobservable.

5.5 Summary

We have performed a detailed analysis of resonant stop production at the LHC, both for the 10 and 14 TeV runs, for values of the baryon number violating coupling λ''_{312} an order of magnitude below the current experimental limit. Benchmark points have been chosen for this purpose, which start just beyond the reach of the Tevatron and end close at the LHC search limit. We find that the same-sign dilepton final states, both with and without a tagged b, are most helpful in identifying the signal. The trilepton signals can also be sometimes useful, especially when decays of the resonant into higher neutralinos, the heavier chargino or the gluino open up. At 14(10) TeV, we can probe stop masses up to 1500 GeV and values of λ''_{eff} down to 0.05 (0.06) depending on the combination of various SUSY parameters. For cases of stop mass below a TeV, the effective mass distributions can enable us to distinguish between the resonant process and contributions from R-parity conserving SUSY processes. For higher stop masses, one has to rely on cross sections or the charge asymmetry.

In conclusion, resonant stop production is a potentially interesting channel to look for SUSY in its baryon-number violating incarnation. Values of the B-violating coupling(s) more than an order below the current experimental limits can be definitely probed at the LHC, both at 10 and 14 TeV. If such interactions really exist, our suggested strategy can not only yield detectable event rates but also point towards resonant production as opposed to pair-production of SUSY particles.

SIGNATURES OF HIGGS

CHAPTER

6

PROBING THE CP-VIOLATING NATURE OF HWW COUPLINGS

“Because nothing is as perfect as you can imagine it.”
– Chuck Palahniuk

The most well-motivated explanation for electroweak symmetry breaking is the Higgs mechanism. Although the Higgs boson remains the only unobserved particle in the Standard Model (SM), there are both experimental and theoretical bounds on its mass. The LEP bound of 114 GeV has now been supplemented with the Tevatron bounds which rule out Higgs masses between 158 – 173 GeV [146, 147].

Here we consider the possibility of the Higgs boson existing in the range 130 – 150 GeV where the decay width of $H \rightarrow WW$ is appreciable. Between the publication of the original paper containing this research and writing this thesis, LHC data has ruled out the SM Higgs above 127 GeV at 95% CL [11, 12]. However, the variables defined here remain useful even in the still allowed mass range with the understanding that a larger integrated luminosity would be required for a statistically significant observation. We stress that the magnitudes of the asymmetries defined here do not change significantly with the Higgs mass and the requirement of large luminosity is purely due to the reduced branching ratio into WW for a low-mass Higgs which leads to smaller cross sections for the channels we consider. Moreover, the presence of anomalous couplings changes the acceptance of cuts in the $H \rightarrow WW$ channel which is primarily responsible

for ruling out the region in question and therefore, the results for the SM Higgs cannot be used without modification.

In such a situation, we wish to probe whether the HWW-coupling is exactly follows the prescription of the standard model. Such couplings can be probed in the relatively clean leptonic channels and previous studies for HWW and HZZ couplings at the LHC can be found in [148, 149, 150, 151, 152, 153, 154]. Many studies for both HWW and HZZ anomalous couplings also exist in the context of a future e^+e^- collider [155, 156, 157, 158, 159, 160], $e\gamma$ collider [161] and photon collider [162, 163]. LEP limits on anomalous Higgs couplings can be found in [164].

The primary production channel at the LHC is through gluon-gluon fusion and would in principle be the cleanest to probe the HWW vertex. However, the decay $H \rightarrow W^+W^-$ leads to an opposite-sign dilepton signature which is prone to large backgrounds from $pp \rightarrow W^+W^-$. This background is generally eliminated by retaining only relatively collimated leptons with an appropriate cut[165]. However, these cuts are no longer useful when one wishes to probe the presence of anomalous couplings because of the difference made by the anomalous couplings in angular distributions of dilepton events. We therefore choose to probe the associated production channel instead. A study for probing the anomalous couplings in the vector-boson fusion channel can be found in [166]. One could also consider Higgs production via $pp \rightarrow ZH$. However, if the HWW vertex has anomalous couplings, it would be natural to expect the HZZ vertex to also have such couplings. In that case, one is left to disentangle the interference of both HWW and HZZ vertices and this will further complicate the study of the HWW interaction.

Thus we explore the production of the Higgs via $pp \rightarrow WH$, and its subsequent decay, again through the HWW coupling. The interplay of anomalous coupling in both the production and decay vertices makes the resulting phenomenology richer and more complicated, but free from contamination from other effects. The environment of a hadron collider and the presence of two neutrinos in the final decay products makes the reconstruction of the event and the extraction of a non-standard HWW vertex difficult. However, as we shall see, there are significant differences in angular distributions which may point to the presence of anomalous contributions. We will also specifically address the issue of effect of initial and final state radiation on the variables as this is a fundamental concern at the LHC.

The paper is organised as follows. In the next section, we acquaint the reader with the anomalous couplings, and go on to discuss model-independent strategies for probing the CP-violating anomalous coupling, in a parton level Monte Carlo approach. Our event selection criteria are also discussed there. Section 6.2 contains our numerical results, including various distributions and asymmetries relevant for the analysis. In section 6.3, we report the results of a study where hadronisation and initial and final state radiation are included, and try to convince the reader that these do not alter the

conclusions of a parton level study in most cases. Our conclusions are presented in section 6.4.

6.1 The anomalous coupling and its simulation

The HWW vertex can receive corrections from higher dimensional operators like $\frac{(\Phi^\dagger\Phi)}{\Lambda^2}W_{\mu\nu}W^{\mu\nu}$ and $\frac{(\Phi^\dagger\Phi)}{\Lambda^2}W_{\mu\nu}\tilde{W}^{\mu\nu}$. The general HWW vertex may then be written in a model-independent way as $\Gamma_{\mu\nu}W^\mu W^\nu H$ where:

$$\Gamma_{\mu\nu} = \frac{igM_W}{2} \left(ag_{\mu\nu} + \frac{b}{M_W^2}(p_{1\mu}p_{2\nu} + p_{1\nu}p_{2\mu} - (p_1 \cdot p_2)g_{\mu\nu}) + \frac{\tilde{b}}{M_W^2}\epsilon_{\mu\nu\rho\sigma}p_1^\rho p_2^\sigma \right) \quad (6.1)$$

where p_1 and p_2 are the momenta of the two gauge bosons. For this study, we assume a completely phenomenological origin of b and \tilde{b} . The Standard Model vertex then corresponds to $b = 0$, $\tilde{b} = 0$ and $a = 1$. We particularly wish to investigate the effect of non-zero values of \tilde{b} which would lead to CP -violation. Therefore, we set b to zero all along. We also include the possibility of a complex \tilde{b} , arising out of some absorptive part in the effective interaction.

6.1.1 Simulation

To investigating the kinematical consequences of the CP -violating anomalous vertex at the LHC, we first use a parton-level Monte Carlo analysis with leptons in the final state. In section 6.3, we will show that the results of this simplified analysis are not altered by showering and hadronisation effects. We factorize the entire matrix element into two pieces $pp \rightarrow H\ell\nu$ ($\ell = e, \mu$) and $H \rightarrow WW^* \rightarrow \ell\nu\bar{f}f'$ [167]. Since the Higgs is a scalar, we expect that this does not affect the spin correlations. Both matrix elements have been calculated using Form [168]. For the first part of our study, we perform a simple smearing of the lepton momenta to approximate detector effects with a Gaussian distribution of width given by $\sigma(E) = aE + b\sqrt{E}$, with $a = 0.02$ and $b = 0.05$ ¹. The lepton identification efficiency has been assumed to be 100%.

We present our calculations for a proton-proton centre-of-mass energy of 14 TeV. The signal rates are too small at 7 and 8 TeV to be accessible at the current run with the projected luminosity. The cross section is calculated using the CTEQ6L1 parton distribution functions [140] with the renormalisation and factorisation scales both set at $\sqrt{\hat{s}}$, the subprocess centre-of-mass energy.

The modification of the leading order (LO) decay width in the $H \rightarrow f\bar{f}'\bar{f}f'$ channel has also been calculated and taken into account in each case. We focus on same-sign

¹B. Mellado; private communication

dileptons (SSD), when only one of the W s from the Higgs decays leptonically. It is less profitable to look into exclusive opposite-sign dilepton because of the large background from W^+W^- production. In Higgs searches, this background is generally suppressed using a cut on the angle between the two leptons — the ones from W^+W^- production are mostly back-to-back whereas those from Higgs decay are highly collimated. Since the excess events due to the term proportional to \tilde{b} tend to also increase the angle between the opposite-sign leptons, we cannot really use this as a criterion for cutting out the background. We can also look at trilepton states when both the W s decay into leptonic final states but we omit them for this work due to very low cross sections.

The Tevatron has certain bounds on the cross section of Higgs production. The CDF bounds in the SSD channel with 7.1 fb^{-1} data on the ratio of the Higgs production cross section to the SM rate in the electron and muon channels are 9.63 (4.99) on Higgs masses of 130 (150) GeV[169]. The combined CDF and DØ results[146] put a much stronger upper bound on the Higgs cross sections by combining various channels. However, the anomalous coupling affects only the associated WH production for which the bounds are not as strong. We present the results in our paper for a value $|\tilde{b}| = 0.2$ which satisfies the above CDF bounds.

6.1.2 Backgrounds and Cuts

At the LHC, the largest contribution to the background for SSD comes from semileptonic B -meson decays in $b\bar{b}$ production where one of the B -mesons oscillates into its charge conjugate state. It has been well-known for some time that the isolation cuts alone are not enough to suppress this background[143] but an additional cut on the transverse momentum (p_T) is required. We found that demanding an additional p_T -cuts along with a cut on missing transverse energy (\cancel{E}_T) is very effective for suppressing this background. We require two isolation cuts on the leptons, viz. the sum of p_T of all particles within a cone of 0.2 around the lepton should be less than 10 GeV and the separation from the nearest jet should be less than 0.4. However, these cuts are only fully relevant after parton showering and hadronisation and therefore will be considered in detail in section 6.3. Therefore, the set of cuts used for the parton-level analysis are:

1. Lepton rapidity : $|\eta| < 2.5$
2. Minimum transverse momenta of the hardest and second hardest leptons : $p_T(\ell_1) > 40 \text{ GeV}$ and $p_T(\ell_2) > 30 \text{ GeV}$ respectively
3. Missing transverse energy: $\cancel{E}_T > 30 \text{ GeV}$

These cuts suppress the $b\bar{b}$ background completely and reduce the contribution of $Zb\bar{b}$, $Wb\bar{b}$ to very small amounts. The $t\bar{t}$ background is still in the range of several

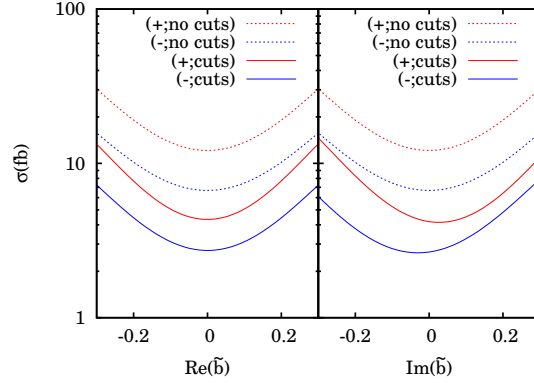


Figure 6.1: The behaviour of the cross section ($m_H = 150$ GeV) in the SSD channel for different values of $\text{Re}(\tilde{b})$ and $\text{Im}(\tilde{b})$ (right) and the final cross section after all the cuts. $\text{Im}(\tilde{b})$ is set to zero in the left panel and $\text{Re}(\tilde{b})$ is zero in the right. The dashed line with label “nocuts” refers to the cross section before any cuts are applied whereas the solid lines correspond to the cross section after cuts. The signs \pm refer to the charge of the SSD.

femtobarns and can be further suppressed using a veto on b-tagged jets and also restricting the number of hard jets in the final state. Since both these cuts are dependent on showering and hadronisation effects, we shall examine them only in section 6.3.

The effect of cuts for SSD on different values of \tilde{b} can be seen in Figure 6.1. We change only one out of $\text{Re}(\tilde{b})$ and $\text{Im}(\tilde{b})$ at a time. Changing $\text{Re}(\tilde{b})$ increase the p_T of the leptons however, this increase is similar for both $\text{Re}(\tilde{b}) > 0$ and $\text{Re}(\tilde{b}) < 0$. The case for non-zero $\text{Im}(\tilde{b})$ however, is different. $\text{Im}(\tilde{b}) < 0$ enhances the p_T for the lepton from W^+ whereas $\text{Im}(\tilde{b}) > 0$ enhances the p_T for the lepton from W^- . This causes an asymmetry in the cross section after the cuts even though there is no asymmetry to start with. This is illustrated in Table 6.1 where we present the cut flow table for the SM case and for $\text{Im}(\tilde{b}) = \pm 0.2$ for both $\ell^+\ell^+$ and $\ell^-\ell^-$ final states. The corresponding cross sections with $\text{Re}(\tilde{b}) = 0.2$ for $m_H = 150(130)$ GeV are (7.64)3.49 fb for $\ell^+\ell^+$ and 4.35 (2.08) fb for $\ell^-\ell^-$.

6.2 Numerical Results

After applying the cuts described in the previous sections, we are left with a fairly pure sample of events. Therefore we shall present the distributions for signal events only. Since the strength of the cross section for different values of the anomalous coupling are already given in Figure 6.1, we will be presenting only the normalised distributions

| m_H | 130 GeV | | | 150 GeV | | |
|---------------------|---------|-------|-------|---------|-------|-------|
| $(\tilde{b}; \pm)$ | Cut 1 | Cut 2 | Cut 3 | Cut 1 | Cut 2 | Cut 3 |
| (0.0; +) | 3.80 | 1.56 | 1.49 | 5.97 | 3.06 | 2.99 |
| (0.0; -) | 3.09 | 1.11 | 1.06 | 4.53 | 2.08 | 2.02 |
| (0.2 <i>i</i> ; +) | 7.69 | 2.81 | 2.77 | 13.86 | 6.21 | 6.16 |
| (0.2 <i>i</i> ; -) | 5.03 | 2.44 | 2.30 | 8.38 | 4.97 | 4.77 |
| (-0.2 <i>i</i> ; +) | 7.15 | 2.81 | 2.77 | 12.87 | 8.66 | 8.29 |
| (-0.2 <i>i</i> ; -) | 5.28 | 1.74 | 1.71 | 8.75 | 3.63 | 3.59 |

Table 6.1: The effect of cuts on the SSD cross section for non-zero $\text{Im}(\tilde{b})$; the \pm signs refer to the charge of the SSD. The cross sections are in fb and are evaluated at $\sqrt{s} = 14$ TeV. The cuts are explained in the text.

for the rest of this work. We also present distributions only for Higgs mass (m_H) of 150 GeV since the cross section in this case is larger. The distributions for $m_H = 130$ GeV are qualitatively similar. The asymmetry distributions are shown for both Higgs masses and it will be seen that $m_H = 130$ GeV is in fact more sensitive to some of them.

The first variable of interest is the difference in transverse momenta of the leptons. The two leptons in the SSD channel are labeled in descending order of their p_T . We then define $\Delta p_T = p_T^{(1)} - p_T^{(2)}$. The charge of the SSD points out whether we have a W^+ or W^- initiated process. Figure 6.2 shows the distribution for both W^\pm -type processes. The sign of $\text{Re}(\tilde{b})$ does not affect the hardness of the distribution. Therefore, we show only one curve corresponding to $\text{Re}(\tilde{b}) = 0.2$. However, the difference due to change in sign of $\text{Im}(\tilde{b})$ is reflected in the two curves corresponding to $\text{Im}(\tilde{b}) = \pm 0.2$.

Next, we consider the distribution in the angle between the two same-sign leptons. In the absence of any cuts, the distribution peaks at $\theta = 0$, i.e. $\cos \theta = 1$. However, the p_T cuts remove nearly all these highly collinear events. The peak for SM curve is shifted from $\cos \theta = 1$ to $\cos \theta \sim 0.5$. Figure 6.3 shows how the distribution changes for non zero $\text{Re}(\tilde{b})$ and $\text{Im}(\tilde{b})$. The effect of the anomalous coupling is to enhance the back-to-back nature of the distribution. The forward peak is almost completely diminished. A quantitative measure of this change can be made by measuring the asymmetry around $\cos \theta = 0$.

We then look at the $\Delta\phi$ distribution, where $\Delta\phi$ is defined as $\phi_{\ell_1} - \phi_{\ell_2}$ and ϕ stands for the azimuthal angle. In this case however, we adopt a different ordering of the leptons. We wish to identify which lepton is more likely to come from Higgs decay (ℓ_2) and which from the main hard interaction (ℓ_1). Since one of the W s from the Higgs decays into jets, we would expect the lepton from Higgs decay to be closer to at least one of the jets than the other lepton. We therefore pick the lepton with the smallest distance to any of the jets as ℓ_2 and then construct $\Delta\phi$. Contrary to the previous distributions, this

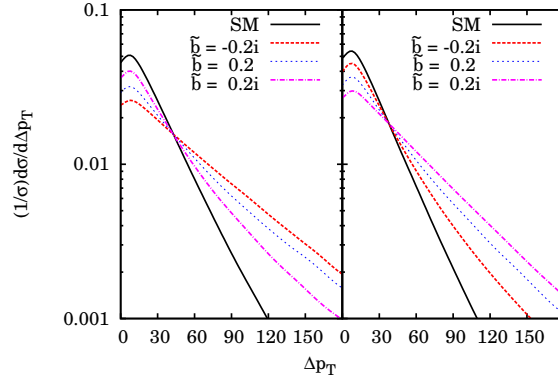


Figure 6.2: The normalised Δp_T distribution between two same-sign leptons for $m_H = 150$ GeV. The left(right) panel corresponds to $\ell^+\ell^+$ ($\ell^-\ell^-$) final states.

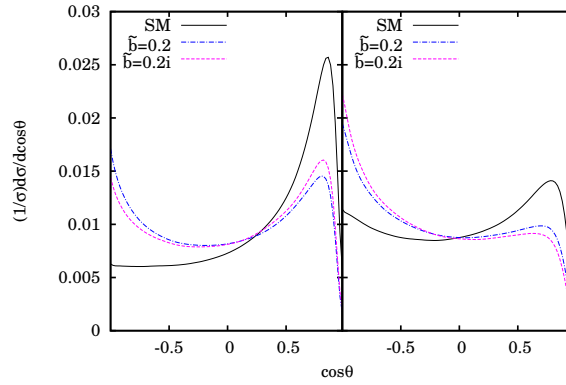


Figure 6.3: The normalised distribution of cosine of the angle between two same-sign leptons for $m_H = 150$ GeV. The effect of changing either $\text{Re}(\tilde{b})$ or $\text{Im}(\tilde{b})$ is to enhance the back-to-back nature of the leptons. The left panel shows the distributions for $\ell^+\ell^+$ whereas the right panel shows the $\ell^-\ell^-$.

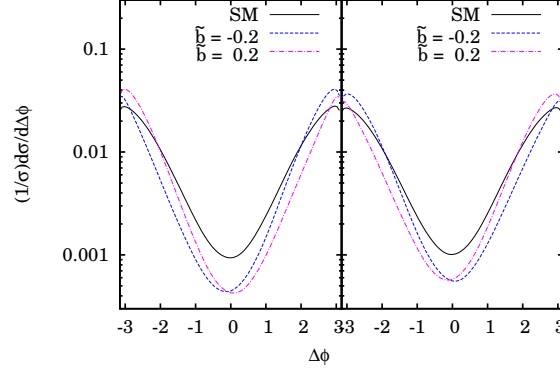


Figure 6.4: Effect of positive (dashed) and negative (dot-dashed) values of $\text{Re}(\tilde{b})$ on the $\Delta\phi$ distributions for $m_H = 150$ GeV. The left panel corresponds to $\ell^+\ell^+$ and the right to $\ell^-\ell^-$ final states.

distribution is particularly sensitive to the sign of $\text{Re}(\tilde{b})$ but not to the sign of $\text{Im}(\tilde{b})$. The effect of different $\text{Re}(\tilde{b})$ on both $\ell^+\ell^+$ and $\ell^-\ell^-$ can be seen from Figure 6.4. A non-zero $\text{Im}(\tilde{b})$ only changes the height of the dip and the distribution is symmetric about $\Delta\phi = 0$ whereas flipping the sign of $\text{Re}(\tilde{b})$ flips the distribution as well.

Since the $\Delta\phi$ distribution has a central dip and also shows left-right symmetry for the standard model case, we can construct two kinds of asymmetries, viz.

$$A_{\text{SSD1}} = \frac{\sigma(\Delta\phi > 0) - \sigma(\Delta\phi < 0)}{\sigma(\Delta\phi > 0) + \sigma(\Delta\phi < 0)} \quad (6.2)$$

$$A_{\text{SSD2}} = \frac{\sigma(|\Delta\phi| < \pi/2) - \sigma(|\Delta\phi| > \pi/2)}{\sigma(|\Delta\phi| < \pi/2) + \sigma(|\Delta\phi| > \pi/2)} \quad (6.3)$$

The first is a left-right asymmetry which captures the change in the sign of $\text{Re}(\tilde{b})$ but remains unaffected by $\text{Im}(\tilde{b})$. The effect of $\text{Re}(\tilde{b})$ on A_{SSD1} is shown in Figure 6.5. The sign of the asymmetry is oppositely correlated to the sign of the coupling. We also look at A_{SSD2} distribution given in Figure 6.6 which describes how central the $\Delta\phi$ distribution is. We notice that the effect of both $\text{Re}(\tilde{b})$ and $\text{Im}(\tilde{b})$ is similar in this regard. Therefore if A_{SSD2} shows a significant deviation from the SM value but A_{SSD1} does not, it would point to the presence of a non zero $\text{Im}(\tilde{b})$.

For a reasonable estimation at the LHC, we require that the asymmetries be reasonable separated from the SM value by at least three standard deviations. Using the formula in equation (5), for a value of $\text{Re}(\tilde{b}) = 0.2$ and $m_H = 150$ GeV for $\ell^+\ell^+$ events, we find that a luminosity of 30fb^{-1} gives an asymmetry $A_{\text{SSD1}} = -0.210 \pm 0.065$ and $A_{\text{SSD2}} = -0.886 \pm 0.031$, both of which are inconsistent with the SM values of

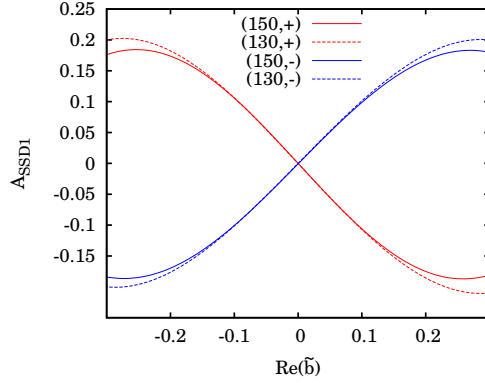


Figure 6.5: The asymmetry A_{SSD1} for different values of $\text{Re}(\tilde{b})$ for $\ell^+\ell^+$ (red) and $\ell^-\ell^-$ (blue) with $\text{Im}(\tilde{b}) = 0$. The labels refer to the Higgs mass and the sign of the SSD.

$A_{\text{SSD1}} = -0.002$ and $A_{\text{SSD2}} = -0.786$ by the required factor.² A 5σ difference can be achieved with 50 fb^{-1} data. The corresponding 3σ measurement for $m_H = 130 \text{ GeV}$ can be done with 50 fb^{-1} giving $A_{\text{SSD1}} = -0.222 \pm 0.074$ and $A_{\text{SSD2}} = -0.88 \pm 0.036$. A 5σ measurement would require 140 fb^{-1} .

To complement the $\Delta\phi$ variable which is sensitive to the sign of $\text{Re}(\tilde{b})$, we would also like to construct a variable that is sensitive to the sign of $\text{Im}(\tilde{b})$. We first reconstruct the W that has decayed into jets and obtain its rapidity, η_W . We then construct $\Delta\eta = |\eta_1 - \eta_W| - |\eta_2 - \eta_W|$. Where $\eta_{1,2}$ are the rapidities of the leptons ordered in the descending order of p_T . We use the difference from η_W to make the variable invariant under Lorentz boosts in the beam direction. This variable is most likely to be modified after taking into account initial and final state radiation (ISR and FSR) effects as the number of jets are modified. We shall deal with this concern in Section 6.3.

We also construct a similar variable, $\Delta|\eta| = |\eta_1| - |\eta_2|$ which shows sensitivity to $\text{Im}(\tilde{b})$ and is much less sensitive to $\text{Re}(\tilde{b})$. It also has the added advantage that one need not reconstruct the W and therefore can look into inclusive SSD final states and is therefore expected to be more robust to FSR effects. However, it should be noted that this variable is not invariant under longitudinal boosts.

The distributions of $\Delta\eta$ and $\Delta|\eta|$ are shown in Figure 6.7 and 6.8 respectively. In both the cases, the $\ell^+\ell^+$ final state is particularly sensitive to $\text{Im}(\tilde{b}) < 0$ whereas the $\ell^-\ell^-$ one is sensitive to $\text{Im}(\tilde{b}) > 0$. Therefore, we can use these variables to confirm the presence of a non-zero $\text{Im}(\tilde{b})$ as only one of $\ell^+\ell^+$ or $\ell^-\ell^-$ will show a significant deviation from the SM value. The first variable is useful because it shows a larger

²The sensitivities have been calculated using $\frac{\delta A}{A} = \frac{2(N^-\sqrt{N^+} - N^+\sqrt{N^-})}{(N^+)^2 - (N^-)^2}$.

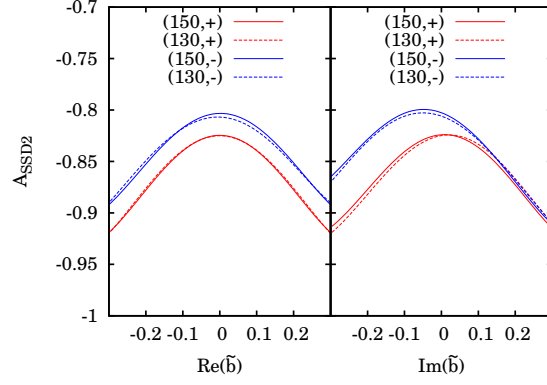


Figure 6.6: The asymmetry A_{SSD2} for different values of the anomalous couplings. The labels indicate the Higgs mass and the sign of the SSD.

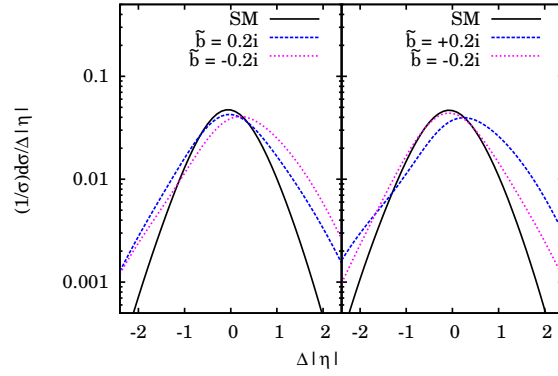


Figure 6.7: Effect of positive (dashed) and negative (dot-dashed) values of $\text{Im}(\tilde{b})$ on the $\Delta\eta$ distributions for $m_H = 150$ GeV. The left panel corresponds to $\ell^+\ell^+$ and the right to $\ell^-\ell^-$ final states.

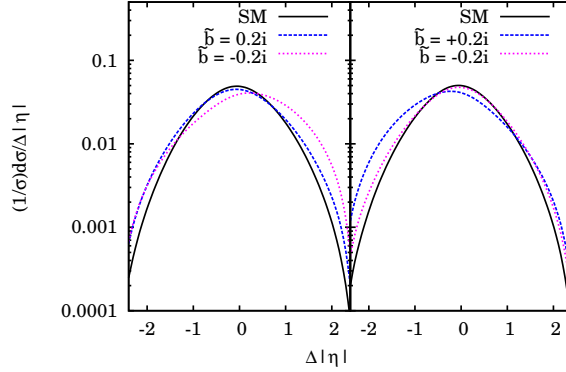


Figure 6.8: Effect of positive (dashed) and negative (dot-dashed) values of $\text{Im}(\tilde{b})$ on the $\Delta|\eta|$ distributions for $m_H = 150$ GeV. The left panel corresponds to $\ell^+\ell^+$ and the right to $\ell^-\ell^-$ final states.

asymmetry and can therefore be used with lower luminosity. However, the shift in the curve is independent of the sign of $\text{Im}(\tilde{b})$. The second variable on the other hand, has a lower asymmetry but changes sign depending on the sign of $\text{Im}(\tilde{b})$. We also find that the effect of non-zero $\text{Re}(\tilde{b})$ is much smaller and is un-correlated with its sign. Here too, we can construct left-right asymmetries to better parametrise this difference.

$$A_{\text{SSD3}} = \frac{\sigma(\Delta\eta > 0) - \sigma(\Delta\eta < 0)}{\sigma(\Delta\eta > 0) + \sigma(\Delta\eta < 0)} \quad (6.4)$$

$$A_{\text{SSD4}} = \frac{\sigma(\Delta|\eta| > 0) - \sigma(\Delta|\eta| < 0)}{\sigma(\Delta|\eta| > 0) + \sigma(\Delta|\eta| < 0)} \quad (6.5)$$

The distribution of the asymmetry A_{SSD3} for different values of $\text{Re}(\tilde{b})$ and $\text{Im}(\tilde{b})$ is shown in Figure 6.9. We can see that $\text{Re}(\tilde{b})$ affects both $\ell^+\ell^+$ or $\ell^-\ell^-$ symmetrically whereas $\text{Im}(\tilde{b})$ shows a very pronounced asymmetry depending on sign. For $\ell^+\ell^+$ events observed with an integrated luminosity of $30(50) \text{ fb}^{-1}$ and $\tilde{b} = -0.2i$, we get an asymmetry $A_{\text{SSD3}} = 0.288 \pm 0.061(0.241 \pm 0.070)$ for $m_H = 150(130)$ GeV with as compared to the SM value of -0.01 (same for both Higgs masses). The distribution of A_{SSD4} is shown in Figure 6.10. The left panel shows the dependence on $\text{Re}(\tilde{b})$. The asymmetry distribution is symmetric with respect to its sign but is of opposite sign for $\ell^+\ell^+$ and $\ell^-\ell^-$ states. The right panel shows the effect of $\text{Im}(\tilde{b})$. We see that in this case as well, the sign of $\text{Im}(\tilde{b})$ causes pronounced asymmetry in either $\ell^+\ell^+$ or $\ell^-\ell^-$ states. This asymmetry can therefore supplement the conclusions from A_{SSD3} . For $\ell^+\ell^+$ states with $\tilde{b} = -0.2i$ and $30(50) \text{ fb}^{-1}$ integrated luminosity, A_{SSD4} takes the values $0.217 \pm 0.062(0.191 \pm 0.071)$ for $m_H = 150(130)$ GeV.

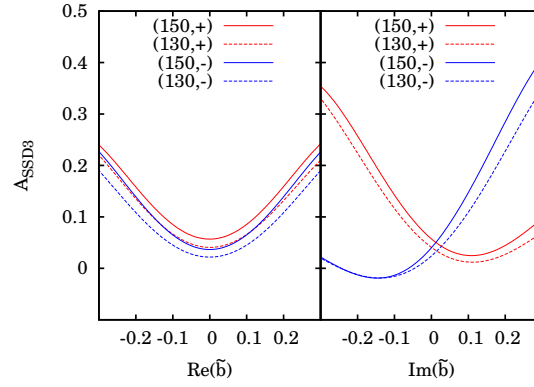


Figure 6.9: The asymmetry A_{SSD3} for different values of the anomalous couplings. The labels indicate the Higgs mass and the sign of the SSD.

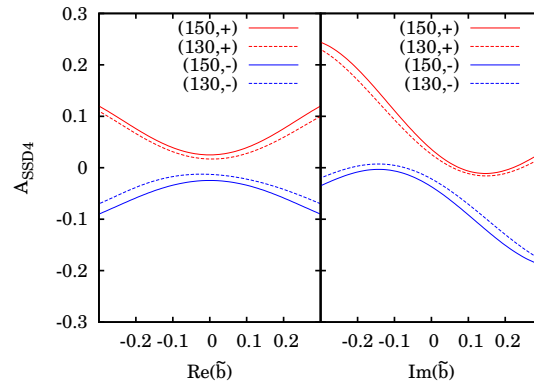


Figure 6.10: The asymmetry A_{SSD4} for different values of the anomalous couplings. The labels indicate the Higgs mass and the sign of the SSD.

In all we find that the presence of anomalous couplings makes the Δp_T distribution harder and enhances the back-to-back region in the $\cos \theta$ distribution. Since the reliable construction of the asymmetries requires accumulation of a large data set, we first test the presence of anomalous couplings using these two distributions. We can then use the three asymmetry variables to for positive and negative SSD to determine what kind of anomalous coupling is present. Let the labels (+) and (-) refer to the charge of the SSD. Then we can conclude the following:

- $A_{\text{SSD1}}(\pm) = 0 \Rightarrow \text{Re}(\tilde{b}) = 0$
- $A_{\text{SSD1}}(+) \neq 0 \Rightarrow \text{Re}(\tilde{b}) \neq 0; \text{sign}(\text{Re}(\tilde{b})) = -\text{sign}(A_{\text{SSD1}}(+))$
- $|A_{\text{SSD3,SSD4}}(+)| < |A_{\text{SSD3,SSD4}}(-)| \Rightarrow \text{Im}(\tilde{b}) > 0$
- $|A_{\text{SSD3,SSD4}}(+)| > |A_{\text{SSD3,SSD4}}(-)| \Rightarrow \text{Im}(\tilde{b}) < 0$

Since the asymmetry variables listed above are not explicitly CP-violating, it is possible that they might also be affected by the presence of CP-conserving anomalous coupling b . We therefore wish to determine if it is possible to get similar results from a non-zero value of b and whether it is possible to distinguish the effect of the two kinds of couplings.

We perform a similar calculation of $pp \rightarrow h\ell\nu$ and $h \rightarrow \ell\nu jj$ using the HWW vertex given in equation 6.1 with $\tilde{b} = 0$ instead. The cross section of Higgs production after including b is then required to also be within the Tevatron bounds. This corresponds to a value of $|b| \leq 0.05$ which will be used for the rest of this section. We then examine the three asymmetries defined in the previous section with the same cuts.

We find that the $\Delta\phi$ asymmetry A_{SSD1} and the $\Delta|\eta|$ -based A_{SSD4} are both completely unaffected by the presence of b . Therefore, these two together can constitute robust variables at the LHC for confirming the presence of a CP-violating anomalous HWW coupling. The second $\Delta\phi$ -based asymmetry, A_{SSD2} is more negative in the case of CP-conserving anomalous couplings. However, the difference is small and measuring it with accuracy will require a large luminosity. The $\Delta\eta$ -based A_{SSD3} shows similar behaviour between non zero values b and $\text{Im}(\tilde{b})$. We can further discriminate between b or \tilde{b} type coupling by examining the Δp_T distribution which falls off much slower in the case of the CP conserving coupling. This can set apart the presence of $\text{Im}(\tilde{b})$ quite distinctly. As an illustration, we present a comparison in Figure 6.11. We find that difference in the distributions for $b > 0 (b < 0)$ is probed best in $\ell^+\ell^+$ ($\ell^-\ell^-$) channels irrespective of the sign of $\text{Im}(\tilde{b})$. In both cases, we find the distributions are distinct enough to allow us to separate the effects from the two couplings.

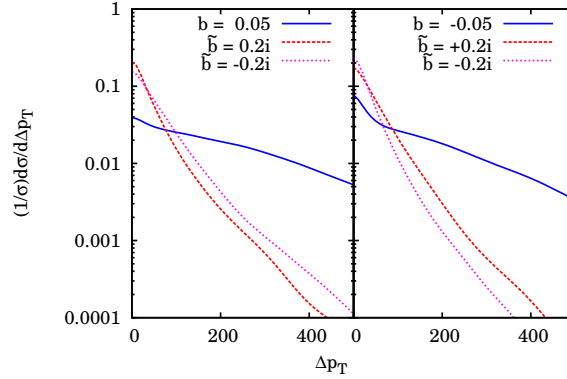


Figure 6.11: Comparison of the normalised Δp_T distribution between two same-sign leptons for $m_H = 150$ GeV for values of b and \tilde{b} . The left(right) panel corresponds to $\ell^+\ell^+$ ($\ell^-\ell^-$) process.

6.3 Effect of showering and hadronisation

Until now we have been working under the simplified scheme of parton-level Monte-Carlo analysis. However, initial and final-state radiation play a very important role at the LHC. In particular the entire partonic system can acquire a transverse momentum due to recoil from ISR. One therefore needs to examine whether the effects of showering destroy the correlations we had examined in the previous section. In this section, we investigate this in the context of the distributions and asymmetries defined above.

We have started by obtaining unweighted events from the parton-level code, which are then passed through PYTHIA8[170, 73] using the LHEF file format[171]. PYTHIA8 performs the initial and final state showers and hadronisation after which we use Fast-Jet 2.4.1 with the anti-kt algorithm[104] with a cone size parameter of 0.4 to form the jets. Leptons are considered isolated if the sum of E_T of particles around the lepton within a cone of 0.2 is less than 10 GeV and the separation with the nearest jet is greater than 0.4. All the variables and asymmetries are defined as before.

As an illustration, we first present the $\Delta\phi$ distributions for a $\ell^+\ell^+$ final state for a value of $\tilde{b} = 0.2$ in Figure 6.12. It can be seen that the distribution retains the correct left-right asymmetry. The $\Delta\eta$ distribution for $\ell^-\ell^-$ and a value of $\tilde{b} = 0.2i$ is shown in Figure 6.13 and the $\Delta|\eta|$ distribution is shown in Figure 6.14. In these cases too, we see that the distribution is fairly unchanged. Both these distributions can therefore be thought of as a robust variables for LHC analyses.

We also present the values of the asymmetry variable constructed in the previous sections in Table 6.2. The variable A_{SSD1} is the most robust as the values change only

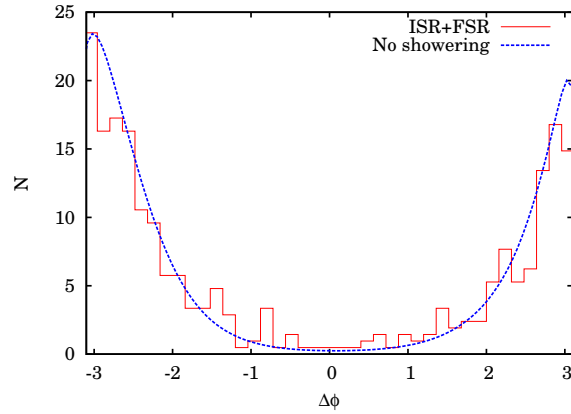


Figure 6.12: Comparison of the $\Delta\phi$ distribution before and after including ISR and FSR for $\ell^+\ell^+$ final states and a value of $\tilde{b} = 0.2$ and $m_H = 150$ GeV for 30 fb^{-1} .

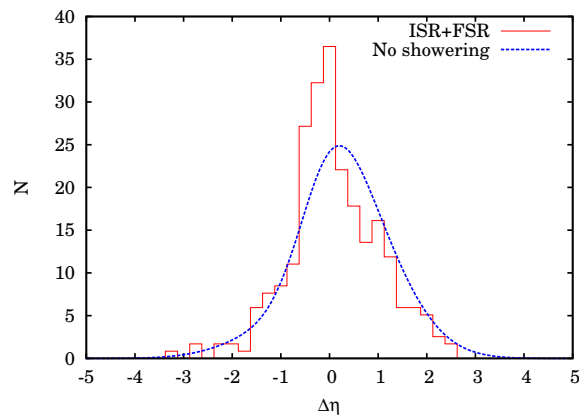


Figure 6.13: Comparison of the $\Delta\eta$ distribution before and after including ISR and FSR for $\ell^-\ell^-$ final states and a value of $\tilde{b} = 0.2i$ and $m_H = 150$ GeV for 30 fb^{-1} .

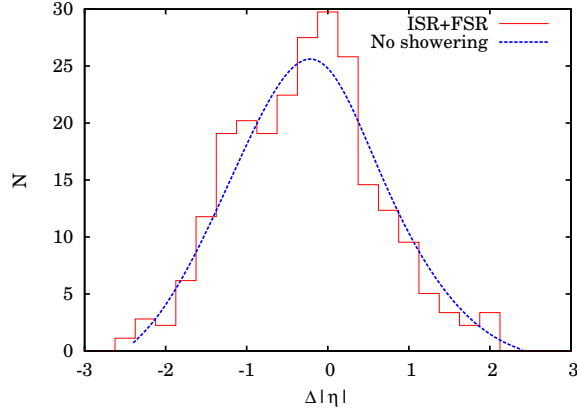


Figure 6.14: Comparison of the $\Delta|\eta|$ distribution before and after including ISR and FSR for $\ell^-\ell^-$ final states and a value of $\tilde{b} = 0.2i$ and $m_H = 150$ GeV for 30 fb^{-1} .

very slightly. The $\Delta\eta$ dependent $A_{\text{SSD}3}$ still shows an asymmetry based on sign of $\text{Im}(\tilde{b})$ but the effect is diluted after taking ISR effects into account.

| | | $\tilde{b} = 0$ | $\tilde{b} = 0.2$ | $\tilde{b} = -0.2$ | $\tilde{b} = 0.2i$ | $\tilde{b} = -0.2i$ |
|-------------------|-------|-----------------|-------------------|--------------------|--------------------|---------------------|
| $A_{\text{SSD}1}$ | W^+ | 0.03(0.00) | -0.27(-0.21) | 0.19(0.21) | 0.08(0.00) | -0.07(0.00) |
| | W^- | -0.08(0.00) | 0.27(0.20) | -0.19(-0.20) | -0.03(0.00) | 0.03(0.00) |
| $A_{\text{SSD}2}$ | W^+ | -0.73(-0.79) | -0.82(-0.89) | -0.80(-0.87) | -0.76(-0.88) | -0.77(0.87) |
| | W^- | -0.61(-0.77) | -0.78(-0.86) | -0.80(-0.86) | -0.78(-0.88) | -0.70(-0.83) |
| $A_{\text{SSD}3}$ | W^+ | 0.05(-0.01) | 0.06(0.17) | 0.06(0.17) | 0.03(0.04) | 0.12(0.31) |
| | W^- | 0.02(-0.03) | 0.10(0.15) | 0.06(0.15) | 0.12(0.29) | 0.03(0.02) |
| $A_{\text{SSD}4}$ | W^+ | -0.01(-0.01) | 0.02(0.08) | 0.04(0.08) | -0.01(-0.01) | 0.13(0.22) |
| | W^- | -0.05(-0.01) | -0.08(-0.06) | -0.14(-0.06) | -0.11(-0.17) | -0.03(-0.01) |

Table 6.2: Asymmetries after ISR and FSR for $m_H = 150$ GeV. The value from parton-level calculations is given in the parentheses for comparison.

6.4 Conclusions

We have systematically examined the effects of a CP-violating HWW coupling on Higgs production and decay at the LHC. We probe this coupling via the WH associated production followed by $H \rightarrow WW^* \rightarrow \ell\nu f\bar{f}'$ which gives rise to same-sign dilepton final states. We take into account the Tevatron limits on the Higgs cross section to restrict the values of real and imaginary parts of the anomalous coupling. We find that,

besides enhancing the production cross section, it also causes significant deviations in various kinematic correlations between leptons in the final state.

We have presented several variables whose distributions show significant deviation from the standard model case. We also define asymmetries constructed from three of them, viz. $\Delta\phi$, $\Delta\eta$ and $\Delta|\eta|$, which can show significant deviation from SM predictions. Trends in the Δp_T and $\cos\theta$ distributions may be used to first ascertain the presence of an anomalous coupling. The left-right asymmetry in the $\Delta\phi$, $\Delta\eta$ and $\Delta|\eta|$ distributions can be used to probe its nature in detail. The errors due to statistical and systematic effects are out of the scope of this current work. However, the reader may refer to [150] for a detailed analysis.

After imposing cuts required to suppress the SM backgrounds, the asymmetries can be discerned at the $3(5)\sigma$ level at 14 TeV, with an integrated luminosity of $30(50) \text{ fb}^{-1}$ for a Higgs of mass 150 TeV. The asymmetries for a Higgs mass of 130 GeV can be similarly determined at $3(5)$ sigma with $50(140) \text{ fb}^{-1}$. It should be noted that our calculation is done at the leading order, and the inclusion of an appropriate next-to-leading order K-factor is expected to enhance the signal rates. We also present and compare various distributions at the parton level and after showering and hadronisation. We find that our conclusions are largely unchanged, even after taking the latter effects into account.

CHAPTER

7

CONCLUSIONS

In this thesis, we have tried to address two main questions — that of discovering supersymmetry by looking for third generation squarks and that of determining the nature of Higgs coupling to W-bosons.

Supersymmetry

Supersymmetry, if present, will be detectable at the LHC via production of coloured superparticles, viz. the squarks and the gluinos. Since the naturalness argument requires only a light stop to stabilize the higgs mass, we concentrate on discovering the third generation squark sector of the MSSM.

We investigate the signals of supersymmetry in a scenario where only the third family squarks and sleptons can be produced at the LHC, in addition to the gluino, charginos and neutralinos. The final states in such cases are marked by a multiplicity of top and/or bottom quarks. We study in particular, the case when the stop, sbottom and gluino masses are near the TeV scale due to which, the final state t's and b's are very energetic. We point out the difficulty in b-tagging and identifying energetic tops and suggest several event selection criteria which allow the signals to remain significantly above the standard model background. We show that such scenarios with gluino mass up to 2 TeV can be successfully probed at the LHC. Information on $\tan\beta$ can also be obtained by looking at associated Higgs production in the cascades of accompanying neutralinos.

We also show that a combined analysis of event rates in the different channels and the effective mass distribution allows one to differentiate this scenario from the one where all three sfermion families are accessible.

Next, we present a re-interpretation of the recent ATLAS limits on supersymmetry in channels with jets (with and without b-tags) and missing energy, in the context of light third family squarks, while the first two squark families are inaccessible at the 7 TeV run of the LHC. In contrast to interpretations in terms of the high-scale based constrained minimal supersymmetric standard model, we primarily use the low-scale parametrisation of the phenomenological MSSM, and translate the limits in terms of physical masses of the third family squarks. Side by side, we also investigate the limits in terms of high-scale scalar non-universality, both with and without low-mass sleptons. Our conclusion is that the limits based on zero-lepton channels are not altered by the mass-scale of sleptons, and can be considered more or less model-independent.

Finally, we investigate the detectability of R-parity violating resonant production of a stop, driven by baryon number violating interactions in supersymmetry. We work in the framework of minimal supergravity models with the lightest neutralino being the lightest supersymmetric particle which decays within the detector. We look at various dilepton and trilepton final states, with or without b-tags. A detailed background simulation is performed, and all possible decay modes of the lighter stop are taken into account. We find that higher stop masses are sometimes easier to probe, through the decay of the stop into the third or fourth neutralino and their subsequent cascades. We also comment on the detectability of such signals during the 7 TeV run, where, as expected, only relatively light stops can be probed. Our conclusion is that the resonant process may be probed, at both 10 and 14 TeV, with the R-parity violating coupling λ''_{312} as low as 0.05, for a stop mass of about 1 TeV. The possibility of distinguishing between resonant stop production and pair-production is also discussed.

Higgs

The LHC has promising data from its searches for the SM Higgs. However, once a Higgs-like resonance is discovered, it will be crucial to measure its properties and, in particular, its couplings to the massive gauge bosons to confirm its identity.

We investigate the possibility of probing an anomalous CP-violating coupling in the HWW vertex at the LHC. We consider the production of the Higgs in association of a W and then decay via the $H \rightarrow WW$ channel taking into account the limits on the Higgs production cross section from the Tevatron. We select the same-sign dilepton final state arising from leptonic decays of two of the three Ws and apply cuts required to suppress the standard model background. Several kinematical distributions and asymmetries that can be used to ascertain the presence of a non-zero anomalous coupling are presented. We find that, for Higgs mass in the range 130-150 GeV and anomalous cou-

plings allowed by the Tevatron data, these distributions can be studied with an integrated luminosity of $30\text{-}50\text{ fb}^{-1}$ at the 14 TeV run. For a smaller Higgs mass, a larger luminosity will be needed. Attention is specifically drawn to some asymmetries that enable one to probe the real and imaginary parts (as well as their signs) of the anomalous coupling, in a complementary manner. The asymmetries are slightly enhanced for lower Higgs masses. We also explicitly demonstrate that showering and hadronisation do not affect the utility of these variables, thus affirming the validity of parton level calculations.

Appendix

APPENDIX

A

MSSM IN PYTHIA 8

PYTHIA 8 [170] is a general-purpose Monte Carlo event generator [172] for a full simulation of high-energy collision events. It includes a comprehensive library of hard-scattering processes, particle decays, initial- and final-state parton-shower models [173, 174], hadronization through string fragmentation [175] and models of beam remnants and multiple interactions [176, 177]. It contains a native implementation of a wide variety of SM and BSM processes and also provides a standard interface [171, 178] to external programs which may be used by a standalone generator.

This appendix describes work [179] done in collaboration with Peter Skands at CERN as the part of a short-term studentship funded by the project “MCnet” (contract number MRTN-CT-2006-035606). The work was done during my tenure as a PhD student and this appendix details my particular contributions to the code PYTHIA 8.

Supersymmetry is considered one of the best motivated extensions of the SM due to its ability to address many outstanding theoretical and experimental issues. In particular, the Minimal Supersymmetric extension of the Standard Model (MSSM) is currently a popular candidate for a BSM theory. The MSSM extends the SM by the addition of one pair of SUSY generators which implies the presence of one superpartner to each SM state. The MSSM particle spectrum therefore has squarks (\tilde{q}_i), sleptons ($\tilde{\ell}_i$) and gauginos (\tilde{B} , \tilde{W}^i and \tilde{g}) as the supersymmetric counterparts of quarks, leptons and gauge bosons respectively. The requirement of self-consistency of the theory via anomaly cancellation also demands two Higgs doublet fields H_u and H_d . Since MSSM has two Higgs doublets, EWSB leaves us with with five physical Higgs degrees of freedom viz.

the CP-even h_0 and H_0 , the CP-odd A_0 and two charged Higgs bosons H^\pm . The superpartners of the Higgses — the fermionic “Higgsinos” — mix with the gauginos to form neutralinos and charginos. In particular, the neutral Higgsinos (\tilde{H}_1 and \tilde{H}_2) mix with the neutral $U(1)$ and $SU(2)$ gauginos (\tilde{B} and \tilde{W}^3) to form the mass eigenstates called the neutralinos ($\tilde{\chi}_i^0; i = 1 - 4$.) Similarly, the charged Higgsino mixes with the charged $SU(2)$ gaugino to form charginos ($\tilde{\chi}_i^\pm; i = 1, 2$.) The next-to-minimal supersymmetric extension of the SM (nMSSM) extends this scenario by adding one extra singlet Higgs field. This adds another member to the neutralinos and the neutralino mixing matrix is enlarged to 5×5 . The current implementation of PYTHIA 8 includes the nMSSM extension and allows processes with CP, flavour or R-parity violation.

PYTHIA 8 uses the standard PDG codes for numbering the superpartners [6] and the particle spectrum is read in via an SLHA file [180, 181]. We use the super-CKM basis (in the conventions of the SLHA2 [181]) for describing the squark sector which allows non-minimal flavour violation. The mass-eigenstates of the squarks are then related to the left- and right-handed squarks via a 6×6 complex mixing matrix. Our implementation can therefore be used to study both CP violation and flavour violation in the squark sector.

$$\begin{pmatrix} \tilde{u}_1 \\ \tilde{u}_2 \\ \tilde{u}_3 \\ \tilde{u}_4 \\ \tilde{u}_5 \\ \tilde{u}_6 \end{pmatrix} = R^u \begin{pmatrix} \tilde{u}_L \\ \tilde{c}_L \\ \tilde{t}_L \\ \tilde{u}_R \\ \tilde{c}_R \\ \tilde{t}_R \end{pmatrix}; \quad \begin{pmatrix} \tilde{d}_1 \\ \tilde{d}_2 \\ \tilde{d}_3 \\ \tilde{d}_4 \\ \tilde{d}_5 \\ \tilde{d}_6 \end{pmatrix} = R^d \begin{pmatrix} \tilde{d}_L \\ \tilde{s}_L \\ \tilde{b}_L \\ \tilde{d}_R \\ \tilde{s}_R \\ \tilde{b}_R \end{pmatrix} \quad (\text{A.1})$$

The neutralino mixing matrix \mathcal{N} is a 4×4 (5×5 in the case of nMSSM) mixing matrix describing the transformation of the gauge eigenstate fermions ($-i\tilde{B}$, $-i\tilde{W}_3$, H_1 , H_2) into the mass eigenstates ($\tilde{\chi}_1^0, \tilde{\chi}_2^0, \tilde{\chi}_3^0, \tilde{\chi}_4^0$). The two chargino mixing matrices \mathcal{U} and \mathcal{V} describe the diagonalization of the chargino mass matrix from the gauge eigenstates ($-iW^+$, H^+) to ($\tilde{\chi}_1^+$, $\tilde{\chi}_2^+$). Supplementary conventions for vertices and most of the cross-section formulae are taken from [182], as detailed below.

A.1 Couplings

PYTHIA 8 reads particle masses and mixing matrices via the SUSY Les Houches Accord (SLHA2) framework [181]. (Read-in of SLHA1 spectra [180] is also supported, but mixing the two standards is strongly discouraged, as the internal translation from SLHA1 to SLHA2 has only been designed with the original SLHA1 in mind.) The raw data read in by the `SusyLesHouches` class is accessed by the `CoupsUSY` class which uses the information to construct all the SUSY couplings. The couplings are

defined according to [182] for all cases except for couplings of superparticles to Higgs bosons which are defined according to [183].

The running of electroweak and strong couplings is carried over from the corresponding one-loop calculations in the Standard Model. The `GAUGE` block can be used to set the boundary values of all three SM couplings at the SUSY breaking scale. By default, the masses of W and Z are assumed to be the pole masses and are used to calculate the on-shell value of $\sin^2 \theta_W = 1 - m_W^2/m_Z^2$. If externally provided in the SLHA file, the value of $\sin \theta_W$ can be set to the running value using the flag `SUSY:sin2thetaWMode = 2` (see the PYTHIA 8 HTML user reference included with the code [170]). The ratio of the two Higgs vacuum expectation values ($\tan \beta$) is read in from the low scale value provided by the `MINPAR` and `EXTPAR` blocks. The default value of the Higgs mixing angle (α_H) is set to the SM limit ($\beta - \pi/2$) which is then overwritten by the contents of the `HMIX` block.

Since the SLHA interface has been extended and can now be used to pass information on any new particles and decays [178], the presence of the `MODSEL` block is used as an indicator of SUSY models and PYTHIA 8 will initialize the `COUPLSUSY` class only if this block is present. Skipping the `MODSEL` block is acceptable for Les Houches Event files (LHEF) as long as the user supplies an external decay table for all required cascade decays.

A.2 R-parity violation

The most general MSSM superpotential allows both lepton and baryon-number violating processes. This is generally avoided by demanding invariance under an R-parity defined as $(-1)^{3B-L+2S}$. From this definition, all SM particles are even whereas all superpartners are odd under R-parity. A well known consequence of this is that the Lightest SUSY particle (LSP) must be stable. A neutral, weakly interacting LSP can therefore be a good candidate for dark matter. However, the imposition of R-parity can be considered an aesthetic requirement rather than a consistency requirement and possible R-parity violating interactions, if present, can be probed by collider experiments. We therefore include R-parity violating production and decay processes in our implementation.

In SLHA conventions, the R-parity violating superpotential is given by

$$\mathcal{W}_{RPV} = \mu_i H_u L_i + \frac{1}{2} \lambda_{ijk} L_i L_j E_k + \lambda'_{ijk} L_i Q_j D_k + \frac{1}{2} \lambda''_{ijk} U_i^c D_j^c D_k^c \quad (\text{A.2})$$

The μ -type terms correspond to bi-linear R-parity violation which causes a mixing between the leptons and neutralinos/charginos. The λ and λ' -type terms lead to lepton number violation whereas λ'' -type terms lead to baryon-number violation. The current implementation does not include the effects of the bi-linear term. The R-parity violating couplings λ_{ijk} are antisymmetric under $i \leftrightarrow j$. Therefore only couplings for $i > j$

are read and the rest are set by the symmetry property. Similarly, λ''_{ijk} is antisymmetric under $j \leftrightarrow k$ and hence only couplings with $j > k$ need to be provided. This implementation includes in particular, the resonant production of a squark via λ'' -type couplings which can be probed at hadron collider experiments. The changes made to showering and hadronization to account for the non-standard colour structure from such terms will be explicitly described in section A.5.

A.3 Cross Sections

The current implementation of SUSY includes all leading-order (LO) $2 \rightarrow 2$ production processes with gluinos, squarks, charginos, and neutralinos in the final state and also $2 \rightarrow 1 \rightarrow 2$ resonant production of squarks via baryon number violating couplings. All available SUSY processes can be turned on using `SUSY:all = on`. Individual subprocesses can then be selected based on the final state by setting `SUSY:idA = PDGcode` and `SUSY:idB = PDGcode`. If only `idA` is provided, all processes with that particle in the final state are turned on. Alternatively, one or more production processes can be turned on using the string `SUSY:processname = on`, again with `SUSY:idA` and `SUSY:idB` providing a further level of subprocess selection. The available subprocess classes are listed in Table A.1.

| Subprocess class | processname |
|------------------------------------|---|
| Chargino and neutralino production | qqbar2chi0chi0, qqbar2chi+-chi0, qqbar2chi+chi-. |
| Gaugino squark production | gg2chi0squark, gg2chi+-squark. |
| Gluino production | gg2gluinogluino, qqbar2gluinogluino. |
| Squark-gluino production | gg2squarkgluino |
| Squark-pair production | gg2squarkantisquark, qqbar2squarkantisquark qq2squarksquark |
| RPV resonant squark production | qq2antisquark |

Table A.1: List of SUSY production processes. In all cases, charge conjugate processes are turned on by default.

The squark-antisquark and squark-squark production processes include contributions from EW diagrams and their interferences. To estimate the size of these contributions, and/or for purposes of comparison to other codes that do not include them,

the cross sections can be restricted to include only the strong-interaction contributions, using the following flags:

- `qqbar2squarkantisquark:onlyQCD = true.`
- `qq2squarksquark:onlyQCD = true.`

The baryon number violating coupling λ''_{ijk} if present, can induce resonant squark production via the process $d_j d_k \rightarrow \tilde{u}_i^*$ which produces a resonant up-type antiquark or via $u_i d_j \rightarrow \tilde{d}_k^*$ or $u_i d_k \rightarrow \tilde{d}_j^*$ which produce a down-type antiquark. The expression for an up-type squark production process is

$$\sigma_{\tilde{u}_i^*} = \frac{2\pi}{3m_i^2} \sum_{jk} \sum_{i'} |\lambda''_{i'jk}(R^u)_{ii'}|^2 \quad (\text{A.3})$$

The expression for down-type squarks is similar, taking into account the symmetry property $\lambda''_{ijk} = -\lambda''_{ikj}$. We implement this production process as `qq2antisquark` and the charge conjugate process ($\bar{q}_i \bar{q}_j \rightarrow \tilde{q}_k$) is included by default.

The supersymmetric Higgs sector is identical in many ways to the Two-Higgs Doublet Model. The Higgs production processes have already been implemented in PYTHIA 8 in the `SigmaHiggs` class. The production of the Higgs bosons can be accessed by including the switch `HiggsBSM:all=on`. For specific Higgs processes, please refer to the HTML user reference included with the code [170].

A.4 Sparticle Decays

SUSY Particle decays are handled by the class `SUSYResonanceWidths`. The user can choose to read in decay tables via SLHA or use the decay widths calculated by PYTHIA. As a default, PYTHIA does not calculate the decay width if a table is externally supplied. Note, however, that while PYTHIA's internal treatment can include sophistications such as matrix-element-based phase-space weighting and running widths, channels read in from an SLHA decay table will be decayed purely according to phase space, with no matrix-element weighting. The internal treatment should therefore be preferable, in most cases, and an option for overriding the automatic read-in of decay tables is provided, by setting the flag `SLHA:useDecayTable = false`.

The decay of a particular particle may be turned off manually using the standard PYTHIA 8 structure `PDGcode:mayDecay = false` or by setting its width to zero in the SLHA decay table. In the former case, the particle will still be distributed according to a Breit-Wigner distribution with non-zero width, whereas it will always be assigned its pole mass in the latter.

Individual decay modes may be switched on/off using the standard PYTHIA 8 methods, documented in the section on “The Particle Data Scheme” in the program’s HTML documentation [170].

The internal treatment of 2-body decays is so far restricted to on-shell particles. A mechanism for effectively generating 3-body decays via sequences of $1 \rightarrow 2$ decays involving off-shell particles is foreseen as an update in the near future (and will be announced in the PYTHIA 8 update notes). An equivalent mechanism is already implemented in PYTHIA 8, e.g., for $h \rightarrow ZZ$ decays for light Higgs bosons.

Currently the following R-parity conserving two-body decays are implemented:

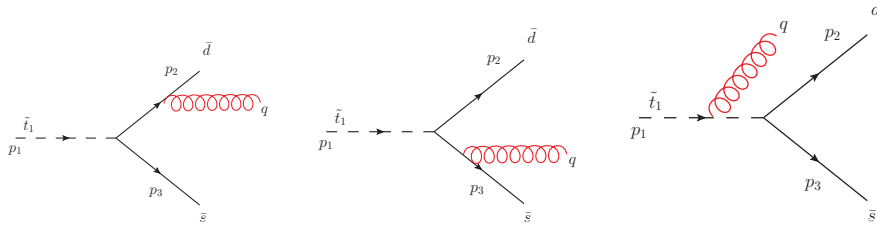
- $\tilde{g} \rightarrow \tilde{q}_i q_j$
- $\tilde{\chi}_i^0 \rightarrow \tilde{q}_i q_j, \tilde{l}_i l_j, \tilde{\chi}_j^0 Z, \tilde{\chi}_j^+ W^-$
- $\tilde{\chi}_i^+ \rightarrow \tilde{q}_i q_j, \tilde{l}_i l_j, \tilde{\chi}_j^+ Z, \tilde{\chi}_j^0 W^+$
- $\tilde{q}_i \rightarrow q_j \tilde{\chi}_k^0, q_j \tilde{\chi}_k^+, \tilde{q}_j Z, \tilde{q}_j W^+$

Besides these, we also include two-body R-parity violating decays of squarks via λ' ($\tilde{q} \rightarrow lq'$) and λ'' -type couplings ($\tilde{q} \rightarrow q'q''$). We also include the three-body decays of neutralinos through λ'' -type couplings via an intermediate squark [184]. For certain final states in three body decays, partial decay via sequential two-body decays may also be kinematically allowed. In this case, we demand that only the off-shell components of the matrix element-squared are allowed to contribute to the three-body decay width. Any interferences between the off-shell and on-shell components are also turned off. The two-body sequential decays then proceed as normal.

The Higgs boson running widths are calculated in the associated classes `ResonanceH` for CP even (h_0, H_0) and the CP odd (A_0) Higgses, and `ResonanceHchg` for charged Higgses (H^\pm). By default, the Higgs decay tables are not overwritten even if they are read via SLHA because PYTHIA 8 performs a more accurate phase space calculation than the flat weighting that is performed for decay widths read in via SLHA. The decays of Higgses into SUSY particles will be included in a future update.

A.5 Showers in R-parity violating case

In this section, we describe PYTHIA’s treatment of QCD radiation in topologies containing colour-epsilon tensors which occurs specifically in the baryon number violating terms of the R-parity violating MSSM. For colour topologies involving the epsilon tensor in colour space (i.e., colour topologies with non-zero baryon number) we first consider the example of $\tilde{t} \rightarrow \bar{q}q$ in the RPV-MSSM model.

Figure A.1: Gluon emission from RPV vertices with ϵ -tensor.

The Lagrangian for the UDD-type interaction terms is

$$\mathcal{L} = -\lambda''_{ijk} \epsilon^{lmn} \left(\tilde{u}_{Ri}^l (\bar{d}^c)^m P_R d_k^m + \tilde{d}_{Rj}^m (\bar{u}^c)^l P_R d_k^m + \tilde{d}_{Rk}^n (\bar{u}^c)^l P_R d_i^m + h.c. \right) \quad (\text{A.4})$$

To extract the behaviour of the radiation function, we look at the ratio of exact matrix element for $\tilde{t}_R(p_1) \rightarrow \bar{d}(p_2)\bar{s}(p_3) + g(q)$ via λ''_{312} to the matrix element for $\tilde{t}_R(p_1) \rightarrow \bar{d}(\hat{p}_2)\bar{s}(\hat{p}_3)$ and retaining only the parts that are soft- or collinear-singular (i.e., which diverge for one or more $q \cdot p_i \rightarrow 0$). Since momentum is explicitly conserved in the shower branching process, the pre- and post-emission momenta must be related by

$$p_1 = \hat{p}_2 + \hat{p}_3 = p_2 + p_3 + q, \quad (\text{A.5})$$

with $p_1^2 = m_1^2$ the invariant mass of the decaying squark.

The Born-level matrix element squared is given by:

$$M_0 = |\lambda''_{312}|^2 (N_c - 1)! (\hat{p}_2 \cdot \hat{p}_3) \quad (\text{A.6})$$

Three diagrams (shown in Fig A.1) contribute to the process where one gluon is emitted from this configuration. The matrix element corresponding to this process i.e. $\tilde{t}_R(p_1) \rightarrow \bar{d}(p_2)\bar{s}(p_3)g(q)$ is denoted by M_1 and, for massless decay products ($p_2^2 = p_3^2 = 0$), is given by

$$\begin{aligned} |M_1|^2 &= 2g^2 |\lambda''_{312}|^2 (N_c - 1)! C_F \times \\ &\left\{ \left[\frac{(p_2 \cdot p_3)}{N_c - 1} \left(\frac{p_1 \cdot p_2}{(p_1 \cdot q)(p_2 \cdot q)} + \frac{p_1 \cdot p_3}{(p_1 \cdot q)(p_3 \cdot q)} + \frac{p_2 \cdot p_3}{(p_2 \cdot q)(p_3 \cdot q)} \right) + \frac{p_2 \cdot q}{p_3 \cdot q} + \frac{p_3 \cdot q}{p_2 \cdot q} \right] \right. \\ &\left. + \frac{1}{N_c - 1} \left(\frac{p_2 \cdot p_3}{p_2 \cdot q} + \frac{p_2 \cdot p_3}{p_3 \cdot q} + \frac{2m_1^2}{p_1 \cdot q} - 2 \right) + \frac{p_2 \cdot p_3}{(p_1 \cdot q)^2} [m_1^2 - p_1 \cdot q] \right\} \quad (\text{A.7}) \end{aligned}$$

$$\begin{aligned} &= 2g^2 |\lambda''_{312}|^2 (N_c - 1)! C_F \times \\ &\left\{ \left[\frac{\hat{s}}{(N_c - 1)} \left(\frac{p_1 \cdot p_2}{(p_1 \cdot q)(p_2 \cdot q)} + \frac{p_1 \cdot p_3}{(p_1 \cdot q)(p_3 \cdot q)} + \frac{p_2 \cdot p_3}{(p_2 \cdot q)(p_3 \cdot q)} \right) + \frac{p_2 \cdot q}{p_3 \cdot q} + \frac{p_3 \cdot q}{p_2 \cdot q} \right] \right. \\ &\left. + \frac{1}{N_c - 1} \left(\frac{2m_1^2}{p_1 \cdot q} - \frac{p_2 \cdot p_3}{p_2 \cdot q} - \frac{p_2 \cdot p_3}{p_3 \cdot q} - 4 \right) + \frac{p_2 \cdot p_3}{(p_1 \cdot q)^2} [m_1^2 - p_1 \cdot q] \right\}. \quad (\text{A.8}) \end{aligned}$$

The ratio of the two squared matrix elements at leading- N_c is then given by:

$$\begin{aligned} \frac{|M_1|^2}{|M_0|^2} = & 8\pi\alpha_s C_F \left[\frac{1}{(N_c - 1)} \left(\frac{p_1 \cdot p_2}{(p_1 \cdot q)(p_2 \cdot q)} + \frac{p_1 \cdot p_3}{(p_1 \cdot q)(p_3 \cdot q)} + \frac{p_2 \cdot p_3}{(p_2 \cdot q)(p_3 \cdot q)} \right) \right. \\ & \left. + \frac{m_1^2}{(p_1 \cdot q)^2} + \frac{1}{m_1^2} \left(\frac{p_2 \cdot q}{p_3 \cdot q} + \frac{p_3 \cdot q}{p_2 \cdot q} \right) \right] + \text{non-singular terms} \end{aligned} \quad (\text{A.9})$$

The antenna pattern represented by this formula can be characterized as follows: the terms on the first line represent three soft-eikonal dipole factors (one for each of the three possible two-particle combinations) and a mass-squared term for the decaying particle. The factor $1/(N_c - 1)$ in front of the dipole factors implies that the normalization of each of these eikonals is half as large as that of the eikonal term in an ordinary $q\bar{q}$ antenna, see, e.g., [185, 186, 187]. These four terms agree with the expression in [184, 188] and correspond to the expression used to generate radiation for this type of colour topology in HERWIG [189]. (Note that, in the HERWIG implementation, the pattern is generated using ordinary full-strength radiation functions, by selecting randomly between each two-particle combination, thereby reproducing the full pattern when summing over events [184, 188].)

The two terms on the last line of A.9 correspond to additional purely collinear singularities for each of the quarks. The factor $1/(N_c - 1)$ is here absent; the collinear singularities have the same strength as those of an ordinary $q\bar{q}$ antenna. The terms labelled “non-singular” are process-dependent and finite in all soft and collinear limits.

Using momentum conservation, we may rewrite the antenna pattern above to only contain the final-state particle momenta,

$$\frac{p_1 \cdot p_2}{(p_1 \cdot q)(p_2 \cdot q)} + \frac{p_1 \cdot p_3}{(p_1 \cdot q)(p_3 \cdot q)} = \frac{p_2 \cdot p_3}{(p_2 \cdot q)(p_3 \cdot q)} + \frac{2}{p_1 \cdot q} \quad (\text{A.10})$$

This reduces the eikonal part of expression to an antenna between the two final-state quarks

$$\begin{aligned} \frac{|M_1|^2}{|M_0|^2} = & 8\pi\alpha_s C_F \left[\frac{2}{(N_c - 1)} \left(\frac{p_2 \cdot p_3}{(p_2 \cdot q)(p_3 \cdot q)} + \frac{1}{p_1 \cdot q} \right) \right. \\ & \left. + \frac{1}{m_1^2} \left(\frac{p_2 \cdot q}{p_3 \cdot q} + \frac{p_3 \cdot q}{p_2 \cdot q} \right) + \frac{m_1^2}{(p_1 \cdot q)^2} \right] \end{aligned} \quad (\text{A.11})$$

The eikonal and the collinear terms here correspond exactly to the standard radiation pattern from a $q\bar{q}$ dipole with an extra term of $\mathcal{O}(\frac{1}{N_c})$. For the present work, we therefore approximate the radiation pattern by retaining a standard-strength dipole between the two quarks. Using $s_{ij} = 2p_i \cdot p_j$, the final expression used in our implementation is:

$$\frac{|M_1|^2}{|M_0|^2} = 8\pi\alpha_s C_F \left(\frac{2s_{23}}{s_{2q}s_{3q}} + \frac{s_{2q}}{s s_{3q}} + \frac{s_{3q}}{s s_{2q}} \right) \quad (\text{A.12})$$

The implementation of the additional terms could then subsequently be incorporated into PYTHIA 8 as a matrix-element correction [190, 191], presumably mostly relevant if B -violating processes should indeed be observed in nature.

A.6 Validation

To summarise, we present here, some validations performed on the code. All validations have been performed using point SPS1a (cMSSM parameters $m_0 = 250$, $m_{1/2} = 100$, $A_0 = 0$, $\mu > 0$ and $\tan \beta = 10$). However, since the masses and mixings of superparticles at low scale depend on renormalization group running, we the complete list of masses and mixing matrices used in our validations is given in Table A.3. The spectrum was generated using SoftSUSY 2.0.5 [192].

The validated cross sections for point SPS1a are presented in Table A.2. All sparticle decays are turned off. The non-default parameters used were chosen mostly for simplicity, and to enable direct comparison with both the PYTHIA 6 [193, 73] and XSUSY [182] implementations:

| | |
|-----------------------------------|----------------------|
| PDF:pSet = 8 | (CTEQ6L1) |
| SigmaProcess:factorscale2 = 4 | ($\sqrt{\hat{s}}$) |
| SigmaProcess:renormScale2 = 4 | ($\sqrt{\hat{s}}$) |
| SigmaProcess:alphaSvalue = 0.1265 | |
| SigmaProcess:alphaSorder = 1 | |

| Process | Cross Section (fb) | | | | | |
|------------------------|-------------------------------------|--------------------------------------|-------------------------------------|--------------------------------------|--------------------------------------|--------------------------------------|
| gg2squarkantisquark | $\tilde{d}_L \tilde{d}_L^*$ 95.1 | $\tilde{u}_L \tilde{u}_L^*$ 103.1 | $\tilde{s}_L \tilde{s}_L^*$ 95.1 | $\tilde{b}_1 \tilde{b}_1^*$ 179.2 | $\tilde{t}_1 \tilde{t}_1^*$ 780.2 | |
| qqbar2squarkantisquark | $\tilde{d}_L \tilde{d}_L^*$ 59.9 | $\tilde{u}_L \tilde{u}_L^*$ 89.6 | $\tilde{d}_L \tilde{u}_L^*$ 64.6 | $\tilde{s}_L \tilde{s}_L^*$ 30.8 | $\tilde{b}_1 \tilde{b}_1^*$ 48.7 | $\tilde{t}_1 \tilde{t}_1^*$ 154.3 |
| onlyQCD | 63.9 | 97.4 | 87.6 | 30.7 | 48.3 | 153.5 |
| qq2squarksquark | $\tilde{d}_L \tilde{d}_L$ 130 | $\tilde{u}_L \tilde{u}_L$ 459 | $\tilde{d}_L \tilde{u}_L$ 765 | $\tilde{s}_L \tilde{s}_L$ 5.11 | $\tilde{b}_1 \tilde{b}_1$ 1.06 | |
| onlyQCD | 106 | 374 | 523 | 4.08 | 0.83 | |
| qq2squarkgluino | $\tilde{g} \tilde{d}_L$ 2.01 | $\tilde{g} \tilde{u}_L$ 4.34 | $\tilde{g} \tilde{s}_L$ 0.345 | $\tilde{g} \tilde{c}_L$ 0.197 | $\tilde{g} \tilde{b}_1$ 0.163 | |
| gg2gluinogluino | $\tilde{g} \tilde{g}$ 0.142 | | | | | |
| qqbar2gluinogluino | $\tilde{g} \tilde{g}$ 2.97 | | | | | |

Table A.2: Cross sections for various SUSY processes using PYTHIA 8

| PDG code | Mass (GeV) | Mixing | | | | | |
|------------------------|------------|-----------------|-------------------|--------------------|---------------|-----------------|------------------|
| \tilde{g} 1000021 | 607.714 | | | | | | |
| $\tilde{\chi}_i^0$ | | \tilde{B} | \tilde{W}_3 | \tilde{H}_1 | \tilde{H}_2 | | |
| 1000022 | 96.688 | 0.986 | -0.053 | 0.146 | -0.053 | | |
| 1000023 | 181.088 | 0.099 | 0.945 | -0.270 | 0.156 | | |
| 1000025 | -363.756 | -0.060 | 0.088 | 0.696 | 0.710 | | |
| 1000035 | 381.729 | -0.117 | 0.311 | 0.649 | -0.684 | | |
| $\tilde{\chi}_i^+$ | | U | | | V | | |
| | | \tilde{W} | \tilde{H} | | \tilde{W} | \tilde{H} | |
| 1000024 | 181.696 | 0.917 | -0.399 | | 0.973 | -0.233 | |
| 1000037 | 379.939 | 0.399 | 0.917 | | 0.233 | 0.973 | |
| \tilde{d} | | \tilde{d}_L | \tilde{s}_L | \tilde{b}_L | \tilde{d}_R | \tilde{s}_R | \tilde{b}_R |
| 1000001 | 568.441 | 1.000 | 0.000 | 0.000 | 0.000 | 0.000 | 0.000 |
| 1000003 | 568.441 | 0.000 | 1.000 | 0.000 | 0.000 | 0.000 | 0.000 |
| 1000005 | 513.065 | 0.000 | 0.000 | 0.939 | 0.000 | 0.000 | 0.345 |
| 2000001 | 545.228 | 0.000 | 0.000 | 0.000 | 1.000 | 0.000 | 0.000 |
| 2000003 | 545.228 | 0.000 | 0.000 | 0.000 | 0.000 | 1.000 | 0.000 |
| 2000005 | 543.727 | 0.000 | 0.000 | -0.345 | 0.000 | 0.000 | 0.939 |
| \tilde{u} | | \tilde{u}_L | \tilde{c}_L | \tilde{t}_L | \tilde{u}_R | \tilde{c}_R | \tilde{t}_R |
| 1000002 | 561.119 | 1.000 | 0.000 | 0.000 | 0.000 | 0.000 | 0.000 |
| 1000004 | 561.119 | 0.000 | 1.000 | 0.000 | 0.000 | 0.000 | 0.000 |
| 1000006 | 399.668 | 0.000 | 0.000 | 0.554 | 0.000 | 0.000 | 0.833 |
| 2000002 | 549.259 | 0.000 | 0.000 | 0.000 | 1.000 | 0.000 | 0.000 |
| 2000004 | 549.259 | 0.000 | 0.000 | 0.000 | 0.000 | 1.000 | 0.000 |
| 2000006 | 585.786 | 0.000 | 0.000 | 0.833 | 0.000 | 0.000 | -0.554 |
| \tilde{e} | | \tilde{e}_L | $\tilde{\mu}_L$ | $\tilde{\tau}_L$ | \tilde{e}_R | $\tilde{\mu}_R$ | $\tilde{\tau}_R$ |
| 1000011 | 202.916 | 1.000 | 0.000 | 0.000 | 0.000 | 0.000 | 0.000 |
| 1000013 | 202.916 | 0.000 | 1.000 | 0.000 | 0.000 | 0.000 | 0.000 |
| 1000015 | 134.491 | 0.000 | 0.000 | 0.282 | 0.000 | 0.000 | 0.959 |
| 2000011 | 144.103 | 0.000 | 0.000 | 0.000 | 1.000 | 0.000 | 0.000 |
| 2000013 | 144.103 | 0.000 | 0.000 | 0.000 | 0.000 | 1.000 | 0.000 |
| 2000015 | 206.868 | 0.000 | 0.000 | 0.959 | 0.000 | 0.000 | -0.282 |
| $\tilde{\nu}$ | | $\tilde{\nu}_e$ | $\tilde{\nu}_\mu$ | $\tilde{\nu}_\tau$ | | | |
| 1000012 | 185.258 | 1.000 | 0.000 | 0.000 | | | |
| 1000014 | 185.258 | 0.000 | 1.000 | 0.000 | | | |
| 1000016 | 184.708 | 0.000 | 0.000 | 1.000 | | | |

Table A.3: Masses and mixing matrices corresponding to SPS1a calculated using Soft-Susy 2.0.5

BIBLIOGRAPHY

- [1] R. Cahn and G. Goldhaber, *The experimental foundations of particle physics (Second Edition)*. Cambridge University Press, 2009.
- [2] G. 't Hooft and M. Veltman, *Regularization and Renormalization of Gauge Fields*, *Nucl.Phys.* **B44** (1972) 189–213. *** Nobel Prize ja href=http://www.nobel.se/announcement-99/physics99.html;1999;ja ***.
- [3] M. E. Peskin and D. V. Schroeder, *An Introduction to quantum field theory*. Addison Wesley Publishing Company, 1995.
- [4] V. D. Barger and R. Phillips, *Collider Physics (Updated Edition)*. Addison Wesley Publishing Company, 1996.
- [5] **JADE** Collaboration, W. Bartel *et al.*, *Observation of Planar Three Jet Events in $e^+ e^-$ Annihilation and Evidence for Gluon Bremsstrahlung*, *Phys.Lett.* **B91** (1980) 142.
- [6] **Particle Data Group** Collaboration, K. Nakamura *et al.*, *Review of particle physics*, *J.Phys.G* **G37** (2010) 075021.
- [7] **ALEPH Collaboration, DELPHI Collaboration, L3 Collaboration, OPAL Collaboration, LEP Electroweak Working Group** Collaboration, A *Combination of preliminary electroweak measurements and constraints on the standard model*, hep-ex/0511027.

- [8] J. D. Hobbs, M. S. Neubauer, and S. Willenbrock, *Tests of the Standard Electroweak Model at the Energy Frontier*, *Rev.Mod.Phys.* (2010) [arXiv:1003.5733].
- [9] **CDF** Collaboration, T. Aaltonen *et al.*, *Precise measurement of the W -boson mass with the CDF II detector*, arXiv:1203.0275.
- [10] **The LEP Electroweak Working Group** Collaboration Taken from CDF's updated analysis of W Mass <http://www-cdf.fnal.gov/physics/ewk/2012/wmass/>.
- [11] **ATLAS Collaboration** Collaboration, G. Aad *et al.*, *Combined search for the Standard Model Higgs boson using up to 4.9 fb⁻¹ of pp collision data at \sqrt{s} = 7 TeV with the ATLAS detector at the LHC*, *Phys.Lett.* **B710** (2012) 49–66, [arXiv:1202.1408].
- [12] **CMS** Collaboration, S. Chatrchyan *et al.*, *Combined results of searches for the standard model Higgs boson in pp collisions at \sqrt{s} = 7 TeV*, arXiv:1202.1488.
- [13] **ATLAS** Collaboration, *Combined search for the Standard Model Higgs boson using up to 4.9 fb⁻¹ of pp collision data at \sqrt{s} = 7 TeV with the ATLAS detector at the LHC*, arXiv:1202.1408.
- [14] **Muon G-2** Collaboration, G. Bennett *et al.*, *Final Report of the Muon E821 Anomalous Magnetic Moment Measurement at BNL*, *Phys.Rev.* **D73** (2006) 072003, [hep-ex/0602035]. Summary of E821 Collaboration measurements of the muon anomalous magnetic moment, each reported earlier in Letters or Brief Reports. Revised version submitted to Phys.Rev.D.
- [15] F. Jegerlehner and A. Nyffeler, *The Muon $g-2$* , *Phys.Rept.* **477** (2009) 1–110, [arXiv:0902.3360].
- [16] A. Strumia and F. Vissani, *Neutrino masses and mixings and...*, hep-ph/0606054.
- [17] **DAYA-BAY** Collaboration, F. An *et al.*, *Observation of electron-antineutrino disappearance at Daya Bay*, arXiv:1203.1669. 5 figures.
- [18] **MINOS** Collaboration, P. Adamson *et al.*, *Measurement of the neutrino mass splitting and flavor mixing by MINOS*, *Phys.Rev.Lett.* **106** (2011) 181801, [arXiv:1103.0340]. 5 pages, 4 figures.
- [19] F. Zwicky, *On the Masses of Nebulae and of Clusters of Nebulae*, *Astrophys.J.* **86** (1937) 217–246.

- [20] D. Clowe, M. Bradac, A. H. Gonzalez, M. Markevitch, S. W. Randall, *et al.*, *A direct empirical proof of the existence of dark matter*, *Astrophys.J.* **648** (2006) L109–L113, [astro-ph/0608407].
- [21] **WMAP** Collaboration, E. Komatsu *et al.*, *Seven-Year Wilkinson Microwave Anisotropy Probe (WMAP) Observations: Cosmological Interpretation*, *Astrophys.J.Suppl.* **192** (2011) 18, [arXiv:1001.4538]. 57 pages, 20 figures. Accepted for publication in ApJS. (v2) References added. The SZ section expanded with more analysis. The discrepancy between the KS and X-ray derived profiles has been resolved. (v3) New analysis of the SZ effect on individual clusters added (Section 7.3). The LCDM parameters have been updated using the latest recombination history code (RECFAST version 1.5).
- [22] M. Cirelli, *Indirect Searches for Dark Matter: a status review*, arXiv:1202.1454. 28 pages, several figures. Extended version of the text prepared for the Proceedings of Lepton-Photon 2011, Mumbai, India, 22-27 Aug 2011. Comments and notifications of inaccuracies, oversights or omissions are welcome (except on ref. [117]).
- [23] **LEP Working Group for Higgs boson searches, ALEPH Collaboration, DELPHI Collaboration, L3 Collaboration, OPAL Collaboration**, R. Barate *et al.*, *Search for the standard model Higgs boson at LEP*, *Phys.Lett.* **B565** (2003) 61–75, [hep-ex/0306033].
- [24] **CDF** Collaboration, F. Abe *et al.*, *Evidence for top quark production in $\bar{p}p$ collisions at $\sqrt{s} = 1.8$ TeV*, *Phys.Rev.* **D50** (1994) 2966–3026.
- [25] **D0** Collaboration, V. Abazov *et al.*, *Observation of Single Top Quark Production*, *Phys.Rev.Lett.* **103** (2009) 092001, [arXiv:0903.0850].
- [26] **CDF** Collaboration, T. Aaltonen *et al.*, *First Observation of Electroweak Single Top Quark Production*, *Phys.Rev.Lett.* **103** (2009) 092002, [arXiv:0903.0885].
- [27] **ATLAS** Collaboration, G. Aad *et al.*, *Expected Performance of the ATLAS Experiment - Detector, Trigger and Physics*, arXiv:0901.0512.
- [28] **CMS Collaboration** Collaboration, G. Bayatian *et al.*, *CMS physics: Technical design report*, .
- [29] **CMS** Collaboration, G. Bayatian *et al.*, *CMS technical design report, volume II: Physics performance*, *J.Phys.G* **G34** (2007) 995–1579.

- [30] **CDF** Collaboration, T. Aaltonen *et al.*, *Evidence for a Mass Dependent Forward-Backward Asymmetry in Top Quark Pair Production*, *Phys.Rev.* **D83** (2011) 112003, [arXiv:1101.0034]. 23 pages, 18 figures, submitted to Physical Review D.
- [31] **D0** Collaboration, V. M. Abazov *et al.*, *Forward-backward asymmetry in top quark-antiquark production*, *Phys.Rev.* **D84** (2011) 112005, [arXiv:1107.4995].
- [32] V. Ahrens, A. Ferroglia, M. Neubert, B. D. Pecjak, and L. L. Yang, *The top-pair forward-backward asymmetry beyond NLO*, *Phys.Rev.* **D84** (2011) 074004, [arXiv:1106.6051].
- [33] W. Hollik and D. Pagani, *The electroweak contribution to the top quark forward-backward asymmetry at the Tevatron*, *Phys.Rev.* **D84** (2011) 093003, [arXiv:1107.2606]. 14 pages, 8 figures.
- [34] **CDF** Collaboration, T. Aaltonen *et al.*, “Combination of CDF top quark pair production cross section measurements with up to 4.6 fb⁻¹.” Conf. Note 9913.
- [35] S. Moch and P. Uwer, *Theoretical status and prospects for top-quark pair production at hadron colliders*, *Phys.Rev.* **D78** (2008) 034003, [arXiv:0804.1476].
- [36] H. P. Nilles, *Supersymmetry, Supergravity and Particle Physics*, *Phys. Rept.* **110** (1984) 1–162.
- [37] G. L. Kane, (ed.), *Perspectives on supersymmetry*. World Scientific, Singapore, 1998.
- [38] S. R. Coleman and J. Mandula, *ALL POSSIBLE SYMMETRIES OF THE S MATRIX*, *Phys.Rev.* **159** (1967) 1251–1256.
- [39] R. Haag, J. T. Lopuszanski, and M. Sohnius, *All Possible Generators of Supersymmetries of the s Matrix*, *Nucl.Phys.* **B88** (1975) 257.
- [40] S. P. Martin, “A Supersymmetry primer.” Published in Kane, G.L. (ed.): *Perspectives on supersymmetry II* 1-153, 1997.
- [41] M. Drees, *An Introduction to supersymmetry*, hep-ph/9611409.
- [42] L. Girardello and M. T. Grisaru, *Soft Breaking of Supersymmetry*, *Nucl.Phys.* **B194** (1982) 65.

- [43] A. H. Chamseddine, R. L. Arnowitt, and P. Nath, *Locally Supersymmetric Grand Unification*, *Phys.Rev.Lett.* **49** (1982) 970.
- [44] R. L. Arnowitt and P. Nath, *SUSY mass spectrum in SU(5) supergravity grand unification*, *Phys.Rev.Lett.* **69** (1992) 725–728.
- [45] G. L. Kane, C. F. Kolda, L. Roszkowski, and J. D. Wells, *Study of constrained minimal supersymmetry*, *Phys. Rev.* **D49** (1994) 6173–6210, [hep-ph/9312272].
- [46] G. Giudice and R. Rattazzi, *Theories with gauge mediated supersymmetry breaking*, *Phys.Rept.* **322** (1999) 419–499, [hep-ph/9801271].
- [47] C. F. Berger, J. S. Gainer, J. L. Hewett, and T. G. Rizzo, *Supersymmetry Without Prejudice*, *JHEP* **0902** (2009) 023, [arXiv:0812.0980].
- [48] S. P. Martin and P. Ramond, *Sparticle Spectrum Constraints*, *Phys.Rev.* **D48** (1993) 5365–5375, [hep-ph/9306314].
- [49] B. Allanach, M. Battaglia, G. Blair, M. S. Carena, A. De Roeck, *et al.*, *The Snowmass points and slopes: Benchmarks for SUSY searches*, *Eur.Phys.J.* **C25** (2002) 113–123, [hep-ph/0202233]. 12 pages, 3 figures Report-no: BNL-HET-02/6, CERN-TH/2002-020, DCPT/02/16, DESY 02-022, FERMILAB-Conf-02/011-T, HEPHY-PUB 751, IPPP/02/08, PM/01-69, SLAC-PUB-9134, UCD-2002-01, UFIFT-HEP-02-2, UMN-TH-2043/02, ZU-TH 3/02.
- [50] Y. Nir and N. Seiberg, *Should squarks be degenerate?*, *Phys.Lett.* **B309** (1993) 337–343, [hep-ph/9304307].
- [51] P. Brax and C. A. Savoy, *Models with inverse sfermion mass hierarchy and decoupling of the SUSY FCNC effects*, *JHEP* **0007** (2000) 048, [hep-ph/0004133].
- [52] S. Dimopoulos, G. Giudice, and N. Tetradis, *Disoriented and plastic soft terms: A Dynamical solution to the problem of supersymmetric flavor violations*, *Nucl.Phys.* **B454** (1995) 59–74, [hep-ph/9504296].
- [53] A. G. Cohen, D. Kaplan, and A. Nelson, *The More minimal supersymmetric standard model*, *Phys.Lett.* **B388** (1996) 588–598, [hep-ph/9607394].
- [54] V. D. Barger, C. Kao, and R.-J. Zhang, *Phenomenology of a string inspired supersymmetric model with inverted scalar mass hierarchy*, *Phys.Lett.* **B483** (2000) 184–190, [hep-ph/9911510].

- [55] A. Pomarol and D. Tommasini, *Horizontal symmetries for the supersymmetric flavor problem*, *Nucl.Phys.* **B466** (1996) 3–24, [hep-ph/9507462].
- [56] H. Baer, P. Mercadante, and X. Tata, *Calculable sparticle masses with radiatively driven inverted mass hierarchy*, *Phys.Lett.* **B475** (2000) 289–294, [hep-ph/9912494].
- [57] H. Baer, C. Balazs, M. Brhlik, P. Mercadante, X. Tata, *et al.*, *Aspects of supersymmetric models with a radiatively driven inverted mass hierarchy*, *Phys.Rev.* **D64** (2001) 015002, [hep-ph/0102156].
- [58] P. Binetruy and E. Dudas, *Gaugino condensation and the anomalous $U(1)$* , *Phys.Lett.* **B389** (1996) 503–509, [hep-th/9607172].
- [59] G. Dvali and A. Pomarol, *Anomalous $U(1)$ as a mediator of supersymmetry breaking*, *Phys.Rev.Lett.* **77** (1996) 3728–3731, [hep-ph/9607383].
- [60] J. L. Feng, K. T. Matchev, and T. Moroi, *Focus points and naturalness in supersymmetry*, *Phys.Rev.* **D61** (2000) 075005, [hep-ph/9909334].
- [61] U. Chattopadhyay, A. Datta, A. Datta, A. Datta, and D. Roy, *LHC signature of the minimal SUGRA model with a large soft scalar mass*, *Phys.Lett.* **B493** (2000) 127–134, [hep-ph/0008228].
- [62] K. Agashe, A. Belyaev, T. Krupovnickas, G. Perez, and J. Virzi, *LHC Signals from Warped Extra Dimensions*, *Phys.Rev.* **D77** (2008) 015003, [hep-ph/0612015].
- [63] U. Baur and L. H. Orr, *Searching for t anti- t Resonances at the Large Hadron Collider*, *Phys. Rev.* **D77** (2008) 114001, [arXiv:0803.1160].
- [64] M. Gerbush, T. J. Khoo, D. J. Phalen, A. Pierce, and D. Tucker-Smith, *Color-octet scalars at the LHC*, *Phys. Rev.* **D77** (2008) 095003, [arXiv:0710.3133].
- [65] V. Barger, T. Han, and D. G. Walker, *Top Quark Pairs at High Invariant Mass: A Model-Independent Discriminator of New Physics at the LHC*, *Phys.Rev.Lett.* **100** (2008) 031801, [hep-ph/0612016].
- [66] U. Baur and L. Orr, *High p_T Top Quarks at the Large Hadron Collider*, *Phys.Rev.* **D76** (2007) 094012, [arXiv:0707.2066].
- [67] R. Frederix and F. Maltoni, *Top pair invariant mass distribution: A Window on new physics*, *JHEP* **0901** (2009) 047, [arXiv:0712.2355].

- [68] R. Kadala, P. Mercadante, J. Mizukoshi, and X. Tata, *Heavy-flavour tagging and the supersymmetry reach of the CERN Large Hadron Collider*, *Eur.Phys.J.* **C56** (2008) 511–528, [arXiv:0803.0001].
- [69] T. Han, R. Mahbubani, D. G. Walker, and L.-T. Wang, *Top Quark Pair plus Large Missing Energy at the LHC*, *JHEP* **0905** (2009) 117, [arXiv:0803.3820].
- [70] S. P. Das, A. Datta, M. Guchait, M. Maity, and S. Mukherjee, *Focus Point SUSY at the LHC Revisited*, *Eur.Phys.J.* **C54** (2008) 645–653, [arXiv:0708.2048]. 17 pages, 4 figures.
- [71] B. S. Acharya, P. Grajek, G. L. Kane, E. Kuflik, K. Suruliz, *et al.*, *Identifying Multi-Top Events from Gluino Decay at the LHC*, arXiv:0901.3367.
- [72] A. Djouadi, J.-L. Kneur, and G. Moultaka, *SuSpect: A Fortran code for the supersymmetric and Higgs particle spectrum in the MSSM*, *Comput.Phys.Commun.* **176** (2007) 426–455, [hep-ph/0211331].
- [73] T. Sjostrand, S. Mrenna, and P. Z. Skands, *PYTHIA 6.4 Physics and Manual*, *JHEP* **05** (2006) 026, [hep-ph/0603175].
- [74] D. E. Kaplan, K. Rehermann, M. D. Schwartz, and B. Tweedie, *Top Tagging: A Method for Identifying Boosted Hadronically Decaying Top Quarks*, *Phys.Rev.Lett.* **101** (2008) 142001, [arXiv:0806.0848].
- [75] L. G. Almeida, S. J. Lee, G. Perez, I. Sung, and J. Virzi, *Top Jets at the LHC*, *Phys.Rev.* **D79** (2009) 074012, [arXiv:0810.0934].
- [76] M. L. Mangano, M. Moretti, F. Piccinini, R. Pittau, and A. D. Polosa, *ALPGEN, a generator for hard multiparton processes in hadronic collisions*, *JHEP* **07** (2003) 001, [hep-ph/0206293].
- [77] I. Hinchliffe, F. Paige, M. Shapiro, J. Soderqvist, and W. Yao, *Precision SUSY measurements at CERN LHC*, *Phys.Rev.* **D55** (1997) 5520–5540, [hep-ph/9610544].
- [78] M. Graesser and J. Shelton, *Probing Supersymmetry With Third-Generation Cascade Decays*, *JHEP* **0906** (2009) 039, [arXiv:0811.4445].
- [79] N. Bhattacharyya, A. Datta, and M. Maity, *Search for Top Squarks at Tevatron Inspired by Dark Matter and Electroweak Baryogenesis*, *Phys.Lett.* **B669** (2008) 311–316, [arXiv:0807.0994].

- [80] N. Desai and B. Mukhopadhyaya, *Signals of supersymmetry with inaccessible first two families at the Large Hadron Collider*, *Phys.Rev.* **D80** (2009) 055019, [arXiv:0901.4883].
- [81] W. Beenakker, S. Brensing, M. Kramer, A. Kulesza, E. Laenen, *et al.*, *Supersymmetric top and bottom squark production at hadron colliders*, *JHEP* **1008** (2010) 098, [arXiv:1006.4771].
- [82] H. Baer, S. Kraml, A. Lessa, S. Sekmen, and X. Tata, *Effective Supersymmetry at the LHC*, *JHEP* **1010** (2010) 018, [arXiv:1007.3897].
- [83] A. Bartl, H. Eberl, B. Herrmann, K. Hidaka, W. Majerotto, *et al.*, *Impact of squark generation mixing on the search for squarks decaying into fermions at LHC*, *Phys.Lett.* **B698** (2011) 380–388, [arXiv:1007.5483].
- [84] H. Li, W. Parker, Z. Si, and S. Su, *Sbottom Signature of the Supersymmetric Golden Region*, *Eur.Phys.J.* **C71** (2011) 1584, [arXiv:1009.6042].
- [85] S. Bornhauser, M. Drees, S. Grab, and J. Kim, *Light Stop Searches at the LHC in Events with two b-Jets and Missing Energy*, *Phys.Rev.* **D83** (2011) 035008, [arXiv:1011.5508].
- [86] K. Huitu, L. Leinonen, and J. Laamanen, *Stop as a next-to-lightest supersymmetric particle in constrained MSSM*, arXiv:1107.2128.
- [87] A. Datta and S. Niyogi, *Entangled System of Squarks from the Third Generation at the Large Hadron Collider*, arXiv:1111.0200. * Temporary entry *.
- [88] Y. Kats, P. Meade, M. Reece, and D. Shih, *The Status of GMSB After $1/\beta$ at the LHC*, arXiv:1110.6444.
- [89] R. Essig, E. Izaguirre, J. Kaplan, and J. G. Wacker, *Heavy Flavor Simplified Models at the LHC*, arXiv:1110.6443.
- [90] X.-J. Bi, Q.-S. Yan, and P.-F. Yin, *Probing Light Stop Pairs at the LHC*, arXiv:1111.2250.
- [91] M. Papucci, J. T. Ruderman, and A. Weiler, *Natural SUSY Endures*, arXiv:1110.6926.
- [92] C. Brust, A. Katz, S. Lawrence, and R. Sundrum, *SUSY, the Third Generation and the LHC*, arXiv:1110.6670.
- [93] L. J. Hall, D. Pinner, and J. T. Ruderman, *A Natural SUSY Higgs Near 126 GeV*, *JHEP* **1204** (2012) 131, [arXiv:1112.2703].

- [94] **ATLAS** Collaboration, G. Aad *et al.*, *Search for squarks and gluinos using final states with jets and missing transverse momentum with the ATLAS detector in $\sqrt{s} = 7$ TeV proton-proton collisions*, arXiv:1102.5290.
- [95] **ATLAS** Collaboration, G. Aad *et al.*, *Search for supersymmetry using final states with one lepton, jets, and missing transverse momentum with the ATLAS detector in $\sqrt{s} = 7$ TeV pp*, *Phys.Rev.Lett.* **106** (2011) 131802, [arXiv:1102.2357].
- [96] **ATLAS** Collaboration, G. Aad *et al.*, *Search for supersymmetry in pp collisions at $\sqrt{s} = 7$ TeV in final states with missing transverse momentum and b-jets*, arXiv:1103.4344.
- [97] **ATLAS** Collaboration, G. Aad *et al.*, “Search for squarks and gluinos using final states with jets and missing transverse momentum with the atlas detector in $\sqrt{s} = 7$ TeV proton-proton collisions.” ATLAS-CONF-2011-086, Jun, 2011.
- [98] **ATLAS** Collaboration, G. Aad *et al.*, “Search for supersymmetry in pp collisions at $\sqrt{s} = 7$ tev in final states with missing transverse momentum, b-jets and no leptons with the atlas detector.” ATLAS-CONF-2011-098, Jul, 2011.
- [99] K. Sakurai and K. Takayama, *Constraint from recent ATLAS results to non-universal sfermion mass models and naturalness*, arXiv:1106.3794.
- [100] K.-i. Hikasa and M. Kobayashi, *Light Scalar Top at $e^+ e^-$ Colliders*, *Phys.Rev.* **D36** (1987) 724.
- [101] C. Boehm, A. Djouadi, and Y. Mambrini, *Decays of the lightest top squark*, *Phys.Rev.* **D61** (2000) 095006, [hep-ph/9907428].
- [102] M. Muhlleitner and E. Popenza, *Light Stop Decay in the MSSM with Minimal Flavour Violation*, *JHEP* **1104** (2011) 095, [arXiv:1102.5712].
- [103] W. Beenakker, R. Hopker, and M. Spira, *PROSPINO: A Program for the production of supersymmetric particles in next-to-leading order QCD*, hep-ph/9611232.
- [104] M. Cacciari, G. P. Salam, and G. Soyez, *The anti- k_t jet clustering algorithm*, *JHEP* **04** (2008) 063, [arXiv:0802.1189].
- [105] J. A. Conley, J. S. Gainer, J. L. Hewett, M. P. Le, and T. G. Rizzo, *Supersymmetry Without Prejudice at the 7 TeV LHC*, *Physical Review D* (2011) [arXiv:1103.1697].

- [106] B. Allanach, *Impact of CMS Multi-jets and Missing Energy Search on CMSSM Fits*, *Phys.Rev.* **D83** (2011) 095019, [arXiv:1102.3149].
- [107] B. Allanach, T. Khoo, C. Lester, and S. Williams, *The impact of the ATLAS zero-lepton, jets and missing momentum search on a CMSSM fit*, *JHEP* **1106** (2011) 035, [arXiv:1103.0969]. * Temporary entry *.
- [108] O. Buchmueller, R. Cavanaugh, A. De Roeck, M. Dolan, J. Ellis, *et al.*, *Supersymmetry in Light of $1/\text{fb}$ of LHC Data*, arXiv:1110.3568. * Temporary entry *.
- [109] S. Sekmen *et al.*, *Interpreting LHC SUSY searches in the phenomenological MSSM*, arXiv:1109.5119.
- [110] D. Feldman, K. Freese, P. Nath, B. D. Nelson, and G. Peim, *Predictive Signatures of Supersymmetry: Measuring the Dark Matter Mass and Gluino Mass with Early LHC data*, *Phys.Rev.* **D84** (2011) 015007, [arXiv:1102.2548].
- [111] P. Athron, S. King, D. Miller, S. Moretti, and R. Nevzorov, *LHC Signatures of the Constrained Exceptional Supersymmetric Standard Model*, *Phys.Rev.* **D84** (2011) 055006, [arXiv:1102.4363].
- [112] S. Scopel, S. Choi, N. Fornengo, and A. Bottino, *Impact of the recent results by the CMS and ATLAS Collaborations at the CERN Large Hadron Collider on an effective Minimal Supersymmetric extension of the Standard Model*, *Phys.Rev.* **D83** (2011) 095016, [arXiv:1102.4033].
- [113] S. Akula, N. Chen, D. Feldman, M. Liu, Z. Liu, *et al.*, *Interpreting the First CMS and ATLAS SUSY Results*, *Phys.Lett.* **B699** (2011) 377–382, [arXiv:1103.1197]. * Temporary entry *.
- [114] **CDF** Collaboration, T. Aaltonen *et al.*, “Search for scalar top decaying into $c + \tilde{\chi}_1^0$ in the met+jets sample.” Search for scalar top decaying into $c + \tilde{\chi}_1^0$ in the MET+jets sample; CDF Note 9834, July, 2009.
- [115] N. Bhattacharyya, A. Choudhury, and A. Datta, *Low mass neutralino dark matter in mSUGRA and more general models in the light of LHC data*, arXiv:1107.1997.
- [116] R. Barbier *et al.*, *R-parity violating supersymmetry*, *Phys. Rept.* **420** (2005) 1–202, [hep-ph/0406039].

- [117] F. Zwirner, *Observable Delta B=2 Transitions Without Nucleon Decay in a Minimal Supersymmetric Extension of the Standard Model*, *Phys. Lett.* **B132** (1983) 103–106.
- [118] H. K. Dreiner and G. G. Ross, *R-parity violation at hadron colliders*, *Nucl. Phys.* **B365** (1991) 597–613.
- [119] R. Barbieri and A. Masiero, *Supersymmetric Models with Low-Energy Baryon Number Violation*, *Nucl. Phys.* **B267** (1986) 679.
- [120] G. Bhattacharyya, D. Choudhury, and K. Sridhar, *New LEP bounds on B violating scalar couplings: R-parity violating supersymmetry or diquarks*, *Phys. Lett.* **B355** (1995) 193–198, [hep-ph/9504314].
- [121] K. Agashe and M. Graesser, *R-parity violation in flavor changing neutral current processes and top quark decays*, *Phys. Rev.* **D54** (1996) 4445–4452, [hep-ph/9510439].
- [122] B. C. Allanach, A. Dedes, and H. K. Dreiner, *Bounds on R-parity violating couplings at the weak scale and at the GUT scale*, *Phys. Rev.* **D60** (1999) 075014, [hep-ph/9906209].
- [123] E. L. Berger, B. W. Harris, and Z. Sullivan, *Single-top-squark production via R-parity-violating supersymmetric couplings in hadron collisions*, *Phys. Rev. Lett.* **83** (1999) 4472–4475, [hep-ph/9903549].
- [124] E. L. Berger, B. W. Harris, and Z. Sullivan, *Direct probes of R-parity violating supersymmetric couplings via single top squark production*, *Phys. Rev.* **D63** (2001) 115001, [hep-ph/0012184].
- [125] K.-i. Hikasa, J. M. Yang, and B.-L. Young, *R-parity violation and top quark polarization at the Fermilab Tevatron collider*, *Phys. Rev.* **D60** (1999) 114041, [hep-ph/9908231].
- [126] P. Chiappetta, A. Deandrea, E. Nagy, S. Negroni, G. Polesello, *et al.*, *Single top production at the CERN LHC as a probe of R-parity violation*, *Phys. Rev.* **D61** (2000) 115008, [hep-ph/9910483].
- [127] T. Plehn, *Single stop production at hadron colliders*, *Phys. Lett.* **B488** (2000) 359–366, [hep-ph/0006182].
- [128] H. Baer, C. Kao, and X. Tata, *Impact of R-parity violation on supersymmetry searches at the tevatron*, *Phys. Rev.* **D51** (1995) 2180–2186, [hep-ph/9410283].

- [129] B. C. Allanach *et al.*, *Measuring supersymmetric particle masses at the LHC in scenarios with baryon-number R -parity violating couplings*, *JHEP* **03** (2001) 048, [hep-ph/0102173].
- [130] B. C. Allanach, A. J. Barr, M. A. Parker, P. Richardson, and B. R. Webber, *Extracting the flavour structure of a baryon-number R -parity violating coupling at the LHC*, *JHEP* **09** (2001) 021, [hep-ph/0106304].
- [131] H. K. Dreiner and S. Grab, *All Possible Lightest Supersymmetric Particles in R -Parity Violating $mSUGRA$* , *Phys. Lett.* **B679** (2009) 45–50, [arXiv:0811.0200].
- [132] J. M. Butterworth, J. R. Ellis, A. R. Raklev, and G. P. Salam, *Discovering baryon-number violating neutralino decays at the LHC*, *Phys. Rev. Lett.* **103** (2009) 241803, [arXiv:0906.0728].
- [133] T. Plehn, M. Spannowsky, M. Takeuchi, and D. Zerwas, *Stop Reconstruction with Tagged Tops*, arXiv:1006.2833.
- [134] **R parity Working Group** Collaboration, B. Allanach *et al.*, *Searching for R parity violation at Run II of the Tevatron*, hep-ph/9906224.
- [135] P. Nath, R. L. Arnowitt, and A. H. Chamseddine, *Applied $N=1$ Supergravity*. World Scientific, Singapore, 1984.
- [136] U. Chattopadhyay and P. Nath, *Upper limits on sparticle masses from $g-2$ and the possibility for discovery of SUSY at colliders and in dark matter searches*, *Phys. Rev. Lett.* **86** (2001) 5854–5857, [hep-ph/0102157].
- [137] B. C. Allanach and M. A. Bernhardt, *Including R -parity violation in the numerical computation of the spectrum of the minimal supersymmetric standard model: SOFTSUSY3.0*, *Comput. Phys. Commun.* **181** (2010) 232–245, [arXiv:0903.1805].
- [138] F. E. Paige, S. D. Protopopescu, H. Baer, and X. Tata, *ISAJET 7.69: A Monte Carlo event generator for $p p$, anti- $p p$, and $e^+ e^-$ reactions*, hep-ph/0312045.
- [139] G. Corcella *et al.*, *HERWIG 6.5 release note*, hep-ph/0210213.
- [140] J. Pumplin *et al.*, *New generation of parton distributions with uncertainties from global QCD analysis*, *JHEP* **07** (2002) 012, [hep-ph/0201195].
- [141] R. M. Barnett, J. F. Gunion, and H. E. Haber, *Discovering supersymmetry with like sign dileptons*, *Phys. Lett.* **B315** (1993) 349–354, [hep-ph/9306204].

- [142] H. K. Dreiner, M. Guchait, and D. Roy, *Like sign dilepton signature for gluino production at CERN LHC with or without R conservation*, *Phys.Rev.* **D49** (1994) 3270–3282, [[hep-ph/9310291](#)].
- [143] Z. Sullivan and E. L. Berger, *Isolated leptons from heavy flavor decays: Theory and data*, *Phys. Rev.* **D82** (2010) 014001, [[arXiv:1003.4997](#)].
- [144] **Particle Data Group** Collaboration, C. Amsler *et al.*, *Review of particle physics*, *Phys. Lett.* **B667** (2008) 1.
- [145] H. K. Dreiner, S. Grab, and M. K. Trenkel, *$S\tau$ LSP Phenomenology: Two versus Four-Body Decay Modes. Example: Resonant Single Slepton Production at the LHC*, *Phys. Rev.* **D79** (2009) 016002, [[arXiv:0808.3079](#)].
- [146] CDF and D0, *Combined CDF and D0 Upper Limits on Standard Model Higgs-Boson Production with up to 6.7 fb^{-1} of Data*, [arXiv:1007.4587](#).
- [147] J. Baglio, A. Djouadi, S. Ferrag, and R. Godbole, *The Tevatron Higgs exclusion limits and theoretical uncertainties: A Critical appraisal*, [arXiv:1101.1832](#).
- [148] B. Zhang, Y.-P. Kuang, H.-J. He, and C. Yuan, *Testing anomalous gauge couplings of the Higgs boson via weak boson scatterings at the CERN LHC*, *Phys.Rev.* **D67** (2003) 114024.
- [149] S. S. Biswal, R. M. Godbole, R. K. Singh, and D. Choudhury, *Signatures of anomalous Higgs interactions at a linear collider*, *Phys. Rev.* **D73** (2006) 035001.
- [150] R. M. Godbole, . Miller, D.J., and M. Muhlleitner, *Aspects of CP violation in the H ZZ coupling at the LHC*, *JHEP* **0712** (2007) 031.
- [151] Y.-H. Qi, Y.-P. Kuang, B.-J. Liu, and B. Zhang, *Anomalous gauge couplings of the Higgs boson at the CERN LHC: Semileptonic mode in WW scatterings*, *Phys.Rev.* **D79** (2009) 055010.
- [152] Z. Zhang, G.-M. Chen, M. Yang, B.-J. Liu, J.-Q. Tao, *et al.*, *Sensitivity to measure the anomalous gauge couplings of the Higgs boson via $W+W+$ scattering at the CERN LHC*, *Phys.Rev.* **D78** (2008) 073010.
- [153] T. Han and Y. Li, *Genuine CP-odd Observables at the LHC*, *Phys.Lett.* **B683** (2010) 278–281.
- [154] N. D. Christensen, T. Han, and Y. Li, *Testing CP Violation in ZZH Interactions at the LHC*, *Phys.Lett.* **B693** (2010) 28–35.

- [155] . Miller, D.J., S. Choi, B. Eberle, M. Muhlleitner, and P. Zerwas, *Measuring the spin of the Higgs boson*, *Phys.Lett.* **B505** (2001) 149–154, [hep-ph/0102023].
- [156] S. Choi, . Miller, D.J., M. Muhlleitner, and P. Zerwas, *Identifying the Higgs spin and parity in decays to Z pairs*, *Phys.Lett.* **B553** (2003) 61–71, [hep-ph/0210077].
- [157] S. D. Rindani and P. Sharma, *Angular distributions as a probe of anomalous ZZH and gammaZH interactions at a linear collider with polarized beams*, *Phys.Rev.* **D79** (2009) 075007.
- [158] S. S. Biswal, D. Choudhury, R. M. Godbole, and Mamta, *Role of polarization in probing anomalous gauge interactions of the Higgs boson*, *Phys.Rev.* **D79** (2009) 035012, [arXiv:0809.0202].
- [159] S. S. Biswal and R. M. Godbole, *Use of transverse beam polarization to probe anomalous VVH interactions at a Linear Collider*, *Phys.Lett.* **B680** (2009) 81–87.
- [160] Y. Takubo *et al.*, *Measuring Anomalous Couplings in $H \rightarrow WW^*$ Decays at the International Linear Collider*, arXiv:1011.5805.
- [161] D. Choudhury and Mamta, *Anomalous Higgs Couplings at an e gamma Collider*, *Phys.Rev.* **D74** (2006) 115019.
- [162] T. Han, Y.-P. Kuang, and B. Zhang, *Anomalous gauge couplings of the Higgs boson at high energy photon colliders*, *Phys.Rev.* **D73** (2006) 055010.
- [163] B. Sahin, *Anomalous WWH couplings in gamma gamma collision with initial beams and final state polarizations*, *J.Phys.G* **G36** (2009) 025012.
- [164] L3 Collaboration, M. Acciarri *et al.*, *Search for anomalous couplings in the Higgs sector at LEP*, *Phys.Lett.* **B489** (2000) 102–114.
- [165] M. Dittmar and H. K. Dreiner, *How to find a Higgs boson with a mass between 155-GeV - 180-GeV at the LHC*, *Phys.Rev.* **D55** (1997) 167–172.
- [166] V. Hankele, G. Klamke, D. Zeppenfeld, and T. Figy, *Anomalous Higgs boson couplings in vector boson fusion at the CERN LHC*, *Phys.Rev.* **D74** (2006) 095001.
- [167] T. Arens, U. Gieseler, and L. Sehgal, *Energy correlation and asymmetry of secondary leptons originating in $H \rightarrow t \text{ anti-}t$ and $H \rightarrow W^+ W^-$* , *Phys.Lett.* **B339** (1994) 127–135.

- [168] J. Vermaseren, *New features of FORM*, math-ph/0010025.
- [169] CDF, *CDF Search for Higgs to WW* Production using a Combined Matrix Element and Neural Network Technique*, .
http://www-cdf.fnal.gov/physics/new/hdg//Results_files/results/hwwmenn_110304/.
- [170] T. Sjostrand, S. Mrenna, and P. Z. Skands, *A Brief Introduction to PYTHIA 8.1*, *Comput.Phys.Commun.* **178** (2008) 852–867.
- [171] J. Alwall *et al.*, *A Standard format for Les Houches event files*, *Comput.Phys.Commun.* **176** (2007) 300–304.
- [172] A. Buckley, J. Butterworth, S. Gieseke, D. Grellscheid, S. Hoche, *et al.*, *General-purpose event generators for LHC physics*, *Phys.Rept.* **504** (2011) 145–233, [arXiv:1101.2599].
- [173] T. Sjöstrand and P. Z. Skands, *Transverse-momentum-ordered showers and interleaved multiple interactions*, *Eur.Phys.J.* **C39** (2005) 129–154, [hep-ph/0408302].
- [174] R. Corke and T. Sjöstrand, *Interleaved Parton Showers and Tuning Prospects*, *JHEP* **1103** (2011) 032, [arXiv:1011.1759].
- [175] B. Andersson, G. Gustafson, G. Ingelman, and T. Sjöstrand, *Parton Fragmentation and String Dynamics*, *Phys.Rept.* **97** (1983) 31–145.
- [176] T. Sjöstrand and P. Z. Skands, *Multiple interactions and the structure of beam remnants*, *JHEP* **0403** (2004) 053, [hep-ph/0402078].
- [177] R. Corke and T. Sjöstrand, *Multiparton Interactions with an x-dependent Proton Size*, *JHEP* **1105** (2011) 009, [arXiv:1101.5953].
- [178] J. Alwall, E. Boos, L. Dudko, M. Gigg, M. Herquet, *et al.*, *A Les Houches Interface for BSM Generators*, arXiv:0712.3311.
- [179] N. Desai and P. Z. Skands, *Supersymmetry and Generic BSM Models in PYTHIA 8*, arXiv:1109.5852.
- [180] P. Z. Skands, B. Allanach, H. Baer, C. Balazs, G. Belanger, *et al.*, *SUSY Les Houches accord: Interfacing SUSY spectrum calculators, decay packages, and event generators*, *JHEP* **0407** (2004) 036, [hep-ph/0311123].
- [181] B. Allanach *et al.*, *SUSY Les Houches Accord 2*, *Comp. Phys. Commun.* **180** (2009) 8–25, [arXiv:0801.0045].

- [182] G. Bozzi, B. Fuks, B. Herrmann, and M. Klasen, *Squark and gaugino hadroproduction and decays in non-minimal flavour violating supersymmetry*, *Nucl.Phys.* **B787** (2007) 1–54, [arXiv:0704.1826].
- [183] J. F. Gunion and H. E. Haber, *TWO-BODY DECAYS OF NEUTRALINOS AND CHARGINOS*, *Phys.Rev.* **D37** (1988) 2515.
- [184] H. K. Dreiner, P. Richardson, and M. H. Seymour, *Parton shower simulations of R-parity violating supersymmetric models*, *JHEP* **0004** (2000) 008, [hep-ph/9912407].
- [185] G. Gustafson and U. Pettersson, *Dipole Formulation of QCD Cascades*, *Nucl.Phys.* **B306** (1988) 746.
- [186] A. Gehrmann-De Ridder, T. Gehrmann, and E. Glover, *Antenna subtraction at NNLO*, *JHEP* **0509** (2005) 056, [hep-ph/0505111]. Erratum added online, 8/18/06.
- [187] A. G.-D. Ridder, M. Ritzmann, and P. Skands, *Timelike Dipole-Antenna Showers with Massive Fermions*, arXiv:1108.6172.
- [188] P. Richardson, *Simulations of R-parity violating SUSY models*, hep-ph/0101105. Ph.D. Thesis.
- [189] G. Corcella, I. Knowles, G. Marchesini, S. Moretti, K. Odagiri, *et al.*, *HERWIG 6: An Event generator for hadron emission reactions with interfering gluons (including supersymmetric processes)*, *JHEP* **0101** (2001) 010, [hep-ph/0011363].
- [190] M. Bengtsson and T. Sjöstrand, *Coherent Parton Showers Versus Matrix Elements: Implications of PETRA - PEP Data*, *Phys.Lett.* **B185** (1987) 435.
- [191] E. Norrbin and T. Sjöstrand, *QCD radiation off heavy particles*, *Nucl.Phys.* **B603** (2001) 297–342, [hep-ph/0010012].
- [192] B. C. Allanach, *SOFTSUSY: a program for calculating supersymmetric spectra*, *Comput. Phys. Commun.* **143** (2002) 305–331, [hep-ph/0104145].
- [193] S. Mrenna, *SPYTHIA, a supersymmetric extension of PYTHIA 5.7*, *Comput.Phys.Commun.* **101** (1997) 232–240, [hep-ph/9609360].